A map-based analysis of the theoretical CO_2 storage capacity in the Rotliegend aquifer of the Dutch offshore

TNO Public ⟩ TNO2025 R10216
20 February 2025

Energy & Materials
Transition
www.tno.nl
+31 88 866 42 56
info@tno.nl

TNO2025 R10216 – 20 February 2025

A map-based analysis of the theoretical CO_2 storage capacity in the Rotliegend aquifer of the Dutch offshore

Author(s)	J.M. (Jo) van Buggenum, B. (Bart) Davids, T. (Thomas) Ravestein
Classification report	TNO Public
Report text	TNO Public
Number of pages	77 (excl. front and back cover)
Number of appendices	2
Sponsor	Ministry of Climate and Green Growth
Programme name	EZK Work Program 2024
Programme number	060.58401
Project name	CO_2 Capacity Prognosis
Project number	01.06.03

Management samenvatting

Deze studie is door TNO-AGE uitgevoerd voor het Ministerie van Klimaat en Groene Groei. De aanleiding hiertoe was dat het opslagpotentieel voor CO_2 in aquifers in het Nederlandse offshore gebied onderbelicht is. Een verbeteringsslag was daardoor wenselijk, anticiperend op de toegenomen interesse in CO_2 opslag m.b.t. Europese en Nederlandse klimaatdoelstellingen. De bevindingen in deze studie kunnen beleidsmakers en exploitanten uit de olie & gas industrie informeren over CO_2-opslag in het Nederlandse offshore gebied en toekomstige verkenningsinspanningen begeleiden.

De Rotliegend-aquifer in het Nederlandse offshore gebied is geïdentificeerd als een potentieel interval voor de opslag van koolstofdioxide (CO_2). Dit aquifer bevindt zich ook in het Nederlandse onshore gebied, echter is dit niet geëvalueerd aangezien er geen politieke steun is voor CO_2 opslag op land. Deze studie evalueert de opslagcapaciteit van deze aquifer met behulp van een verbeterde versie van de conventionele opslagbeoordelingsmethode voor gesloten-systeem aquifers. Traditionele methoden omvatten het samenvoegen van de CO_2-opslagcapaciteit van individuele opslagcomplexen, wat tijdrovend is. Daarom is een methode ontwikkeld om de theoretische CO_2-opslagcapaciteit inclusief een onzekerheidsmarge direct te evalueren met behulp van regionale kaarten.

Het studiegebied komt overeen met de ruimtelijke verdeling van de Slochteren Formatie van het Rotliegend in het Nederlandse deel van de Noordzee. De kern van dit studiegebied wordt begrensd door specifieke geologische en verwachte juridische beperkingen, waaronder een theoretische CO_2-opslagcapaciteitslimiet in het noorden, de afwezigheid van een doorlopende Zechstein afdekkingslaag in het zuiden, de Nederlandse maritieme 3-mijlszone in het oosten en de VK/NL economische zonegrens in het westen.

De studie concludeert:

- De gemiddelde theoretische CO_2-opslagcapaciteit van de Rotliegend-aquifer in het kerngebied is 2215 Mt, met een 80% zekerheidsinterval dat de capaciteit zich tussen 990 Mt en 3650 Mt bevindt;
- Gebieden met de hoogste CO_2-opslagcapaciteit vertonen een duidelijke oost-west oriëntatie, met prominente zones in de noordelijke blokken (van L10 in het oosten tot K10 in het westen) en zuidelijke blokken (van Q2 in het oosten tot P1 in het westen) van het studiegebied;
- De porositeit-dikte kaart correleert sterk met het CO_2 opslagpotentieel, wat betekent dat deze kaart een efficiënte korte route is voor het verkennen van hoge capaciteit aquifer opslagcomplexen.

Contents

List of Figures

List of Maps

List of Tables

1 Introduction

The Rotliegend aquifer in the Dutch offshore has been identified as a potential interval for carbon dioxide (CO_2) storage. In this study, we evaluated the storage capacity of this aquifer using an enhanced version of the conventional storage assessment method for closed-system aquifers. The conventional approach to calculate the storage capacity for such aquifers is well-documented in References 1-3 and Reference 6. An earlier assessment of the storage capacity of the Rotliegend aquifer in the Dutch offshore is documented in Neele et al, 2012 (Reference 4).

Traditionally, regional estimates of CO_2 storage capacity within an aquifer involves aggregating the CO_2 storage capacity of individual storage complexes. This is a time-consuming process. Instead, we developed a method to directly assess the theoretical CO_2 storage capacity using regional maps. This approach provides an estimate of the CO_2 storage capacity of the Rotliegend aquifer, along with the uncertainty range. Moreover, this method also identifies key “sweet spots” where storage potential is highest. Our findings can inform policy decision makers regarding CO_2 storage in the Dutch offshore and guide future exploration efforts, focusing on areas with high potential.

The CO_2 storage capacity in this study is categorized as the theoretical storage capacity. The theoretical storage capacity is the maximum amount of CO_2 that can be stored in the aquifer under ideal practical and technical conditions, considering geological variation (Reference 3 and Reference 5).

The study area, depicted by the grey-shaded region in Figure 1, aligns with the spatial distribution of Rotliegend sandstones from the Slochteren Formation in the Dutch offshore region. These Rotliegend sandstones extend eastward to the Dutch onshore area and westward to the UK offshore region. Within the study area, the red polygon delineates the “core area” of the Rotliegend aquifer (see Figure 1). The storage capacity calculations provided in this report are specifically applicable to this area. The core area is bounded as follows:

- To the north, the core area is limited by a theoretical CO_2 storage capacity of 10 kg/m^2.

This limit approximately corresponds to a net sandstone thickness of 20 meters. Aquifer complexes falling below the 10 kg/m^2 threshold, especially when coupled with a significant likelihood of encountering reservoir compartmentalization in this region, are considered unviable for commercial exploitation.

- To the south, the core area is constrained by the absence of a continuous Zechstein

caprock, rendering the Rotliegend aquifer unsuitable for CO_2 storage. In this part of the Dutch offshore, a continuous caprock is primarily formed by the halites of the ZEZ2H Member and extends southward through the claystones of the ZEZ1G, ZEZ1M, and ZEZ1K-Coppershale Members (see NL stratigraphic nomenclature[1]).

- The eastern boundary corresponds to the Dutch maritime 3-mile zone.
- The western boundary aligns with the UK/NL economic zone boundary.

Additionally, Figure 1 displays the locations of Rotliegend gas fields and the positions where wells have penetrated the Rotliegend or older sediment layers. Notably, small white squares also depict well data calibration points in the current document’s maps (e.g., Map 6, Slochteren Formation porosity).

---

[1] Www.dinoloket.nl/stratigrafische-nomenclator

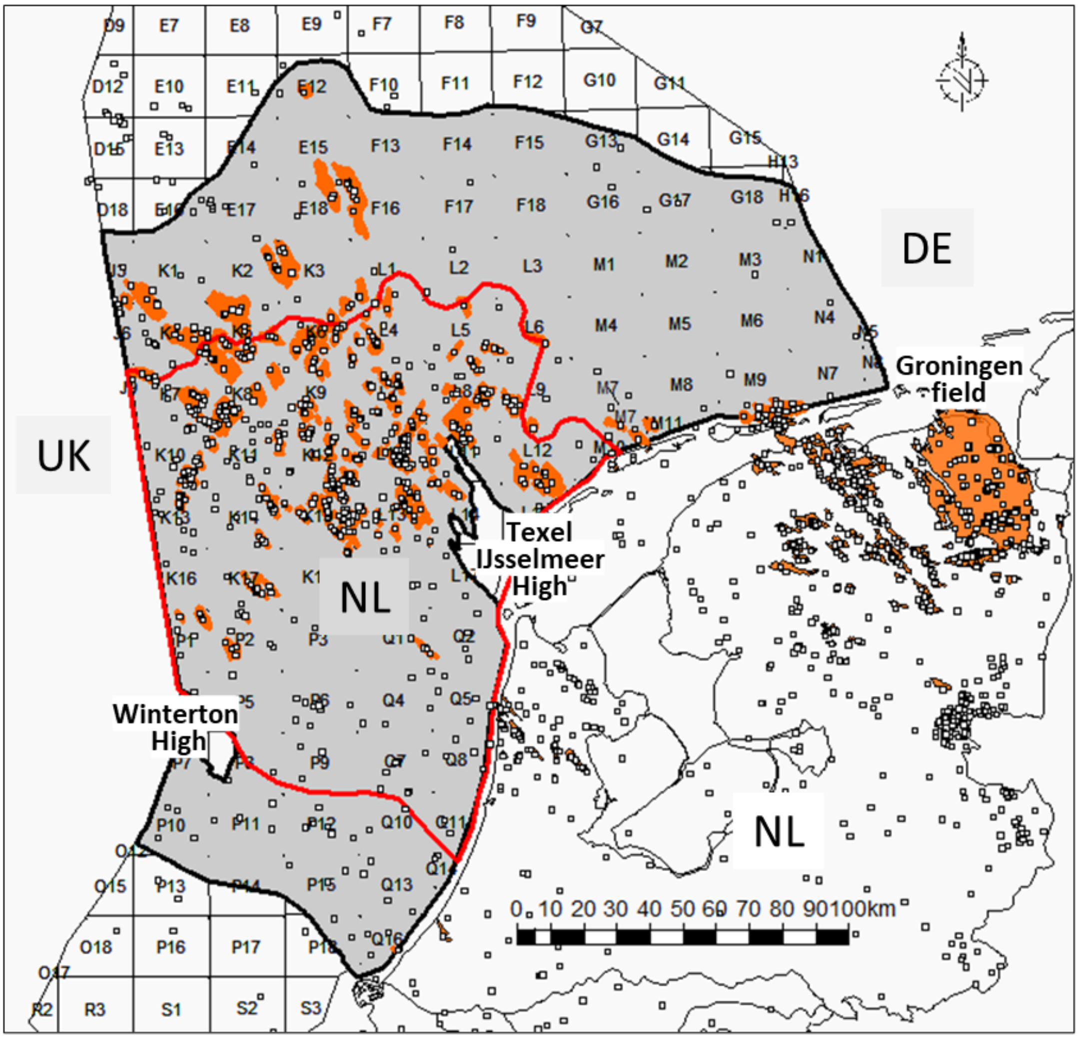

Figure 1: Location map. The study area includes notable geographical landmarks of the Netherlands, along with offshore block numbers. The figure highlights significant geological features, including the extent of the Slochteren sandstone reservoir and the study area (grey area). It also outlines the main region where CO_2 sequestration is expected to be viable within the Rotliegend aquifer (red polygon). The Rotliegend gas fields are marked in both the Dutch onshore and offshore sectors (orange filled polygons). Additionally, the locations of wells that have reached the Rotliegend geological layer are indicated by white squares.

2 Geology

The Rotliegend aquifer is a rock formation located in the Dutch on- and offshore. It is part of the Upper Permian Rotliegend Group. The Rotliegend Group is divided into two formations: the Slochteren Formation and the Silverpit Formation (Figure 1). The Slochteren Formation, located in the southern and central part of the Dutch offshore, consists of sandstone and minor conglomerate and is considered the Rotliegend aquifer here.

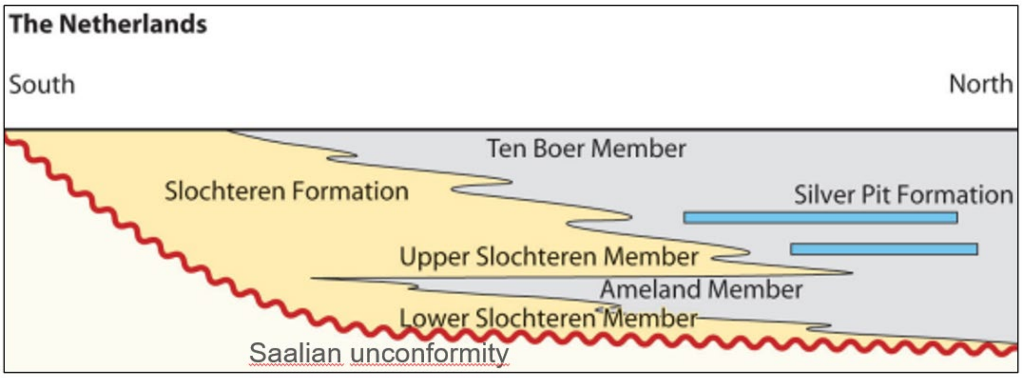

Figure 2: Rotliegend Group stratigraphy (see NL stratigraphic nomenclature[2]). The illustration highlights the sandstone reservoir in yellow, contrasting with the shale lithology depicted in grey. Notably, evaporite intercalations, primarily halite, are represented in blue. The sandstone layers demonstrate onlap against the Saalian (Base Permian) unconformity, which is delineated by a distinctive red wavy line.

The Slochteren sandstones are of fluviatile (wadi), aeolian and sabkha facies. The Silverpit Formation, located in the northern half of the Dutch offshore, consists of shale, siltstone, and evaporites. The Rotliegend sediments were derived from the Variscan mountain chain and the London-Brabant Massif, situated southeast and southwest of the depositional basin, respectively. Deposition took place under arid to semi-arid conditions.

The aquifer’s top seal (caprock) is provided by the shales from the Rotliegend Silverpit Formation and by the evaporites from the Upper Permian Zechstein Group (Figure 3). The evaporites from the Silverpit Formation were deposited in a desert lake in the central part of the basin. Thick accumulation of Zechstein evaporites subsequently developed by marine influxes in the Central European Basin under arid conditions. The aquifer’s bottom seal, below the Saalian unconformity (see Figure 2) is provided by the fluvial and lacustrine shales from the Upper Carboniferous Group.

---

[2] Www.dinoloket.nl/stratigrafische-nomenclator

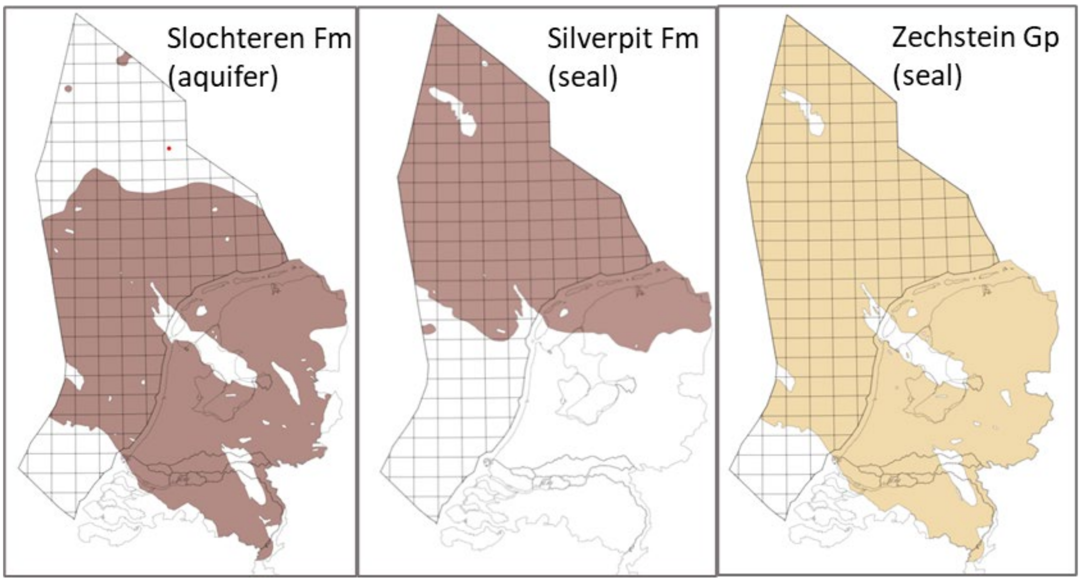

Figure 3: Rotliegend aquifer and caprocks distribution (source NL stratigraphic nomenclature [3]) – In the study area's northern sector, the Slochteren reservoir is sealed by shales from the Silverpit Formation. Conversely, in the southern sector, the reservoir is capped by evaporites, particularly halites from the Zechstein Group. It is important to note that in the northern sector, the Zechstein seal is stratigraphically positioned above the Silverpit seal, thereby providing an additional buffer to prevent any CO_2 leakage from the underlying Rotliegend aquifer.

The study area is subdivided in 3 areas, each with a different composition of geological members.
In the southern part of the study area, the Slochteren Formation is undifferentiated. Therefore, the thickness (Map 3), is defined as the difference between the top and the base of the Slochteren Formation.
In the central part of the study area, the Slochteren Formation is differentiated into an Upper and Lower Slochteren Member separated by the Ameland Member. The thickness of the Rotliegend aquifer is defined as the sum of the thickness of each member.
In the northern part of the study area, the Upper Slochteren Member was not deposited. Therefore, the thickness refers to the Lower Slochteren Member only.

---

[3] www.dinoloket.nl/stratigrafische-nomenclator

3 Method

The new CO_2 storage capacity calculation method currently under discussion is applicable to the Rotliegend aquifer system in the Dutch offshore. This aquifer system is confined between two layers of low-permeability rock that restrict the flow of fluids into and out of the aquifer. The system is considered hydraulically closed, which means that it is not connected to any surface water or groundwater systems outside the system.

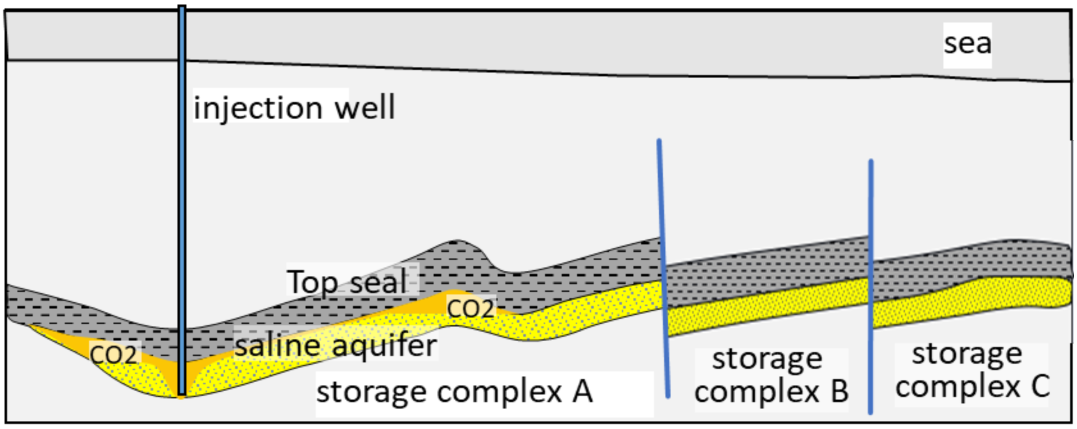

Figure 4: Hydraulic closed aquifer systems (storage complexes). After injection, the system ensures secure containment of both CO_2 and the incumbent water. This is achieved through sealing lithologies that envelop the aquifer reservoir—above, laterally, and below—often reinforced by the presence of sealing faults.

When CO_2 is injected into such an aquifer system, the formation water and the formation rock will experience an increase in reservoir pore fluid pressure. They will be compressed and create storage space. The storage capacity is limited by the maximum pressure at the top of the aquifer before the caprock is fractured, and leakage of CO_2 occurs.
The calculated storage capacity is categorized as the theoretical storage capacity. It is determined by the rock and fluid properties of the aquifer, such as its size and porosity, the compressibility of the formation water and rock, the maximum allowed pressure increase of the aquifer, and the density of the CO_2.

The theoretical storage capacity calculation is defined by the following equation (References 3 and 5):

$$Theoretical\ Storage\ Capacity\ = V_p \times \Delta P \times C_t \times \rho_{CO_2}$$

V_p = Pore Volume
ΔP = Maximum allowed pressure increase
C_t = Total Compressibility of water (C_w) and rock (C_r)
ρ_{CO_2} = CO_2 plume density

The applied workflows for the map-based application of this equation are documented in Appendix B of this report.

In our current study, it is important to recognize that the pressure values, which are critical for the assessment of the ΔP, are specifically linked to the top reservoir depth map (Map 1). Conversely, temperature values, essential for the assessment of the ρ_{CO_2} are specifically associated with the mid reservoir depth map (Map 2). Additionally, the latter map has also been utilized to create the porosity guiding grid (Map 5), which plays an important role in assessing both the V_p (see section 3.1) and C_t (see section 0).

This study made use of the Petrel (version 2022.4.0) software package and all mention of functionality are available there.

3.1 Pore thickness

The applied workflow for the map-based pore volume (V_p) calculation is documented in Appendix B2.

The pore thickness or pore volume (V_p) of the Rotliegend aquifer has been calculated using the thickness (t), net-to-gross ratio (N/G), and porosity (φ) of the Slochteren Formation:

$$V_p \ = \ t \times \varphi \times \frac{N}{G}$$

3.1.1 Thickness

The top and base depths, as well as the thickness of the Slochteren Formation and its members, are available from the NLOG[4] well stratigraphy dataset. To create the thickness map, three individual maps were combined to form the final Slochteren Formation thickness map. In the southern part of the study area, where the Slochteren Formation is undifferentiated, convergent interpolation gridding between the wells was used to create the southern map. In the central part of the study area, where the Slochteren Formation is differentiated into the Upper and Lower Slochteren Member, the thicknesses of these members were first combined into a total thickness. Subsequent convergent interpolation gridding between the wells was then used to create the central map. In the northern part of the study area, where only the Lower Slochteren Formation is present, convergent interpolation gridding between the wells was used to create the northern map. These three maps were combined into a single map and smoothed (filter width: 5, iteration: 1) to display smooth transitions. The result is shown in (Map 3).

3.1.2 Depth

The depth maps for both the top and mid part of the Slochteren Formation are derived from the Base Zechstein depth map, which is based on the interpretation of seismic data. The Base Zechstein depth map, created as part of the Dutch Geological Survey's project 'DGM-diep V5 on- en offshore,' is available for download on the NLOG[5] website. Convergent interpolation gridding of the well thicknesses from the stratigraphy dataset for the Silverpit Formation and the Ten Boer Member was used to create a thickness map. This thickness

---

[4] https://www.nlog.nl/sites/default/files/thematische_data/nlog_stratstelsel.xlsx
[5] https://www.nlog.nl/dgm-diep-v5-en-offshore

map was combined with the Base Zechstein map to create the Top Slochteren depth map (Map 1). The Top Slochteren depth map was then combined with half of the Slochteren thickness map (Map 3) to create the mid-depth map of the Slochteren Formation (Map 2).

3.1.3 Porosity

The porosity map (Map 6) integrates well log evaluation results from the NLOG[6] 'Reservoireigenschappen (version 2017)' dataset with a porosity-depth trend derived from core sample measurements in the NLOG[7] 'nlog_poroperm' dataset. To project the well data onto a map, we applied a convergent gridding algorithm. This method interpolates the point data from wells while considering a specified guiding grid.

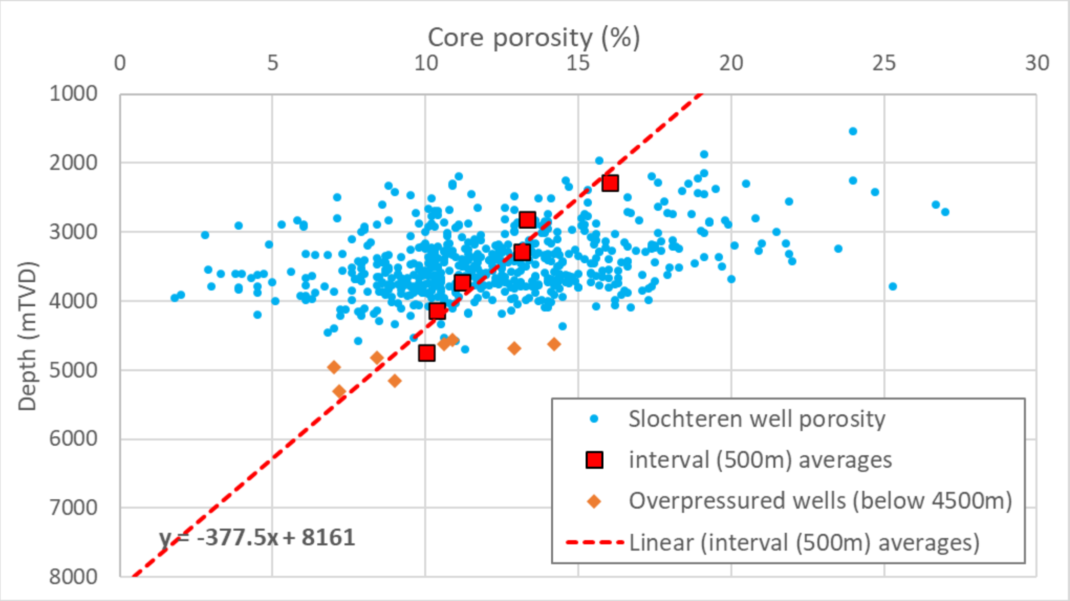

Figure 5: Porosity Core measurement Slochteren Formation. The porosity-versus-depth plot of individual measurements (blue circles and orange diamonds) exhibits a wide dispersion and only a subtle trend. To get a trend over depth, the average porosity has been determined at a 500 m interval (red squares). The Excel least square method was used to fit a linear trendline through the data. This trend is $Depth = -377.5\, x\, \phi\ + 8161$ emerges when plotting averages over 500 m intervals over depth.

The guiding grid (Map 5) was created by applying the following porosity-depth trend equation shown in Figure 5 to the Mid Slochteren Formation Depth map (Map 2):

$$\varphi = \frac{8161 - d}{377.5}$$

Where d is depth.

We applied the default settings for convergent gridding algorithm from Petrel. By utilizing the porosity guiding grid as a trend surface, we ensured that the resulting grid (Map 6) takes the geological structure of the reservoir into account.
Following the methodology outlined in Section 3.1.1, three individual maps were initially created and subsequently merged to produce the final porosity map.

---

[6] https://www.nlog.nl/reservoireigenschappen
[7] https://www.nlog.nl/sites/default/files/thematische_data/nlog_poroperm.xlsx

3.1.4 Net-to-gross

The net-to-gross (Map 4) captures well log evaluation results from the NLOG[8] 'Reservoireigenschappen (version 2017)' dataset. To project the well data onto a map, we utilized a convergent interpolation gridding algorithm, followed by a smoothing process (filter width 10 and 1 iteration) and clipping the map values between 0 and 1.
Following the methodology outlined in Section 3.1.1, three individual net-to-gross maps were initially created and subsequently merged to produce the final net-to-gross map.

3.2 Maximum allowed pressure increase

The applied workflow for the map-based delta P (ΔP), maximum allowed pressure calculation is documented in Appendix B3.

Delta P (ΔP) represents the maximum allowed pressure increase of the aquifer before the caprock is fractured and leakage of CO_2 occurs. ΔP is calculated by subtracting the maximum allowed aquifer pressure from the initial aquifer pressure.
Pressures contained in the Pressure Southern North Sea (PSNS) dataset[9] were used to map the initial pressure regime (hydrostatic normal and overpressures) of the Rotliegend aquifer in the study area.

3.2.1 Hydrostatic pressure

As a first step in mapping the pressure regime of the Rotliegend aquifer a "hydrostatic baseline" was established by plotting formation pressure values from dry wells against the corresponding depth (Figure 6). This excludes pressures from wells that discovered hydrocarbon fields, as these pressures are generally well above the hydrostatic baseline pressures.

The hydrostatic pressure is generally a function of the average density of formation water above the aquifer. The density in turn is a function of salinity and pressure. Because salinity is not well known in the study area, the hydrostatic pressure is inferred from pressure data and a function defined solely dependent on depth.

Along the hydrostatic baseline, we observed a dense cloud of data points. This cloud represents the normal hydrostatic pressure regime within our study area. The hydrostatic baseline was established to the left of this data cloud. Formation pressures to the right of the cloud indicate an over-pressured aquifer. Conversely, formation pressures to the left of the cloud signify a pressure-depleted aquifer.
The hydrostatic baseline is a slightly curved line and a 2nd order polynomial function over depth. The baseline has been determined by manually interpreting the lower bound of the lower data-cloud of the pressure-depth plot (Figure 6):

---

[8] https://www.nlog.nl/reservoireigenschappen
[9] https://www.nlog.nl/en/pressure-southern-north-sea-psns-database

$$Hydrostatic\ baseline\ =\ 4{,}9\ x\ 10^{-6}\ x\ d^2 + 0.088\ x\ d + 1.81$$

Where d is depth.

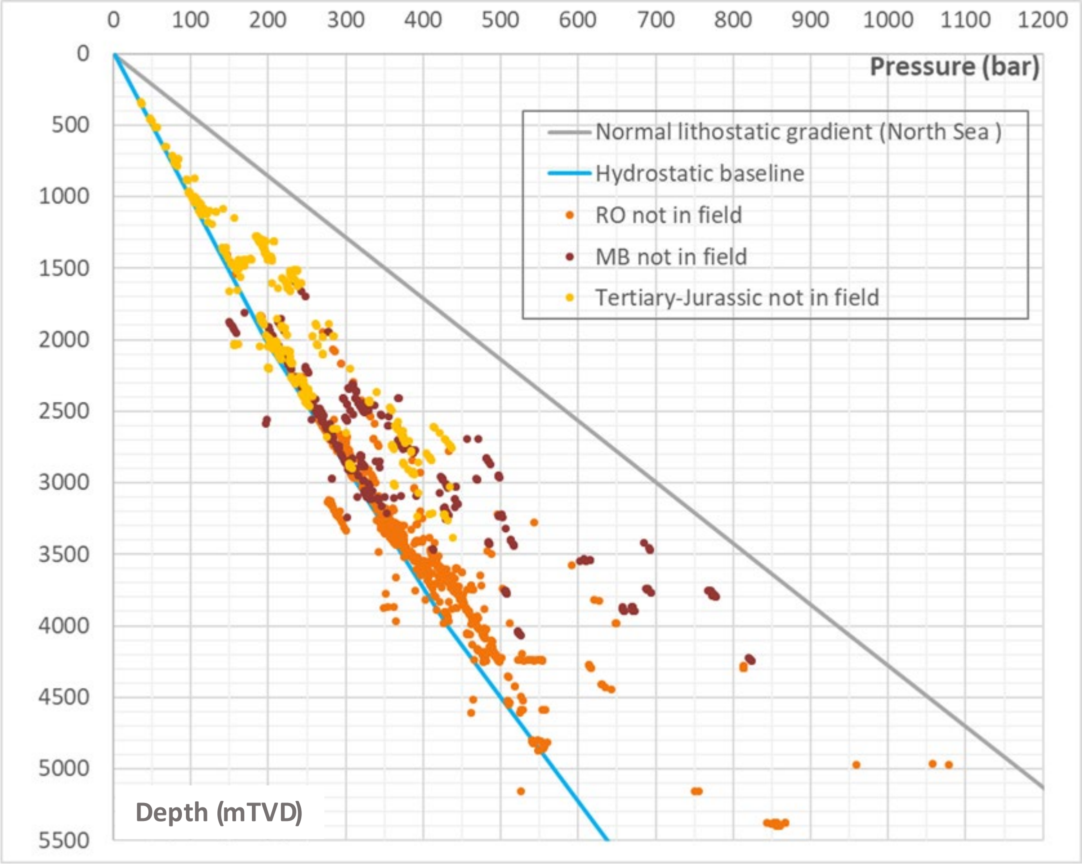

Figure 6: Aquifer formation pressures, Dutch offshore (excluding wells in field). Pressure-versus-depth plot of Repeat Formation Tests (RFT) conducted on Rotliegend (RO), Main Buntsandstein (MB) and younger reservoir formations. Pressure points within an aquifer are generally found in the lower half of the region demarcated by the hydrostatic and lithostatic gradient lines.

The hydrostatic baseline grid (Map 8) is created by applying the hydrostatic baseline equation to the Top Slochteren reservoir map (Map 1).

3.2.2 Overpressure

Formation pressures and overpressures (Verweij et al 2012) were evaluated using data from approximately 200 offshore wells[6] that intersected the Rotliegend interval (Figure 7). Overpressure values were determined as the difference between the measured gas-water contact (or water gradient) pressure and the corresponding hydrostatic baseline pressure. The overpressures were subsequently mapped (Map 9) by using convergent interpolating.

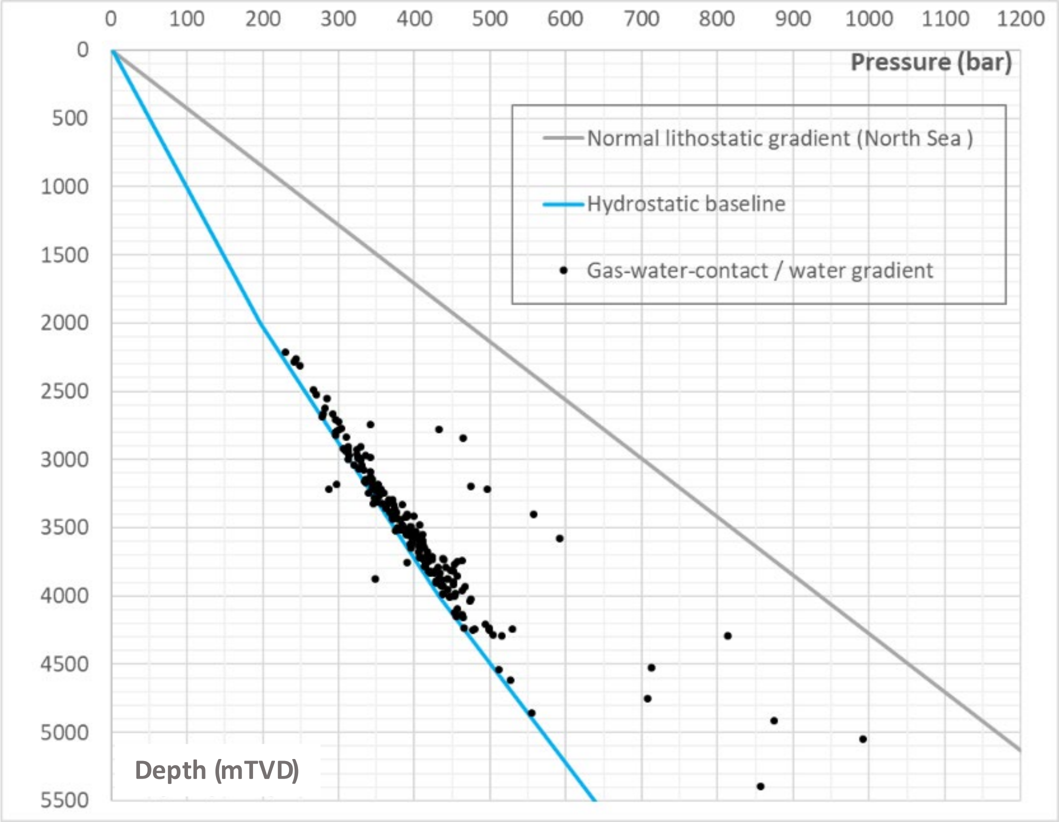

Figure 7: Gas-water-contact and water gradient pressures. The pressure-depth plot for the gas-water contacts and water leg pressures within the Rotliegend aquifer (Dutch offshore) provides valuable insights into the state of the aquifer complexes. A dense cluster of data points adhering closely to the hydrostatic baseline suggests normally pressured aquifers. In contrast, data points significantly above the baseline denote over-pressured aquifers, and those below indicate depleted aquifers. The latter condition typically results from gas extraction in adjacent fields, leading to a reduction in pressure within these aquifer complexes.

The data points situated below the hydrostatic baseline in Figure 7 correspond to wells K10-16, K11-FA-103, L10-13, and L11-02. In the vicinity of these wells, aquifer depletion, caused by gas production from nearby Rotliegend fields, is most pronounced. Specifically, we observe this effect around K11-FA, L10-CDA, and the L11b-A/L08-D complex. Within the slightly over-pressured K&L blocks, these and other depleted aquifer areas are visually represented by blue colors as depicted in Map 9. Notably, the overpressures in these regions remain below 25 bar. Conversely, the blue colors observed in the P&Q blocks indicate normal pressure areas.

3.2.3 Initial pressure

Finally, the hydrostatic baseline grid from Map 8 was added to the Rotliegend aquifer overpressures map (Map 9). This summation yields the Initial pressures Rotliegend aquifer map depicted in Map 10.

3.2.4 Maximum allowed aquifer pressure

The storage capacity of an aquifer is typically constrained by the maximum pressures at its top, just before the caprock fractures and CO_2 leakage occurs. Other potential constraints on storage capacity, such as CO_2 leakage along faults or wells, are not addressed in this paper. To determine the maximum allowed pressure increase of the Rotliegend aquifer, leak-off pressure and formation integrity test data from the PSNS dataset were analyzed. These pressure data were obtained from tests conducted in wells drilled within the Dutch subsurface.

A drilling Leak-Off Test (LOT)[10] is a procedure in the oil and gas industry to determine the strength or fracture pressure of a formation. It is typically conducted immediately after drilling below a new casing shoe and in the caprock, just above the reservoir. During the test, the well is shut in and fluid is pumped into the wellbore to gradually increase the pressure that the formation experiences. At a certain pressure, fluid will enter the formation, or leak off, either moving through permeable paths in the rock or by creating a space by fracturing the rock. The results of the leak-off test dictate the maximum pressure or mud weight that may be applied to the well during drilling operations.

A drilling Formation-Integrity Test (FIT) resembles the drilling Leak-Off Test. However, the primary objective of a FIT test is not to pressurize the wellbore until the formation fractures, but rather to assess the formation's strength against a predetermined limit of the mud weight used in drilling operations.

An analysis of approximately 370 LOT data points from the Dutch subsurface, on- and offshore, (as depicted in Figure 8) reveals a distinct data cloud positioned between the hydrostatic baseline and the normal lithostatic gradient of the North Sea[11]. To deepen our understanding, we have integrated an additional 420 FIT data points into the LOT dataset (as depicted in Figure 9). Notably, the distribution of LOT/FIT data closely aligns with the overall LOT data distribution. Consequently, we can confidently utilize the FIT data alongside the LOT data to substantiate the statistically derived trend lines for the "Lower Bound" and "Mid Gradient". Both terms are further specified below. This combined dataset now comprises a total of 790 datapoints.

---

[10] https://www.drillingmanual.com/leak-off-test-procedures/

[11] Normal lithostatic gradient = 2.34 x Depth / 10

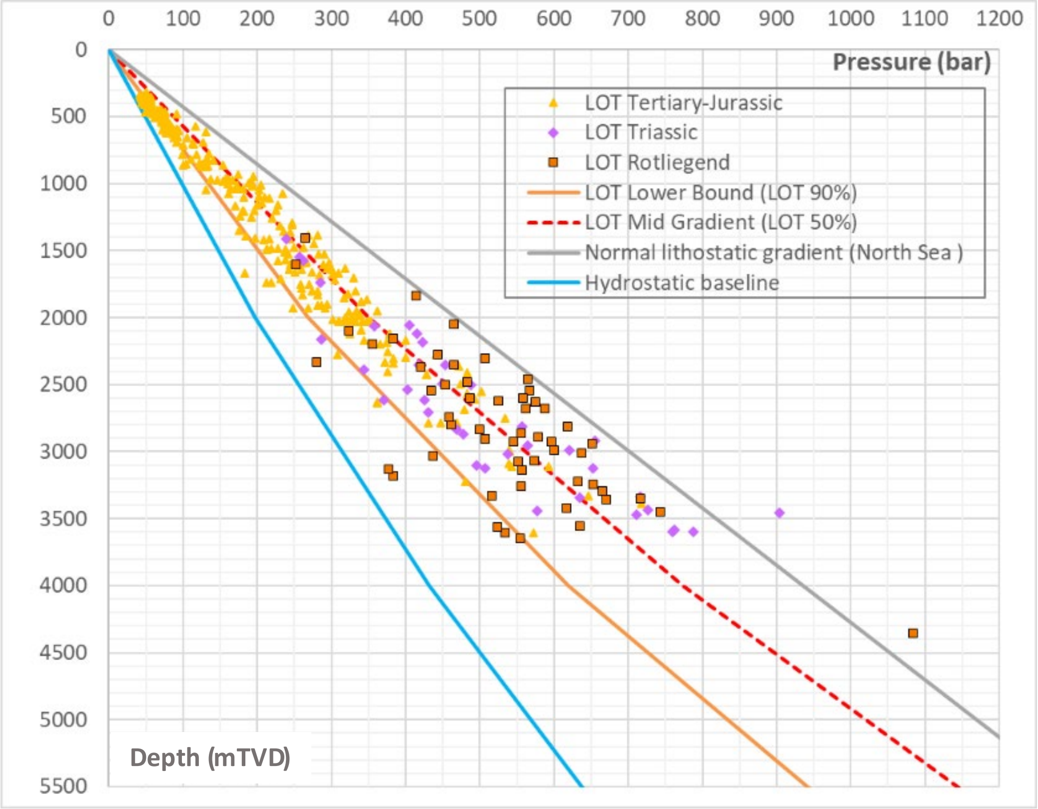

Figure 8: Leak-off-test (LOT) pressures in the Dutch on- and offshore, excluding Formation-integrity-test (FIT) pressures. This figure presents a pressure-versus-depth plot of LOT tests conducted while drilling Rotliegend, Triassic and younger cap rock formations. The LOT measures the pressure at which the cap rock integrity is compromised (fractures). Pressure points within an aquifer are generally found in the upper half of the region demarcated by the hydrostatic and lithostatic gradient lines.

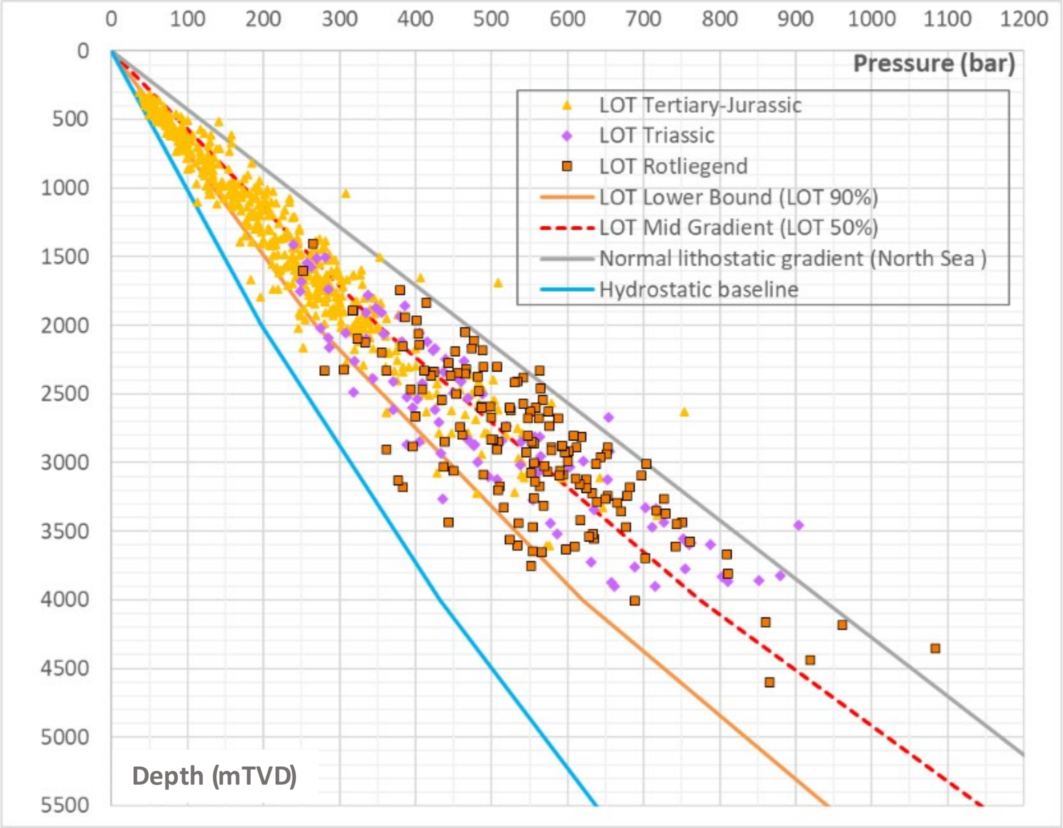

Figure 9: LOT and Formation-integrity-test (FIT) pressures. This figure presents a pressure-versus-depth plot of LOT and FIT tests conducted while drilling Rotliegend (and Zechstein), Triassic and younger cap rock formations. Pressure points within an aquifer are generally found in the upper half of the region demarcated by the hydrostatic and lithostatic gradient lines.

The wide pressure distribution within this data cloud indicates significant variability in the strength of the caprock formation across the study area. However, mapping the caprock strength would necessitate meticulous quality control of the LOT/FIT dataset and detailed knowledge of the tested lithologies and tectonic stress fields. Due to time and resource constraints, we however omitted these investigations from our study. Instead, we determined a maximum pressure range for CO_2 storage based on the available LOT/FIT and mud pressures datasets, anchoring our capacity calculations between the lower boundary trendline of the LOT/FIT dataset (Figure 9, LOT Lower Bound, orange line) and the fracture gradient trendline of the mud pressures dataset (Figure 10, Fracture Gradient, red line).

The lower boundary pressure line corresponds to a curved line that closely approximates the lower LOT pressure values (see Figure 9). In the oil and gas industry, this boundary is commonly known as the “LOT Lower Bound”. It is arbitrarily defined such that 90% of the pressure data points lie above this boundary, while the remaining 10% fall below it. The curvature of this boundary closely follows the regressive trend line of the LOT Mid Gradient pressures (see section 3.2.4). Its mathematical representation is given by the following equation:

$$LOT\ Lower\ Bound\ pressure\ = 1.0 \times 10^{-5} \times d^2 + 0.115 \times d + 5$$

Where d is depth.

The LOT Lower Bound pressure map (Map 11) is created by applying the Top Slochteren depth map (Map 1) to the above equation.

The LOT Mid Gradient pressure line (see Figure 9, red dashed line) represents a regressive trend line derived from the LOT/FIT dataset. This trend line serves as a dividing boundary, where 50% of the pressure data points reside above the line, while the remaining 50% fall below it. The LOT Mid Gradient mathematical representation is given by the following equation:

$$LOT\ Mid\ Gradient\ pressure\ =\ 8.9 \times 10^{-6} \times d^2 + 0.158 \times d - 1$$

Where d is depth.

Significantly, in our present study, the LOT Mid Gradient line does not serve as a pressure boundary limit. Nevertheless, its proximity to the Fracture Gradient boundary (see Figure 10) is worth noting.

The upper boundary of the maximum pressure range in the current paper is defined by the regional “Fracture Gradient”. The Fracture Gradient is the upper bound of the mud weight used during drilling operations. In this study, the Fracture Gradient is a manually derived, slightly curved line that closely follows the upper pressure values of the mud weights used for drilling in the Dutch subsurface (Figure 10). Its mathematical representation has been defined by the following equation:

$$Fracture\ profile\ pressure\ =\ 9.2 \times 10^{-6} \times d^2 + 0.161 \times d - 1$$

Where d is depth.

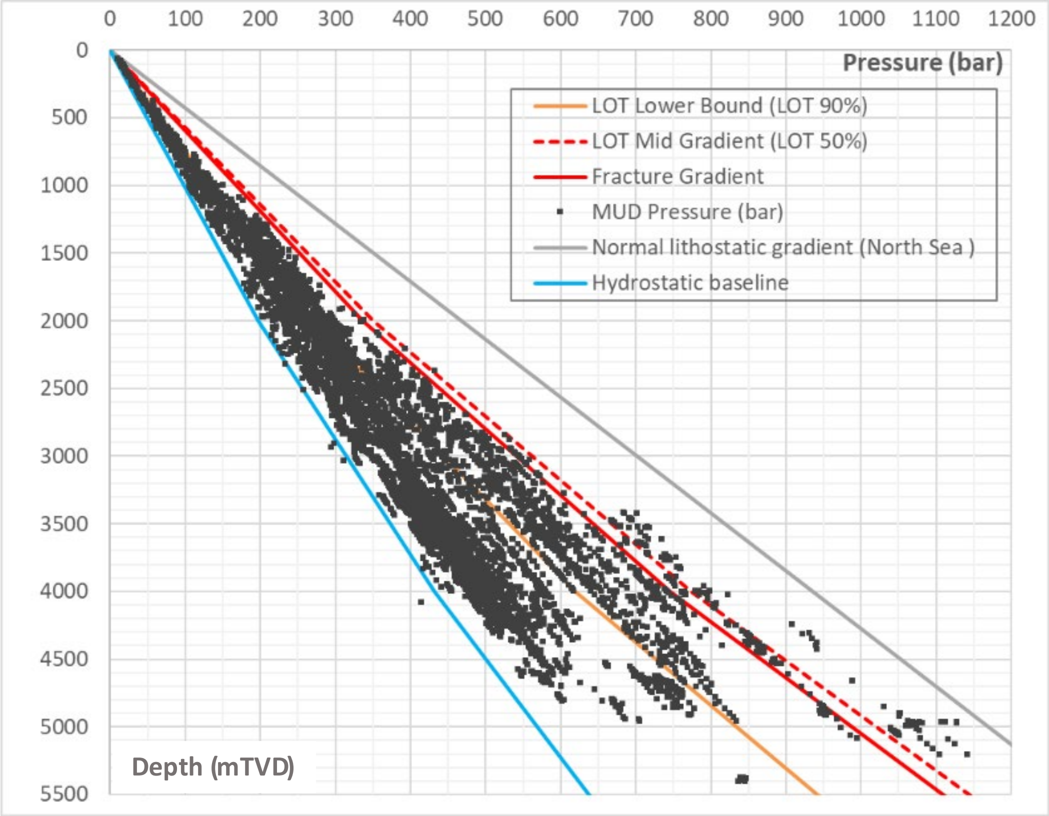

Figure 10: Mud pressures in the Dutch on- and offshore. This figure presents a pressure-versus-depth plot of mud pressures measured while drilling Rotliegend and younger formations. The mud weight pressure serves as an indicator of the cap rock's integrity, reflecting its ability to withstand subsurface pressures. The maximum limit of the mud weight pressure establishes the Fracture Gradient. This gradient represents the critical threshold beyond which the formation is likely to fracture, thereby guiding the safe operational limits for drilling activities.

The Fracture Gradient pressures map (Map 12) is created by applying the Top Slochteren depth map (Map 1) to the above equation.

In our current study concerning CO_2 storage capacity calculations for the Rotliegend aquifer, the maximum allowable aquifer pressure increase is defined as the midpoint pressure between the Lower Bound pressures and the Fracture Gradient pressures. This critical pressure level is visually represented in Figure 11 by the “mid LB-FG gradient” line and is defined by the following equation:

$$Mid\ LB - FG\ gradient\ = 9.6 \times 10^{-6} \times d^2 + 0.133 \times d - 1$$

Where d is depth.

The Mid LB-FG gradient pressures map (Map 13) is created by averaging the LOT Lower Bound pressures map (Map 11) with the Fracture Gradient pressures map (Map 12). The map can also be created by the earlier mentioned Mid LB-FG gradient equation.

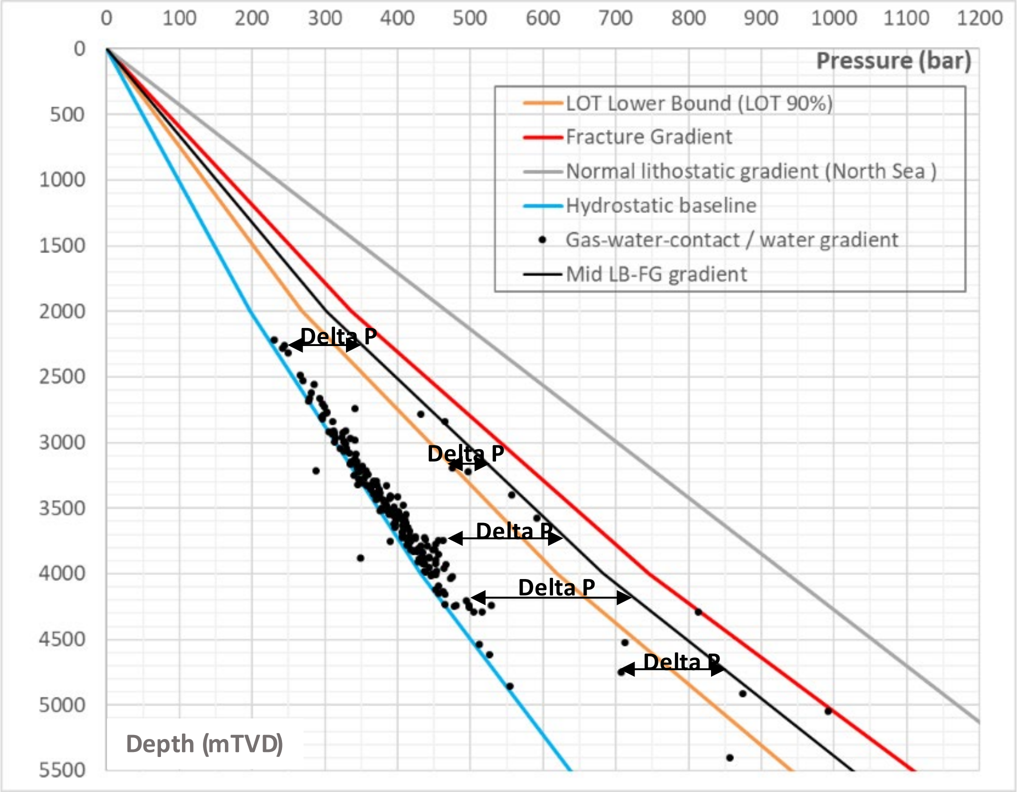

Figure 11: Pressure limits. This figure delineates the regional pressure thresholds—lower (LOT Lower Bound), intermediate (Mid LB-FG gradient), and maximum (Fracture Gradient)—for the cap rock of the Rotliegend and subsequent aquifer complexes. In this study, the established pressure thresholds serve as a basis for evaluating the CO_2 storage capabilities of the Rotliegend. The term "Delta P" represents the allowed increase in pressure within an aquifer complex, from its initial pressure to the Mid LB-FG Gradient pressure at a specific location.

3.2.5 Delta P ($\Delta \boldsymbol{P}$)

Delta P (ΔP) represents the pressure difference within the aquifer before and after CO_2 injection. It is calculated by subtracting the initial aquifer pressures (Figure 11, indicated by the black dots and Map 10) from the maximum allowable aquifer pressures (Figure 11, indicated by the mid LB-FG gradient line and Map 13).

The ΔP pressures map (Map 15) is created by subtracting the Mid LB-FG gradient pressures map (Map 13) from the initial pressures Rotliegend aquifer map (Map 10). Although creating the ΔP pressures map (Map 15) is not part of the currently recommended workflow, it has been included in this report to compare the results of the conventional approach with the novel approach presented in this paper.

3.3 Compressibility

When CO_2 is injected into a closed aquifer system, storage capacity is established through the compression of both the saline water and the surrounding formation rock. Total compressibility C_t is calculated by adding the water (brine) compressibility (C_w) to the pore compressibility (C_p), all with unit 1/bar (bar^{-1}). The applied workflow for the map-based total compressibility (C_t) calculation is documented in Appendix B4. The two compressibility types are provided below.

3.3.1 Water Compressibility

The compressibility of water (or brine) within a saline aquifer is influenced by several factors (Reference 5), including aquifer salinity (Map 16), temperature (Map 19), and the maximum allowable pressure (Map 14).

The Pressure Southern North Sea (PSNS) dataset[12] provided salinity data from formation water samples in wells, which were used to map the salinity of the brine within the Rotliegend aquifer across the study area (Map 16).

The PSNS dataset also provided temperature data used to calculate temperature gradients at well locations. These gradients were then mapped across the study area (Map 17). To estimate the 'mid-reservoir' temperature within the Rotliegend aquifer (Map 18), we multiply the temperature gradient (Map 17) with the depth map corresponding to the mid-Slochteren Formation datum (Map 2). Subsequently, a second version of this map in Fahrenheit (Map 19) was created by multiplying the Celsius map by a factor of 9/5 and adding 32.

The water compressibility map (as shown in Map 20) is defined by the following equation (Reference 5):

$$C_w = \frac{1}{\left\{10^6\left[0.314+\left(\frac{0.58S}{10^6}\right)+\left(\frac{1.9T}{10^4}\right)-\left(\frac{1.45T^2}{10^6}\right)\right]+\left[(8+\left(\frac{50S}{10^6}\right)-\left(\frac{0.125ST}{10^6}\right)\right]p\right\}0.069}$$

S = the salinity of the brine (in ppm, Map 16)
T = the temperature of the brine (in °F, Map 19)
p = the maximum allowed aquifer pressure (in psi, Map 14)

The Petrel version of this equation is shown in Appendix A.

Creating the 'uncorrected' C_w compressibility map (Map 20) is optional and serves as an alternative to the ideal workflow presented here. This workflow generates the 'corrected' C_w compressibility map (Map 29, see section 3.5.2).

---

[12] https://www.nlog.nl/en/pressure-southern-north-sea-psns-database

3.3.2 Pore Compressibility

The pore compressibility of the formation rock (Reference 5) is influenced by its solid rock compressibility (assumed constant as $2.71\text{x}10^{-6}$ 1/bar), by its frame compressibility (Map 21) and by the porosity of the formation (Map 6). The frame compressibility, in turn, depends on the porosity of the formation (Map 6) only (Reference 5). The pore compressibility map (Map 22) is defined by the following equation (Reference 5):

$$C_p = \frac{C_{fr} - C_s(1+\varphi)}{\varphi}$$

C_{fr} = the frame compressibility (in 1/bar, Map 21), see equation below.
C_s = the solid rock compressibility (in 1/bar)
φ = porosity (dimensionless, Map 6)

The frame compressibility map (Map 21) is calculated using the following equation (Reference 7):

$$C_{fr} = 4.943 \times 10^{-3}\varphi^3 - 1.419 \times 10^{-3}\varphi^2 + 1.52 \times 10^{-4}\varphi + 6.198 \times 10^{-7}$$

3.3.3 Total Compressibility

The total compressibility map of the Rotliegend aquifer (Map 23) is created by adding the water compressibility map (Map 20) to the pore compressibility map (Map 22) and is defined by the following equation:

$$C_t = C_w + C_p$$

C_w = Water compressibility (in 1/bar, Map 20)
C_p = Pore compressibility (in 1/bar, Map 22)

Creating the 'uncorrected' C_t compressibility map (Map 20) is optional and serves as an alternative to the ideal workflow presented here. This workflow generates the 'corrected' C_t compressibility map (Map 30, see section 3.5.2).

3.4 CO_2 plume density

The applied workflow for the map-based CO_2 plume density (ρ_{CO_2}) calculation is documented in Appendix B5.

The density of a pure CO_2 plume (denoted as ρ_{CO_2}) within an aquifer depends on both the plume's temperature and pressure (Reference 6). In our current study, we assume for simplicity that the plume consists solely of carbon dioxide and that the plume's midpoint, defining the plume's temperature and maximum allowed pressure limit, coincides with the aquifer midpoint. The CO_2 plume density map of the Rotliegend aquifer (Map 24) is thus defined by the following equation:

CO_2 plume density map (ρ_{CO_2}) =

$$\rho_{CO_2} = 260.416638 + (-7.59534T) + (5.587335p) + (0.038888T^2) + (-0.007272p^2) + (-0.000048T^3) + (0.000001p^3) + (-0.013924\mathrm{Tp}) + (-0.000017T^2\mathrm{p}) + (0.000026\mathrm{T}p^2)$$

T = Aquifer temperature (in deg C, Map 18)
p = Maximum allowed aquifer pressure (in bar, Map 13)

The Petrel version of this equation is shown in Appendix A. For the Microsoft Excel version of this equation see Reference 5.

Creating the ‘uncorrected’ CO_2 plume density map (Map 24) is optional and serves as an alternative to the ideal workflow presented here. This workflow generates the ‘corrected’ CO_2 plume density map (Map 31, see section 3.5.3).

Creating the ‘uncorrected’ C_t compressibility map (Map 20) is optional and serves as an alternative to the ideal workflow presented here. This workflow generates the ‘corrected’ C_t compressibility map (Map 30, see section 3.5.2).

3.5 Map correction

To rigorously assess the CO_2 storage capacity of an aquifer using a map-based approach, a novel in-house method developed by TNO-AGE incorporates essential map corrections. The need for these corrections became evident when the deterministically assessed storage capacities of aquifer storage complexes did not match the map-based assessments of the same complexes. Failing to account for these corrections may result in inaccuracies, potentially leading to a significant overestimation of the CO_2 storage capacity of the Rotliegend aquifer in the Dutch offshore.

Figure 12 provides a visual representation to illustrate the rationale behind the correction of the maximum allowed pressures. The figure illustrates the pressure distribution within a typical aquifer storage complex, also referred to as an aquifer unit. The blue line depicts the initial pressures within the aquifer storage complex before CO_2 injection. Conversely, the green line corresponds to the pressures at the end of CO_2 injection into the aquifer. At this stage, critical pressures are reached at the top of the aquifer (Figure 12, point B) just prior to caprock fracturing and potential CO_2 leakage.

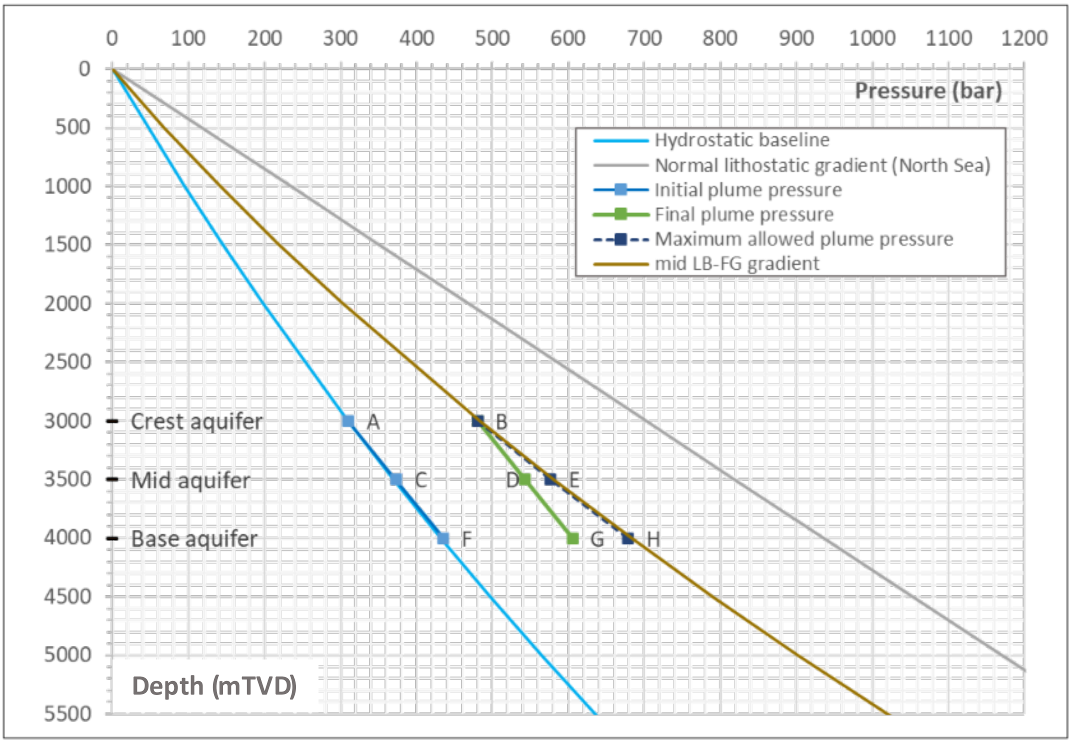

Figure 12: Aquifer storage complex pressures. This figure illustrates the pressure profiles of a generic aquifer complex, with the crest located at 3000 m and the base at 4000 m. The profiles are shown both before CO_2 injection (line A-F) and after CO_2 injection (line B-G). The maximum allowable pressures are denoted by line B-H.

When creating a maximum allowable pressure map, a critical pressure value is created for each grid point on the map. If we overlay an aquifer storage complex onto this map, the corresponding point (referred to as point E in Figure 12) represents the mean critical pressure for the aquifer storage complex. However, it is important to note that the map-based critical pressure determination occurs at the mid-aquifer location, whereas it should be assessed at the top of the aquifer, because that is where the increased aquifer pressure will first intersect with the Mid LB-FG gradient. Consequently, the evaluated ΔP (as indicated by pressure distance C to E in Figure 12) requires correction to align with the ΔP at the top of the aquifer storage complex (as shown by pressure distances A to B and C to D in Figure 12).

The extent of correction may vary among distinct aquifer storage complexes, contingent upon the height of each specific aquifer storage complex. For the map correction calculation, we consider an aquifer storage complex height of 1000 meters. Additionally, we assume that the CO_2 injection point lies at the base of the aquifer, which is 1000 meters below the crest of the aquifer. Consequently, the corrected maximum allowable pressure map (as shown in Map 26) can be utilized for both the aquifer and CO_2 plume storage calculations. It is important to recognize that the inclusion of a uniform aquifer storage complex height of 1000 meters significantly reduces the precision of the map-based CO_2 storage capacity assessment method when compared to the traditional approach of aggregating the CO_2 storage capacities of individual storage complexes. The 1000 m value indicates the average height of the aquifer complexes based on a preliminary survey of the study area.

A correction factor for the maximum allowable pressure map was determined by evaluating the $\frac{\Delta CD}{\Delta CE}$ pressure ratio (Figure 12) across different depths within an aquifer storage complex. Subsequently, these pressure distance ratios were plotted (Figure 13), and from this plot, the following regression equation was derived:

$$Max\ aquifer\ pressure\ correction\ factor = (2 \times 10^{-12} \times d^3) - (3 \times 10^{-8} \times d^2) + (0.0002 \times d) + 0.43$$

Where d is depth.

An analytically derived formulation is given in Ravestein et al., 2024, Box 1.

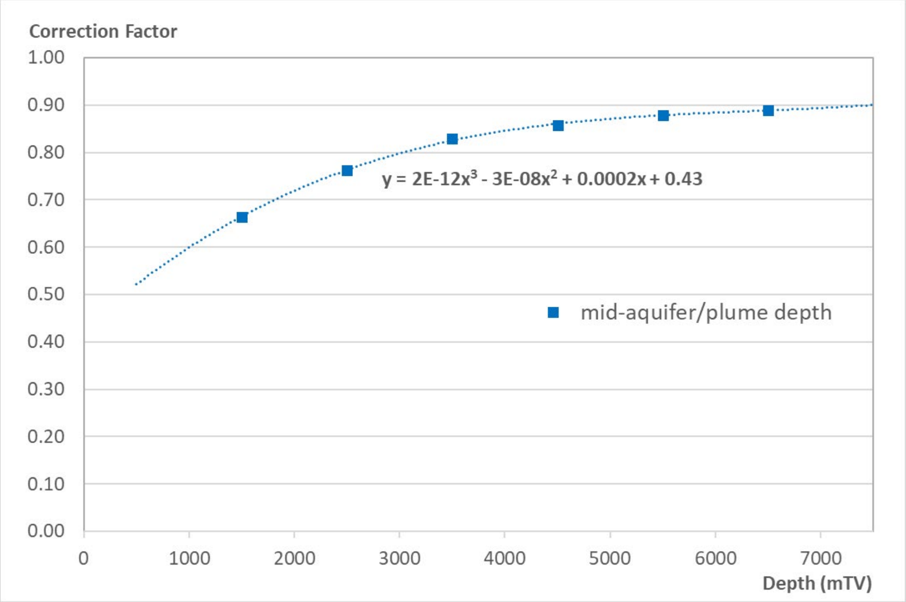

Figure 13: Maximum allowed aquifer pressure correction. This figure illustrates the pressure correction factor that considers the difference between the maximum allowed pressure at the mid-aquifer level and that at the top of the aquifer when calculating the CO_2 storage capacity. A low correction factor leads to a substantial adjustment of aquifer pressures, whereas a high correction factor results in a minor correction (i.e., significant adjustments occur at shallow depths, while minor adjustments occur at greater depths).

The maximum allowed aquifer pressure correction factor equation when applied to the Top Slochteren Formation depth map (Map 1) results in the creation of the Max aquifer pressure correction factor map (Map 25).

Subsequently, the maximum allowed aquifer pressures corrected map (Map 26) is created as follows:

$$Mid\ LB - FG\ gradient\ pressures\ corrected = Hydrostatic\ baseline\ guiding\ grid + Max\ aquifer\ pressure\ correction\ factor \times (Mid\ LB - FG\ gradient\ pressures - Hydrostatic\ baseline\ guiding\ grid)$$

Or

$$Map26 = Map8 + Map25 \times (Map13 - Map8)$$

The maximum allowed aquifer pressures corrected map (Map 26) serves as input for the ΔP correction (section 3.5.1), the Compressibility correction (section 3.5.2) and the CO_2 plume density correction (section 3.5.3).

3.5.1 Delta P ($\Delta \boldsymbol{P}$) correction

The applied workflow for the map-based delta P (ΔP) correction is documented in Appendix B3.

The ΔP pressures corrected map (Map 28) is derived from the difference between the Mid LB-FG gradient pressures corrected map (Map 26) and the Initial pressures Rotliegend aquifer map (Map 10). The ΔP pressures corrected map serves as the input for assessing the CO_2 storage capacity of the Rotliegend aquifer in the Dutch offshore within our current study.

Neglecting the correction of the ΔP map could lead to inaccurate estimations of the storage capacity, potentially overestimating the total CO_2 storage capacity of an aquifer.

3.5.2 Compressibility correction

The correction for compressibility specifically pertains to water compressibility, while it does not apply to pore compressibility. Pore compressibility relies solely on porosity, solid rock- and frame compressibility, independent of the maximum allowed aquifer pressures.

The corrected water compressibility map of the Rotliegend aquifer (Map 29) is created by using the equation described in section 3.3.1. However, instead of using the original maximum allowed aquifer pressures map (Map 14), we are now employing the corrected version (Map 27).

The Total compressibility corrected map (Map 30) is obtained by adding the Water compressibility corrected map (Map 29) to the Pore compressibility map (Map 22).

The Total compressibility corrected map serves as the input for assessing the CO_2 storage capacity of the Rotliegend aquifer in the Dutch offshore within our current study.
Unlike ΔP related storage capacity calculations, which depend solely on maximum allowed aquifer pressures, water compressibility related storage capacity calculations also incorporate the temperature parameter. Notably, in water compressibility storage calculations, the temperature parameter has a more significant impact than the maximum allowable aquifer pressures parameter. Furthermore, the total compressibility is influenced not only by water compressibility but also by pore compressibility in storage capacity calculations. Neglecting the correction of the total compressibility map has therefore a minimal impact on storage capacity estimations. However, it may lead to an underestimation of the total CO_2 storage capacity in the core area of the Rotliegend aquifer in the Dutch offshore by about 1%. Given this limited effect of the compressibility correction

on the CO_2 storage capacity assessment, one might contemplate omitting this correction in future assessments.

3.5.3 CO_2 plume density correction

The extent of a CO_2 density correction can differ across different aquifer storage complexes, depending on the height of the CO_2 plume within each specific complex. The plume height is defined as the vertical distance between the depth at which CO_2 is injected into the aquifer and the crest of the aquifer. In our study, we assume a plume height of 1000 meters. Given that we use a consistent height of 1000 meters for the plume within the aquifer storage complex, we can apply the same corrected maximum allowable pressure map (Map 26) for both the aquifer and CO_2 plume storage calculations.

The corrected CO_2 plume density map of the Rotliegend aquifer (Map 31) is created by using the equation described in section 3.4. However, instead of utilizing the original maximum allowed aquifer pressures map (Map 13), we are now employing the corrected version (Map 26).

Unlike ΔP related storage capacity calculations, which depend solely on maximum allowed aquifer pressures, CO_2 plume density related storage capacity calculations incorporate the temperature parameter. Notably, in CO_2 plume density storage calculations, the temperature parameter has a more significant impact than the maximum allowable aquifer pressures parameter. Neglecting the correction of the CO_2 plume density map has therefore a minimal impact on storage capacity estimations. However, it may lead to an underestimation of the total CO_2 storage capacity of the Rotliegend aquifer in the Dutch offshore by about 1%. Given this limited effect of the compressibility correction on the CO_2 storage capacity assessment, one might contemplate omitting this correction in future assessments.

3.5.4 Correction validation

The purpose of the map corrections is to align the deterministically assessed storage capacities of aquifer storage complexes with the map-based assessment of the same complexes or with the storage capacity of the entire area covering these complexes.

For the validation of the map correction values, we mapped 10 adjacent Rotliegend aquifer storage complexes within the study area. These complexes exhibit varying sizes, expressed in storage capacity, ranging from 4 Mt to 63 Mt. Additionally, their heights (measured from base to crest) span from 870 meters to 1750 meters, with an average height of approximately 1150 meters.

The storage capacity of all 10 complexes was deterministically assessed using the recently introduced TNO-AGE SCADSA tool (Reference 5). Subsequently, the capacities of the individual complexes were summed to determine the total storage capacity for the area. Additionally, the storage capacities for the same 10 complexes were determined using the map-based method. An overview of the results is presented in Table 1. In the table, one can also observe the variation in assessed total storage capacity when correcting for an aquifer's height of 1000 meters compared to 1600 meters.

Table 1: Total storage capacity 10 Rotliegend aquifer storage complexes

Deterministic (mode in SCADSA)	Map-based			Method
	Un-corrected	Corrected [aquifer. h = 1000m]	Corrected [aquifer. h = 1600m]	
205	310	247	211	Total capacity (Mt)
0	51.2%	20.5%	2.9%	% difference

While the map-based total storage capacity assessment for map correction, associated with an aquifer height of 1600 meters, seems to align more closely with the deterministically assessed storage capacity, we however prefer the assessment related to an aquifer height of 1000 meters. The rationale behind this preference lies in the irregular structural shapes of the investigated aquifer complexes. These irregularities occasionally pose challenges, as the SCADSA tool and its current algorithms are primarily optimized for calculating storage capacities in regular structures. Implementation of a shape factor to properly address this issue in the SCADSA tool is pending. For the map-based storage capacity calculation method, irregular structural shapes do not present a challenge. It is therefore reasonable to assume that the actual total theoretical storage capacity of the investigated area will likely be closer to 247 Mt rather than 205 Mt.

4 Results and Conclusions

4.1 Theoretical storage capacity

To assess the theoretical storage capacity of the Rotliegend aquifer, we employed the equation outlined in section 3, along with (corrected) maps specifically relevant to the parameters involved.

$$Theoretical\ Storage\ Capacity\ =\ D_p \times \Delta P_{corr} \times C_{t\,corr} \times \rho_{CO_2\,corr}$$

D_p = Pore Thickness (Map 7)
ΔP_{corr} = Delta P pressures corrected (Map 28)
$C_{t\,corr}$ = Total Compressibility corrected (Map 30)
$\rho_{CO_2\,corr}$ = CO_2 plume density corrected (Map 31)

The theoretical CO_2 storage capacity map (Map 32) illustrates storage thickness expressed in kilograms per square meter. We utilized the ‘volume below surface’ utility from the Petrel software package to calculate the theoretical storage capacity within the Rotliegend core area in the Dutch offshore (the core area is shown by the red polygon in Map 32). The outcome of this calculation reveals a theoretical CO_2 storage capacity for the Rotliegend aquifer in the core area of 2310 Mt. The storage capacity has been calculated assuming the absence of Rotliegend gas fields within the core area. It is estimated that correcting for this assumption will reduce the storage capacity by 2-5% (46-115 Mt).

4.2 Uncertainty

To quantify the uncertainty related to the theoretical CO_2 storage capacity, we developed a probabilistic workflow using the Petrel software package. Within this workflow, we employed the Theoretical Storage Capacity equation (see section 4.1) and incorporated information from the four basic input maps (outlined in section 0). Additionally, the workflow incorporated estimated uncertainty ranges associated with the four input maps (see Table 2). These ranges were estimated from variation within the four input maps and from uncertainty estimates specific to a representative Rotliegend CO_2 storage complex. The uncertainty ranges were modeled as following a normal distribution. The workflow employs a Monte Carlo random sampling procedure for every grid point across the four input maps. Subsequently, the grid point values are multiplied, and the results are aggregated. This random sampling process is repeated 1,000 times. The result of this calculation is shown in Table 3 and Figure 14.

Table 2: Input maps and uncertainty ranges

Map	Map title	Parameter	Unit	Uncertainty	Uncertainty type
Map 7	Pore Thickness	D_p	m/m2	+/- 7.7	absolute
Map 28	Delta P pressures corrected	ΔP	bar	+/- 0.29 × ΔP	relative
Map 30	Total compressibility corrected	C_t	1/bar	+/- 4.97 × 10-6	absolute
Map 31	CO_2 plume density corrected	ρ_{CO_2}	kg/m^3	+/- 29	absolute

Table 3: - Output results probabilistic calculations

Theoretical CO_2 storage capacity	Mean	P90	P50	P10
Mt	2215	990	2030	3650

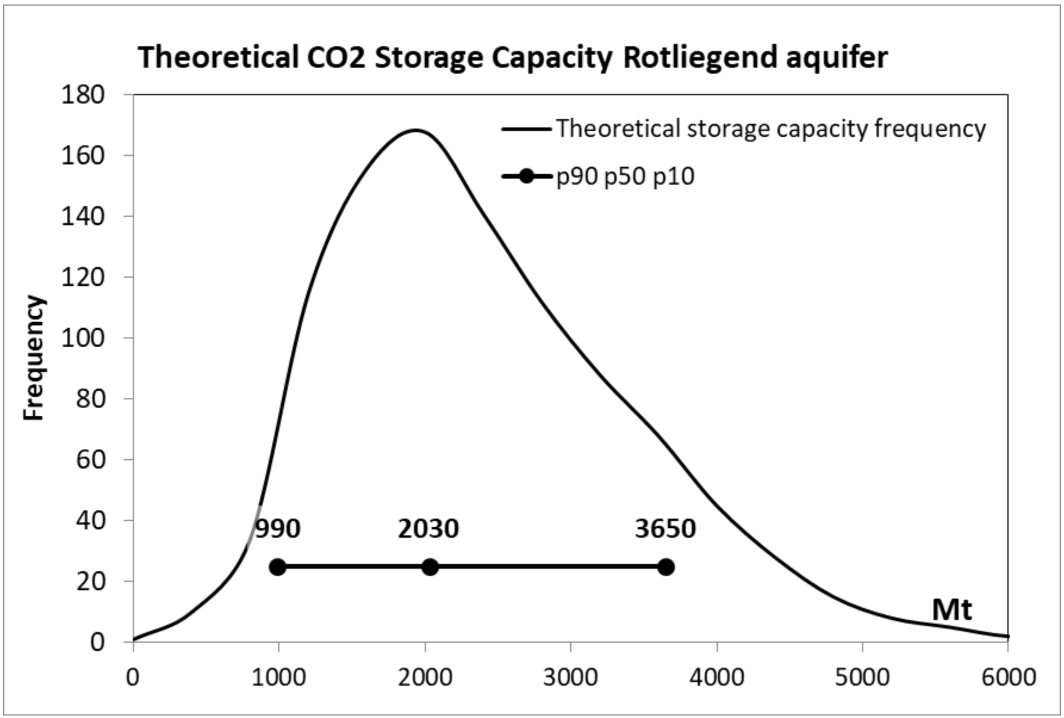

Figure 14: Frequency distribution of the map-based theoretical CO_2 storage capacity, Rotliegend aquifer. The study's outcome, which includes the calculated CO_2 storage capacity and its associated uncertainty, is depicted in this figure and summarized in Table 3.

4.3 Calculation method comparison

Section 4.3 focuses on calculating and comparing a representative range of methods for assessing the CO_2 storage capacity and applying these methods to the Rotliegend aquifer in the Dutch offshore. Table 4 presents a comparison of Theoretical CO_2 storage capacity for the Rotliegend aquifer in the core area, as determined by different methods. The deterministic map-based method (Method 2) is discussed in section 3. Method 2 has been executed with and without map correction as discussed in section 0. Method 1 pertains to the probabilistic analysis discussed in section 4.2. Finally, Method 3 and 4 have been performed to compare to legacy methods as discussed in 4.3.1 and 4.3.2.

Table 4: Theoretical CO_2 storage capacity in the Rotliegend aquifer of the Dutch offshore area of the core area of this study. Calculation comparison with the difference between the various deterministic methods and the mean value of the probabilistic map-based method

Method				Storage capacity (Mt)	Difference (%)
Probabilistic	1a Map-based (corrected maps)		Probabilistic mean	2215	0
			P90	990	
			P50	2030	
			P10	3650	
Probabilistic	1b Map-based (corrected maps)		Probabilistic mean	2770	25.0
Deterministic	2 Map based	Corrected map	Integral	2310	4.3
		Uncorrected map	Integral	2870	29.6
	3 Conventional methods	Mean corrected maps	$V_p \Delta P C_t \rho_{CO_2}$	2510	13.3
		Mean uncorrected maps	$V_p \Delta P C_t \rho_{CO_2}$	3020	36.4
	4 Quick look		$V_p 2\%700$	4160	87.8

4.3.1 Comparison with conventional storage assessment

The conventional method (Reference 3) to calculate the total theoretical CO_2 storage capacity of an aquifer in an area is to multiply the mean values from the V_p, ΔP, C_t and ρ_{CO_2} maps.

$$Theoretical\ Storage\ Capacity\ =\ V_p \times \Delta P \times C_t \times \rho_{CO_2}$$

The mean values that were assessed from the **corrected maps** to calculate the Theoretical storage capacity from the Rotliegend aquifer within the core area are indicated in Table 5.

Table 5: Mean values of specified parameters before correction has been applied.

Variable	Map	Mean value
V_p	7	2.97×10^{11} m^3
ΔP	28	196 bar
C_t	30	6.76×10^{-5} 1/bar
ρ_{CO_2}	31	768 kg/m^3
$Theoretical\ Storage\ Capacity$		3022 Mt

The outcome of the conventional method for assessing the regional storage capacity of an aquifer differs (Table 4, Deterministic, Conventional methods) significantly from the outcome of the new map-based probabilistic approach (Table 4, Deterministic, Map based). In the conventional method, the storage capacity is calculated by multiplying the mean values extracted from the $\boldsymbol{V_p, \Delta P, C_t}$ and $\boldsymbol{\rho_{CO_2}}$ maps. In contrast, the map-based approach takes a more granular approach: it multiplies the values at individual grid points from each of the four maps and then stacks the results. Furthermore, the conventional method fails to consider the $\boldsymbol{\Delta P}$ correction. This difference in methodology significantly affects the outcome of storage capacity estimates, resulting in a potential overestimation of the storage capacity of up to 36% when employing the conventional assessment approach (Table 4, Deterministic, Conventional methods, Mean uncorrected maps).

4.3.2 Efficiency Factor and quick look assessment

In 1996, a relationship (see section 3) was introduced to calculate the theoretical CO_2 storage capacity for a closed-system aquifer (Reference 3). Additionally, a simplified version was developed to facilitate a quick look assessment of the storage capacity for North Sea aquifers. The simplified equation was defined as follows:

$$Theoretical\ Storage\ Capacity_{simplified} = V_p \times Seff \times \rho_{CO_2}$$

$Seff$ = Storage Efficiency Factor (equals $\Delta P \times C_t$)

Typical parameter values for North Sea aquifers are (Reference 3) 2% for the $Seff$ (at ΔP = 105 bar and at $C_t = 19 \times 10^{-5}$ 1/bar) and $700\ \frac{kg}{m^3}$ for ρ_{CO_2} (at average hydrostatic conditions).

The quick look CO_2 storage capacity equation for North Sea aquifers is thus defined as follows:

$$Theoretical\ Storage\ Capacity\ _{quick\ look} = V_p \times 2\% \times 700$$

When incorporating the pore volume of 297×10^9 m^3 from the Rotliegend aquifer in the core area, the quick look assessment yields a Theoretical Storage Capacity of **4160 Mt**.

The Storage Efficiency Factor map (Map 33) for the Rotliegend aquifer in the Dutch offshore was created by multiplying the ΔP pressures corrected map (Map 28) with the Total compressibility corrected map (Map 30).

The Rotliegend aquifer in the core area exhibits an $Seff$ range between 0% and 3.5%, a mean value of 1.1% and a mode value of 0.8% (see Figure 15). Notably, high $Seff$ values occur along a north-south trending strip, while lower values are observed to the east and west (see Map 33). Importantly, $Seff$ values exceeding 2.0% predominantly occur in deep graben areas characterized by low porosity, resulting in a limited contribution to storage capacity.

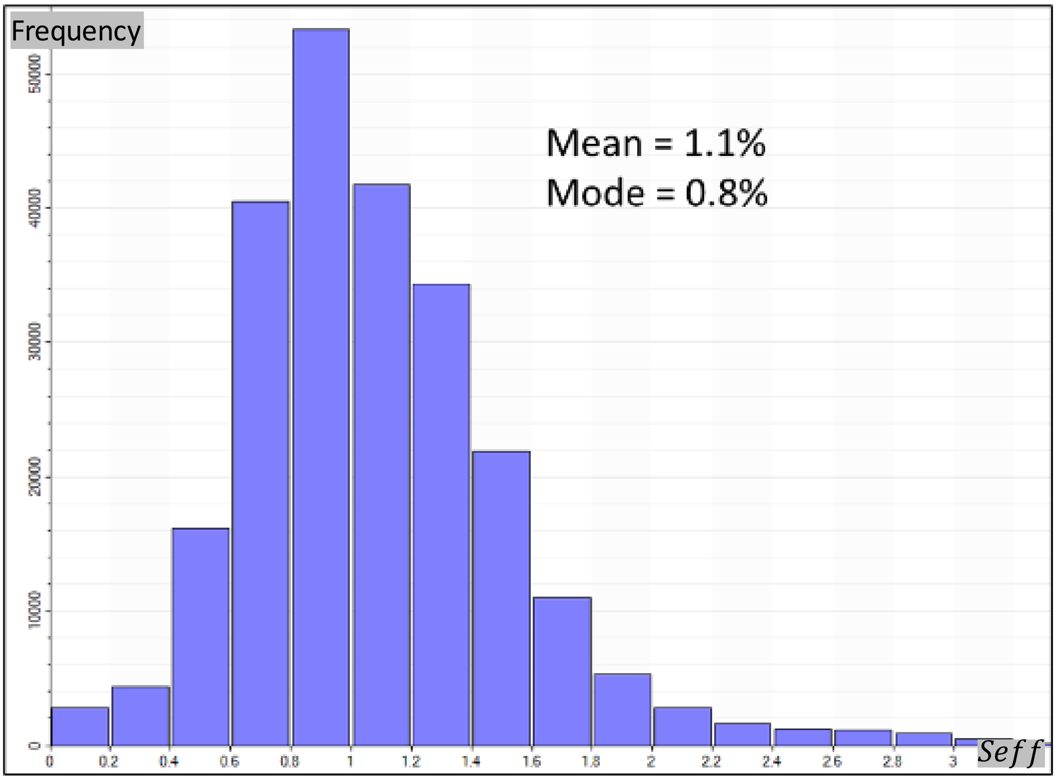

Figure 15: Storage Efficiency Factor (Seff) distribution. This graph represents the frequency of the Seff ascertained from the Storage Efficiency Factor map (Map 33). The depicted frequency statistics are exclusive to the core area, exhibiting a distribution that is predominantly skewed towards higher values. The frequency distribution with a mean of 1.1% is notably below the 2% benchmark Seff from the North Sea aquifers' CO_2 storage capacity quick look assessment (refer to Section 4.3.2).

The mean CO_2 plume density within the Rotliegend aquifer core area was determined using the CO_2 plume density corrected map (refer to Map 31). From this map, the mean density frequency value is 770 kg/m^3 (as shown in Figure 16). Notably, this value is 70 kg/m^3 higher than the estimate obtained from the quick look storage capacity equation (which yields 700 kg/m^3). This discrepancy accounts for 9% of the difference between the conventional assessment (at 2510 Mt) and the quick look assessment (at 4160 Mt).

The CO_2 plume density in the Rotliegend aquifer within the core area exhibits a range spanning from 540 kg/m^3 to 900 kg/m^3, with a mode value of 815 kg/m^3 (as depicted in Figure 16). Notably, lower CO_2 plume density values are concentrated along a north-south trending strip, while higher values are observed to the east and west (as illustrated in Map 31).

Importantly, CO_2 plume density values exceeding 860 kg/m^3 are primarily calculated in the deepest graben areas, which are characterized by very low porosity (< 0.03). Consequently, these areas make only a limited contribution to the overall storage capacity.

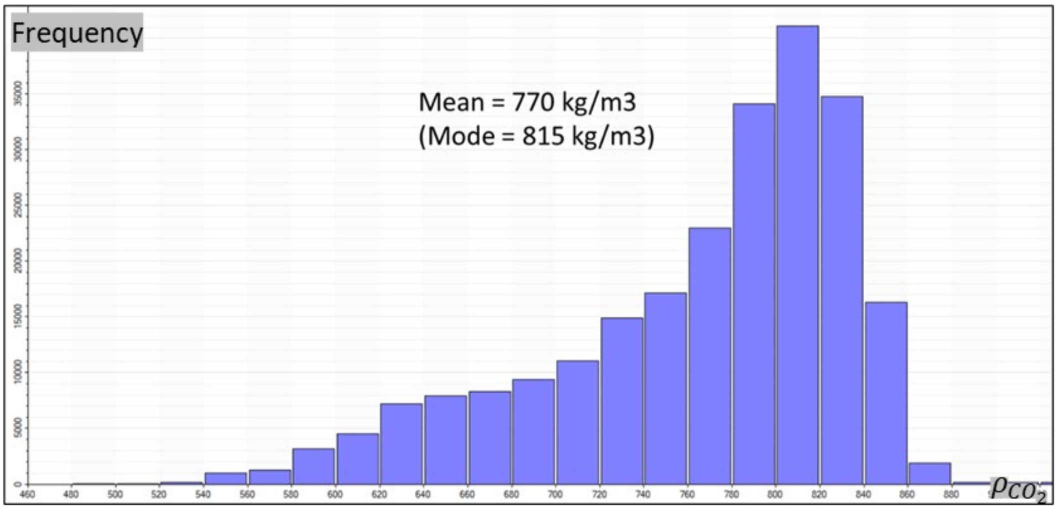

Figure 16: CO_2 plume density distribution. This graph represents the frequency of the CO_2 plume density ascertained from the CO_2 plume density corrected map (Map 31). The depicted frequency statistics are exclusive to the core area, exhibiting a distribution that is predominantly skewed towards lower values. The frequency distribution with a mean of 700 kg/m3 is notably above the 700 kg/m3 benchmark CO_2 plume density from the North Sea aquifers' CO_2 storage capacity quick look assessment (refer to Section 4.3.2).

The results obtained from the quick look method for assessing the regional storage capacity of an aquifer significantly diverge from those generated by the new map-based probabilistic approach (as shown in Table 4). The primary source of divergence between the two methods lies in variations related to the Storage Efficiency Factor ($Seff$). Notably, a significant portion of the $Seff$ discrepancy can be attributed to differences in the total compressibility (C_t) value settings. While both methods maintain the same water compressibility (C_w) value of 3.1x10^{-5} 1/bar, the pore compressibility (C_p) in the quick look assessment employs a value of 15.9x10^{-5} 1/bar. This is 4.1 times higher than the C_r value of 3.7x10^{-5} 1/bar used by the map-based probabilistic method. When considering the effect of ΔP, which differs between the two methods (105 bar vs 161 bar), we calculate the following E.F.'s for both approaches:

Quick look method:

$$Seff = \left(3.1 \times 10^{-5} + 15.9 \times 10^{-5}\right) \times 105 \ = 2\%$$

Map-based probabilistic method:

$$Seff = \left(3.1 \times 10^{-5} + 3.7 \times 10^{-5}\right) \times 161 \ = 1.1\%$$

The divergence in value settings between C_t and ΔP, coupled with variations in the value settings of ρ_{CO_2}, significantly impacts the estimated storage capacity when comparing the quick look method with the map-based probabilistic method. Specifically, the former method predicts a storage capacity of 4160 Mt, while the latter suggests a capacity of 2215 Mt. This discrepancy amounts to 87.8% (as shown in Table 4).

4.4 Conclusions

The probabilistic map-based storage capacity method, using corrected maps, is the preferred method to assess the theoretical storage capacity of the Rotliegend aquifer in the Dutch offshore. This method best reflects the geological differences (and uncertainties) that were mapped and assessed within the study area. The mean theoretical CO_2 storage capacity of the Rotliegend aquifer in the core area is **2215 Mt** with an uncertainty ranging between **990 Mt and 3650 Mt**.

The regions with the highest CO_2 storage capacity exhibit a distinct east-west orientation. Specifically, there are two prominent zones: a northern area, which encompasses blocks K10 to L10, and a southern area, covering blocks P1 to Q2. In the northern part of the study area, situated north of the Rotliegend aquifer core area, the CO_2 storage capacity is notably low or even absent. Conversely, in the southern region, the CO_2 storage capacity is modest. It is important to note that in a significant portion of this southern area, a caprock is absent, rendering it unsuitable for CO_2 storage within this segment of the Rotliegend aquifer.
The observed trends in the theoretical storage capacity map, which highlight areas with the highest CO_2 storage potential, are also prominently reflected in the Pore thickness map. Consequently, we can infer that the latter map serves as an efficient shortcut when exploring for high-capacity aquifer complexes.

It is also important to note that a more meticulous approach, involving detailed mapping and assessment of individual Rotliegend aquifer complexes, is likely to yield greater accuracy compared to the broader regional aquifer assessment. Although this individualized approach is likely to be more accurate, the cumulative sum of the Rotliegend aquifer complexes is still expected to fall within the range of the previously quoted CO_2 storage capacity from the map-based probabilistic method. Additionally, it is important to recognize that mapping and assessing all individual storage complexes within a region can be a time-consuming process.

Utrecht, 20th February 2025

W.W. van Driel,

Deputy Research Manager AGE

5 References

1. Bentham M., Mallows T., Lowndes J., Green A. 2014. CO_2 Storage Evaluation Database (CO_2 Stored), the UK's online storage database, Energy Procedia 63, 5103-5113.
2. Gammer D., Green A., Holloway S., Smith G. 2011. The Energy Technologies Institute's UK CO_2 Storage Appraisal Project (UKSAP). SPE paper 148426, SPE Offshore Europe Oil and Gas Conference, Aberdeen.
3. Holloway, 1996. The underground disposal of carbon dioxide, British Geological Survey, Joule II project CT 92-0031, The Commission of European Communities.
4. Neele, F., ten Veen, J., Wilschut, F., Hofstee C. 2012. Independent assessment of high-capacity offshore CO_2 storage options, TNO-report-060-UT-2012-00414 / B
5. Ravestein, T., Davids, B., van Buggenum, J. 2025. SCADSA – Storage capacity assessment for deep saline aquifers - A tool to assess the capacity for storage of carbon dioxide in deep saline aquifers. TNO public report-R2025 R10218.
6. Span R., Wagner W. 1996. A New Equation of State for Carbon Dioxide Covering the Fluid Region from the Triple-Point Temperature to 1100 K at Pressures up to 800 MPa, Journal of Physical and Chemical Reference Data 25, 1509 (1996).
7. TNO, 2013, Toetsing van de bodemdalingsprognoses en seismische hazard ten gevolge van gaswinning van het Groningen veld. https://www.nlog.nl/sites/default/files/tno_rapport_groningen_15-01-2014_gelakt_pre-scan.pdf
8. Vangkilde-Pedersen, T. et al, 2009. Assessing European capacity for geological storage of carbon dioxide – the EU GeoCapacity project, Energy Procedia 1 (2009) 2663–2670
9. J.M. Verweij, H.J. Simmelink, J. Underschultz, N. Witmans, 2012. Pressure and fluid dynamic characterisation of the Dutch subsurface, Netherlands Journal of Geosciences — Geologie en Mijnbouw, 91 – 4, 465 – 490 (2012).

6 Maps

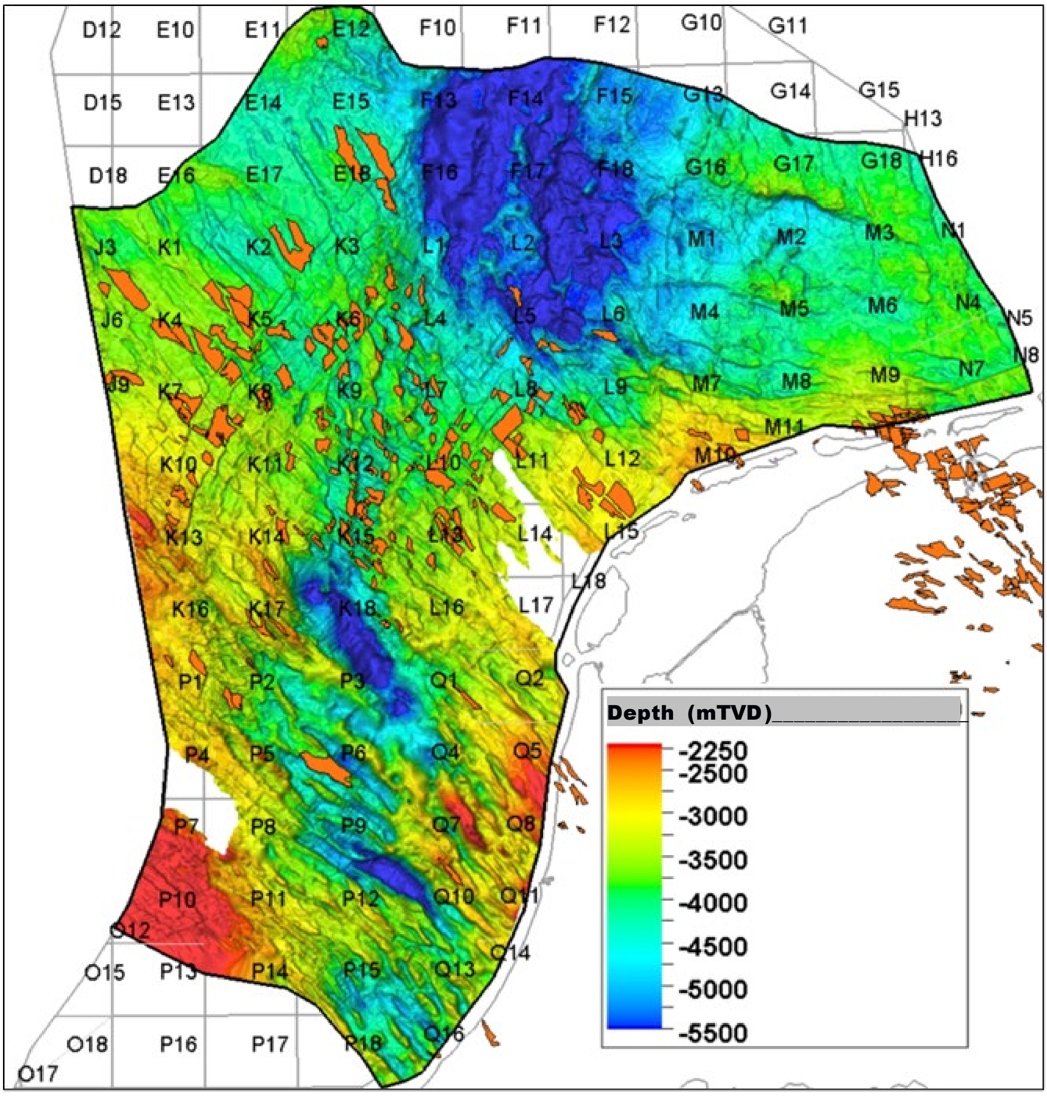

Map 1 - Top Slochteren Formation depth. The creation process and methodology of the map are elaborated in Section 3.1.2 of this report.

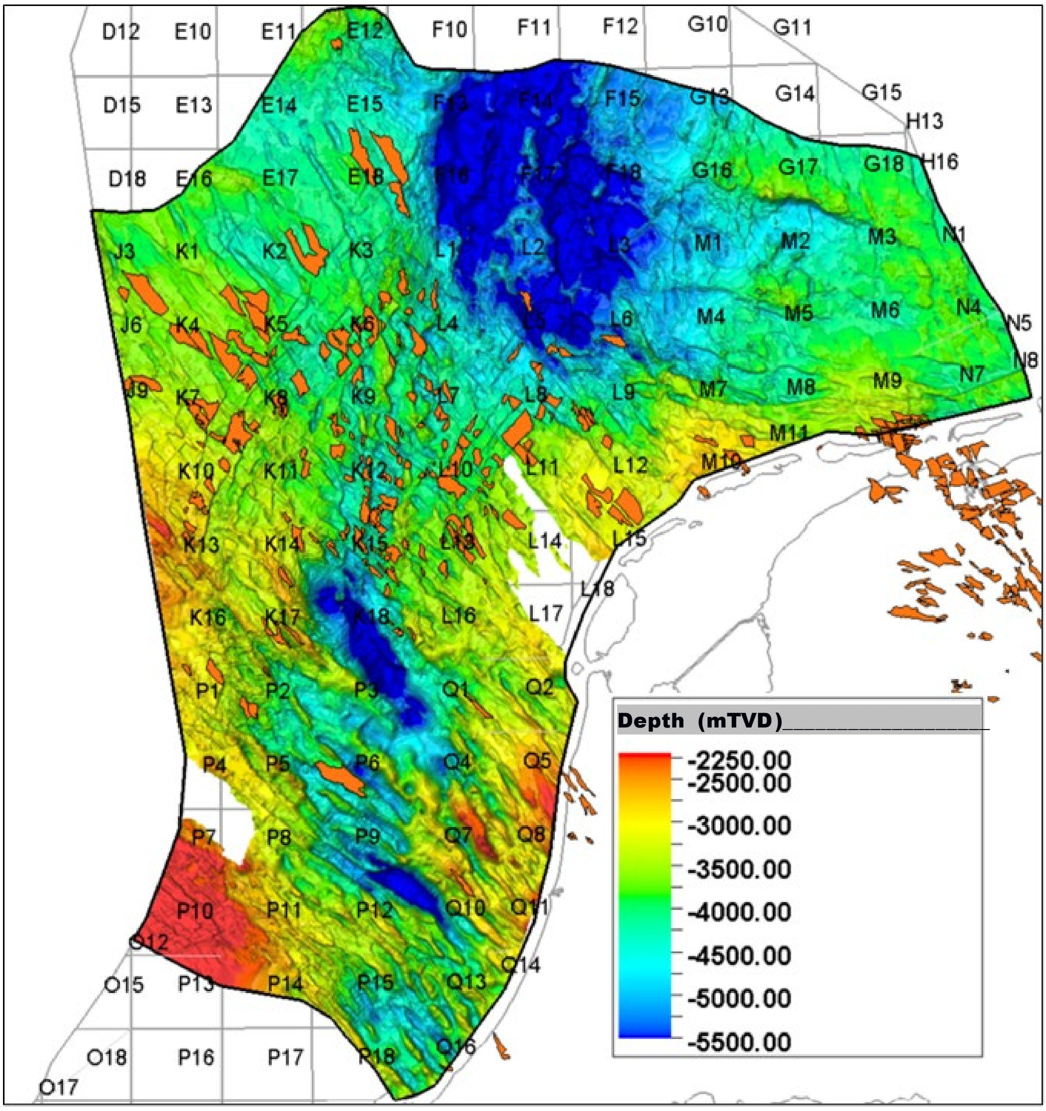

Map 2 – Mid Slochteren Formation Depth. The creation process and methodology of the map are elaborated in Section 3.1.2 of this report.

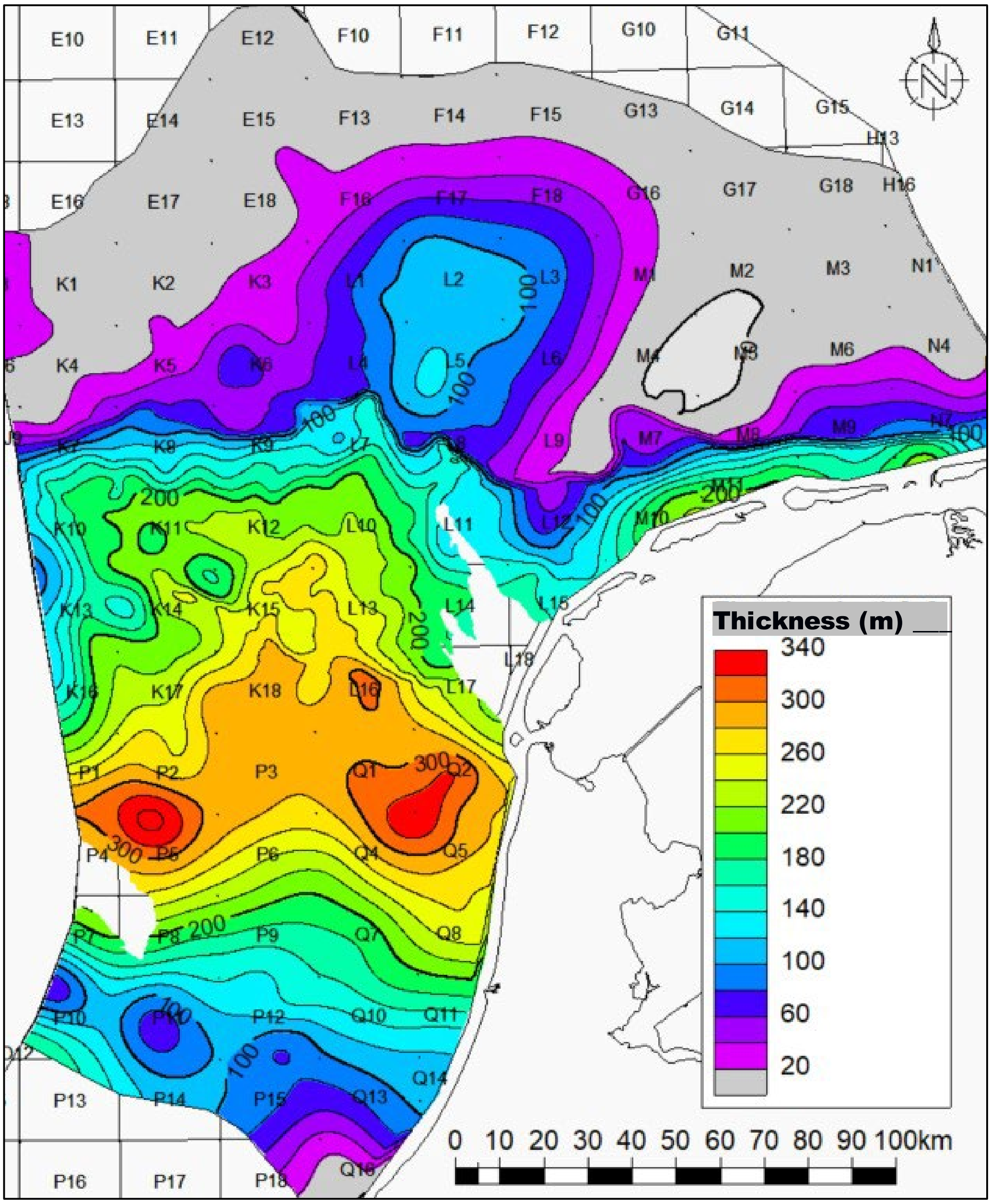

Map 3 - Slochteren Formation thickness. The creation process and methodology of the map are elaborated in Section3.1.2 3.1.1 of this report.

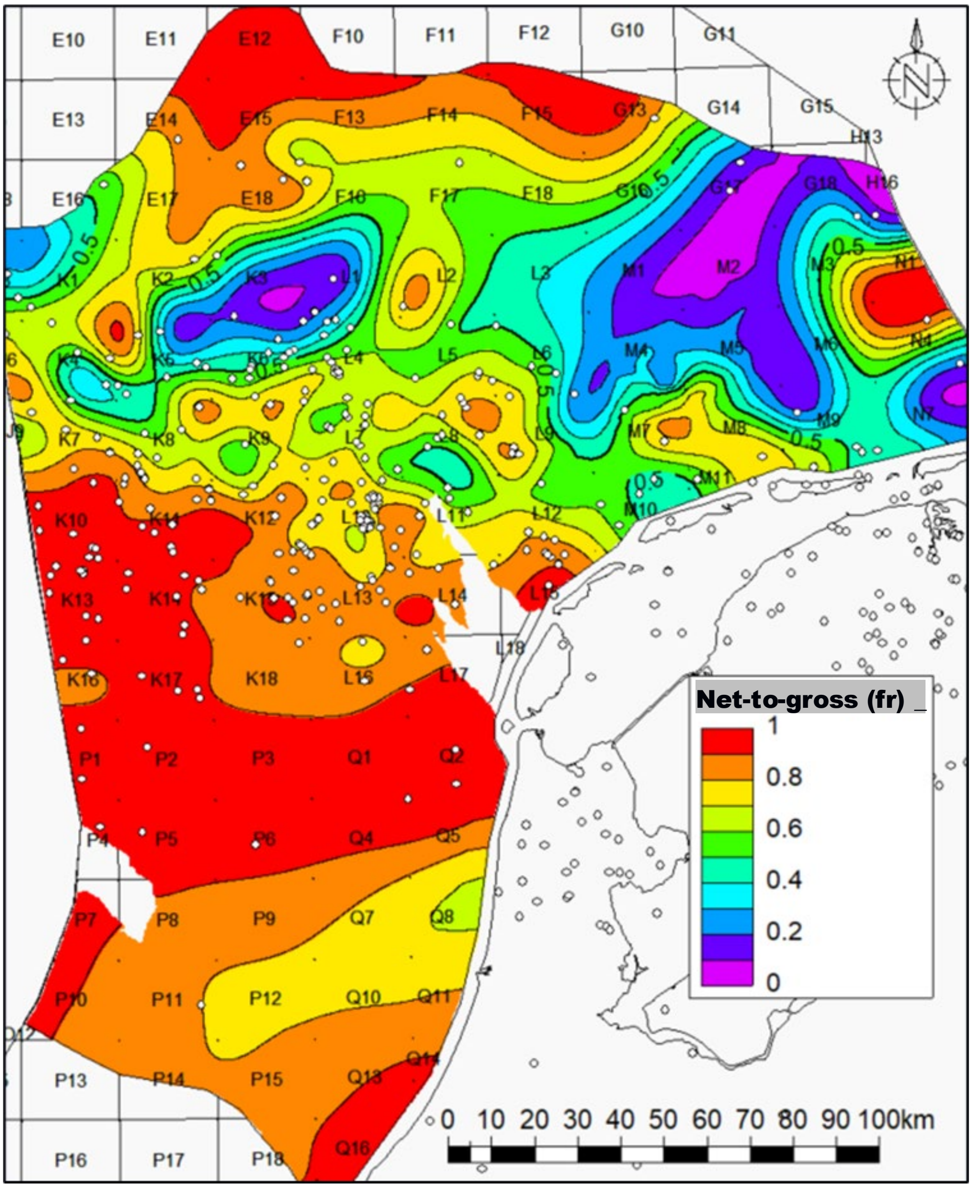

Map 4 - Slochteren Formation net-to gross ratio. The creation process and methodology of the map are elaborated in Section3.1.2 3.1.4 of this report.

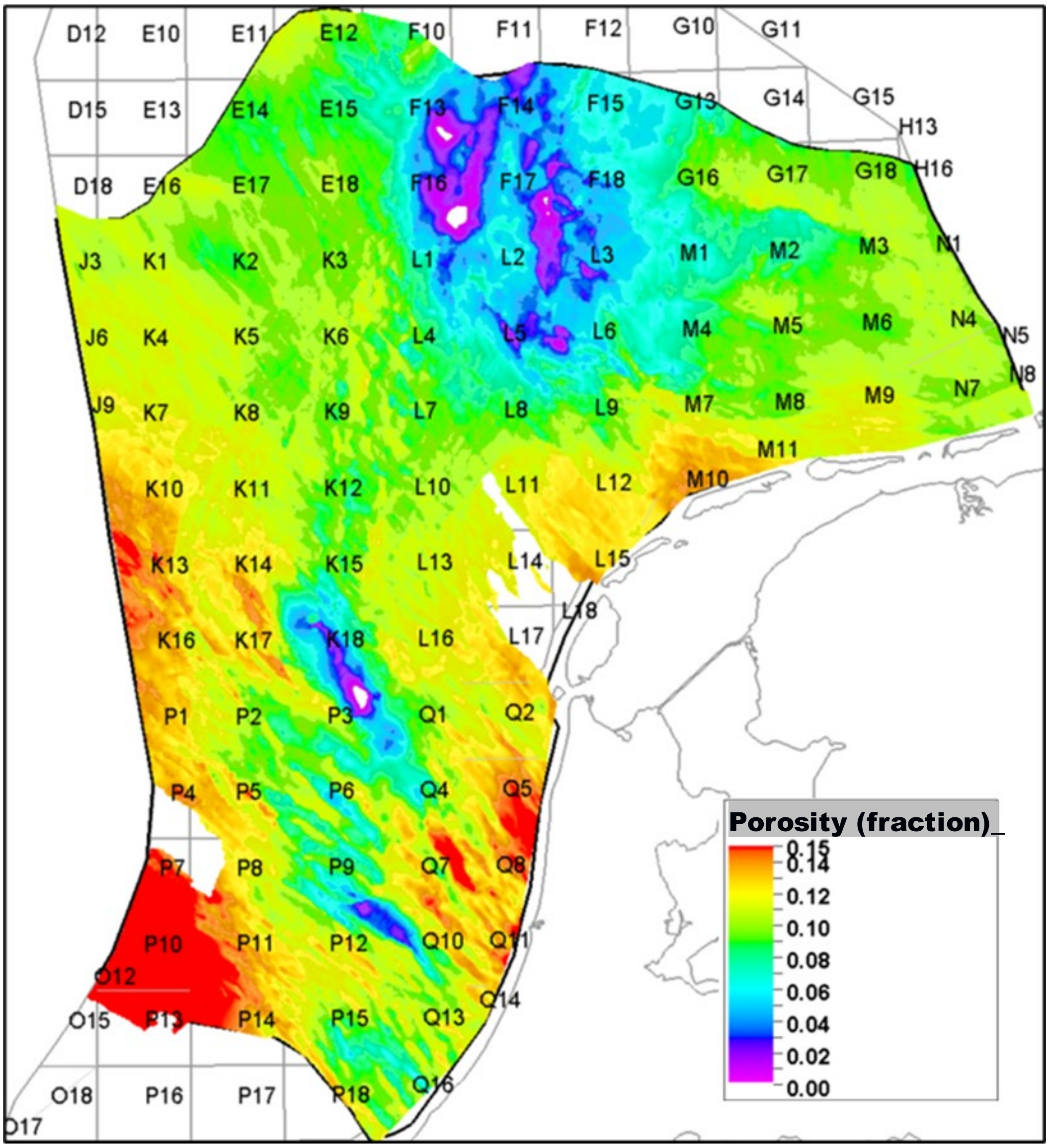

Map 5 – Porosity guiding grid based on depth/porosity trend. The creation process and methodology of the map are elaborated in Section 3.1.3 of this report. The grid is used as a guiding grid for interpolating porosity between wells to create the Slochteren Formation porosity map (Map 6).

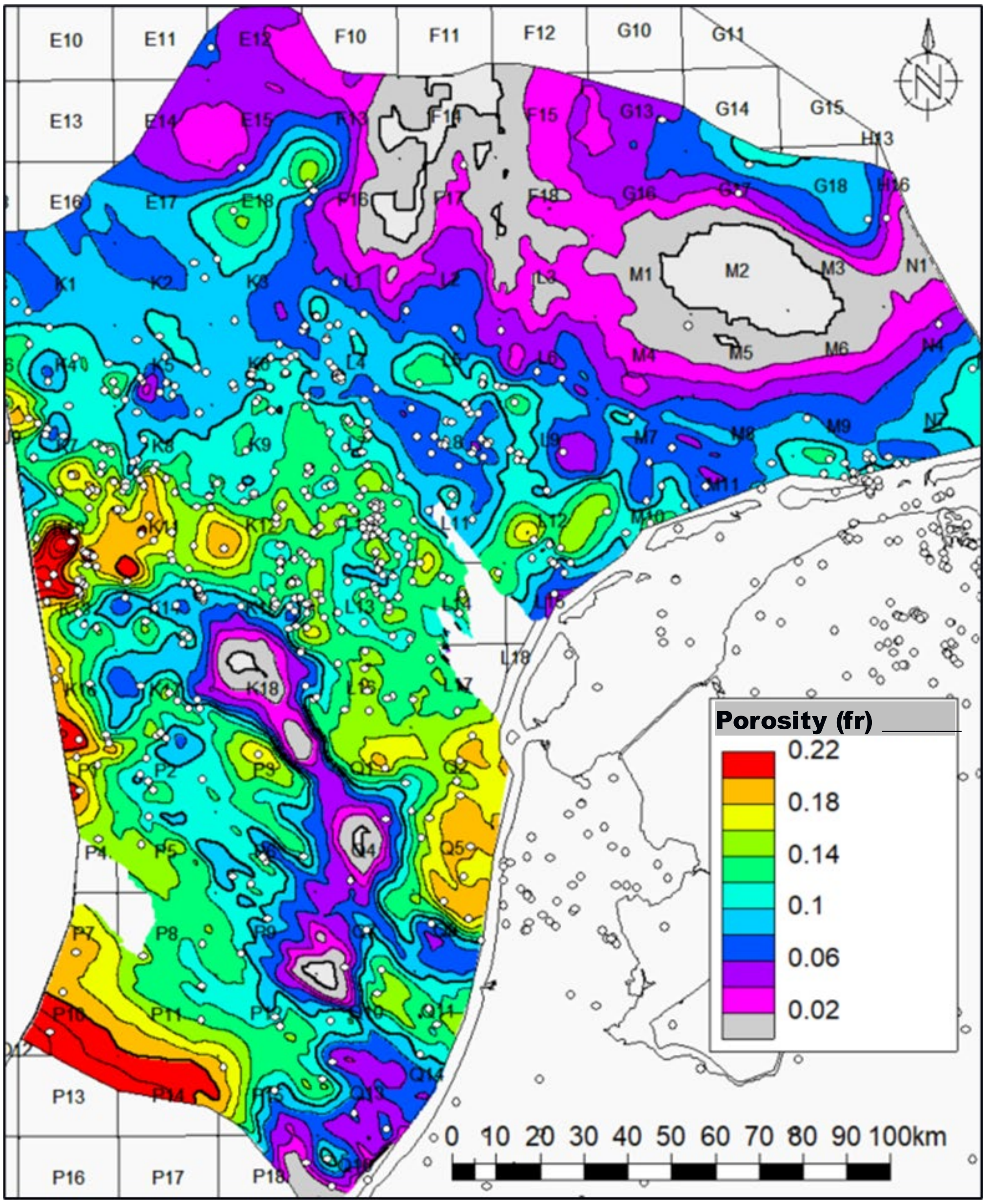

Map 6 - Slochteren Formation porosity. The creation process and methodology of the map are elaborated in Section 3.1.3 of this report.

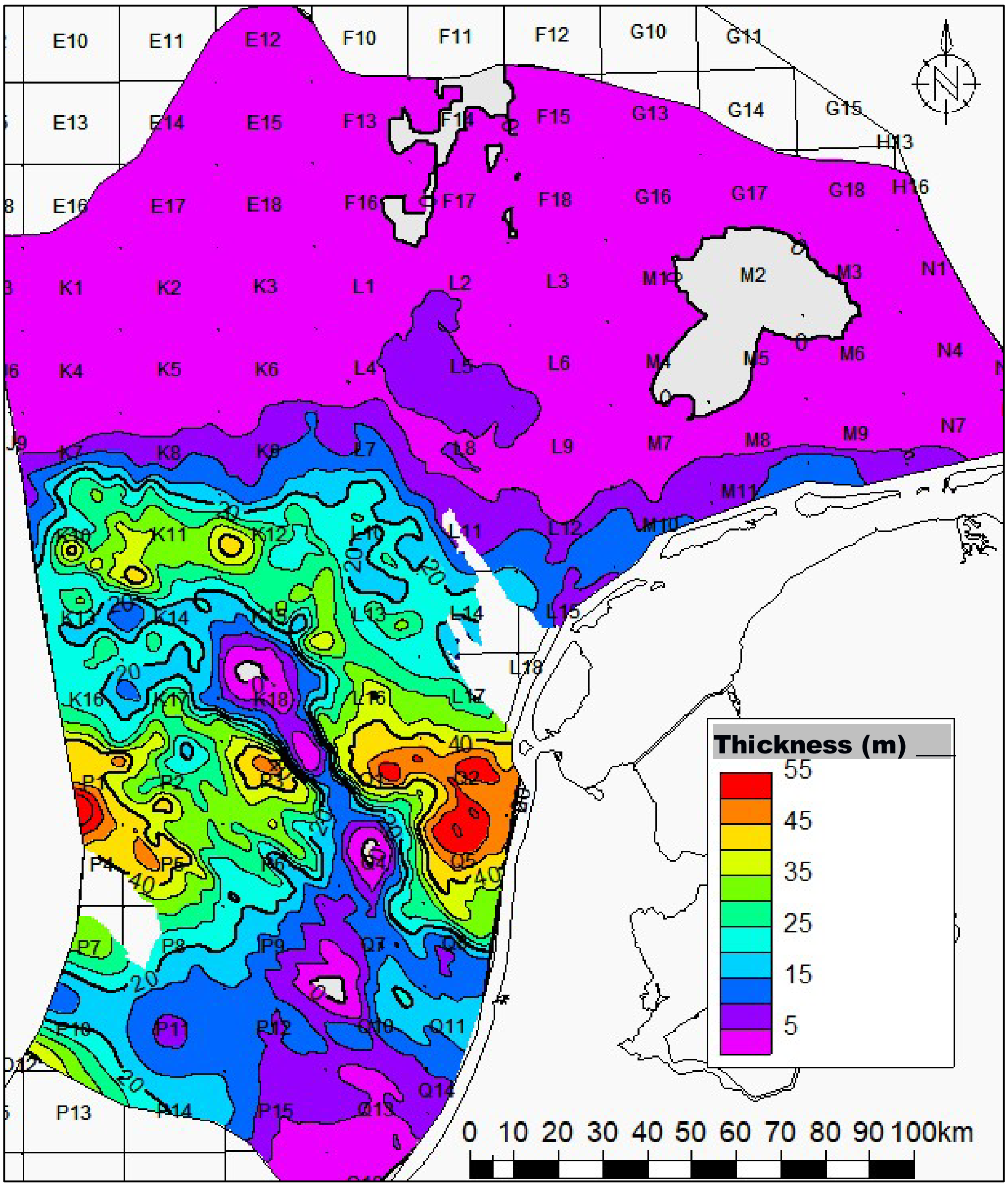

Map 7 - Pore Thickness of the Rotliegend aquifer. The creation process and methodology of the map are elaborated in Section 3.1 of this report.

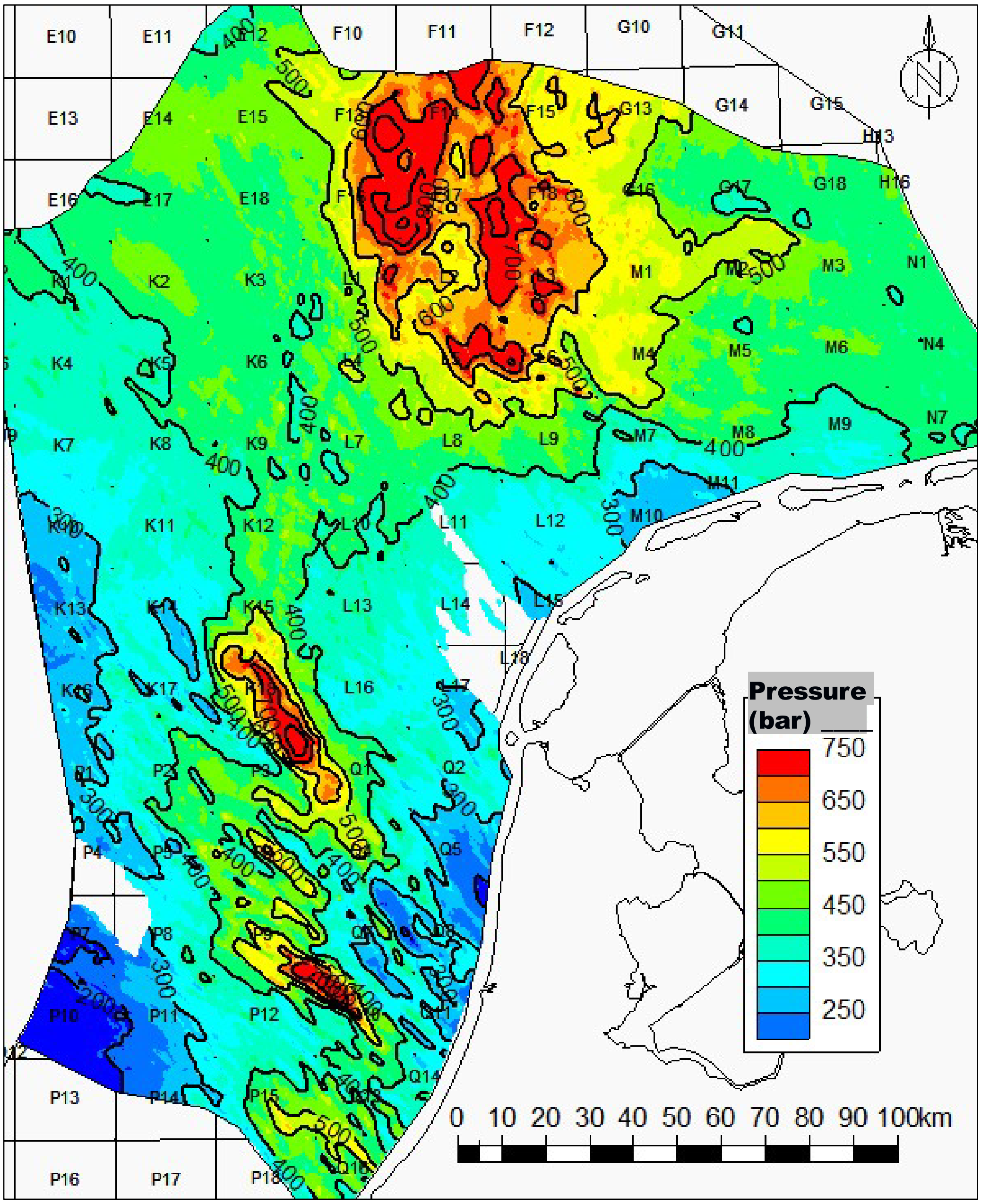

Map 8 – Pressure based on hydrostatic baseline gradient. The term 'pressure' refers to the calculated hydrostatic baseline gradient pressure at the top of the Slochteren reservoir. The creation process and methodology of the map are elaborated in Section 3.2.1 of this report. The grid is used as a guiding grid to create Map 9.

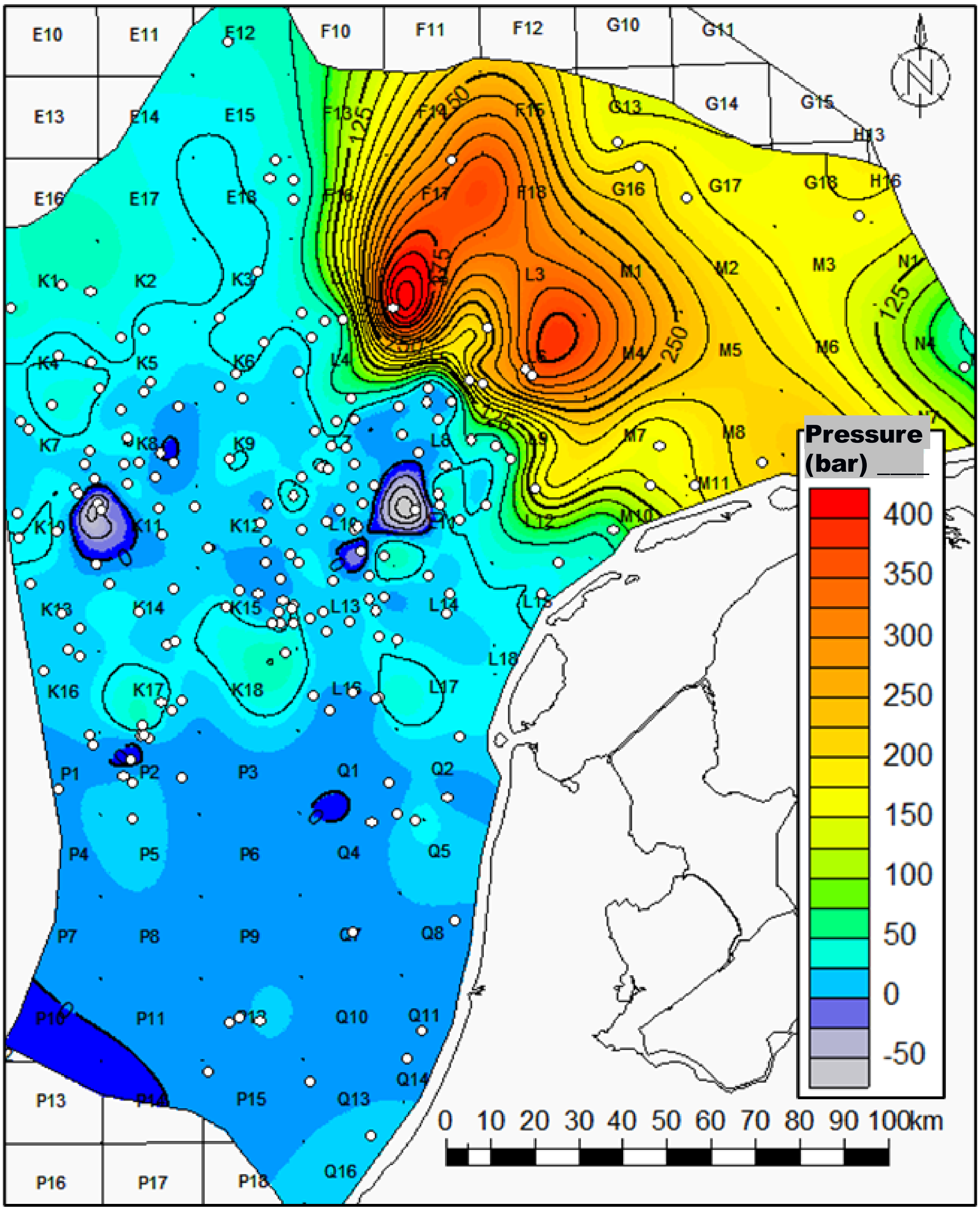

Map 9 - Rotliegend aquifer overpressures. The creation process and methodology of the map are elaborated in Section 3.2.2 of this report.

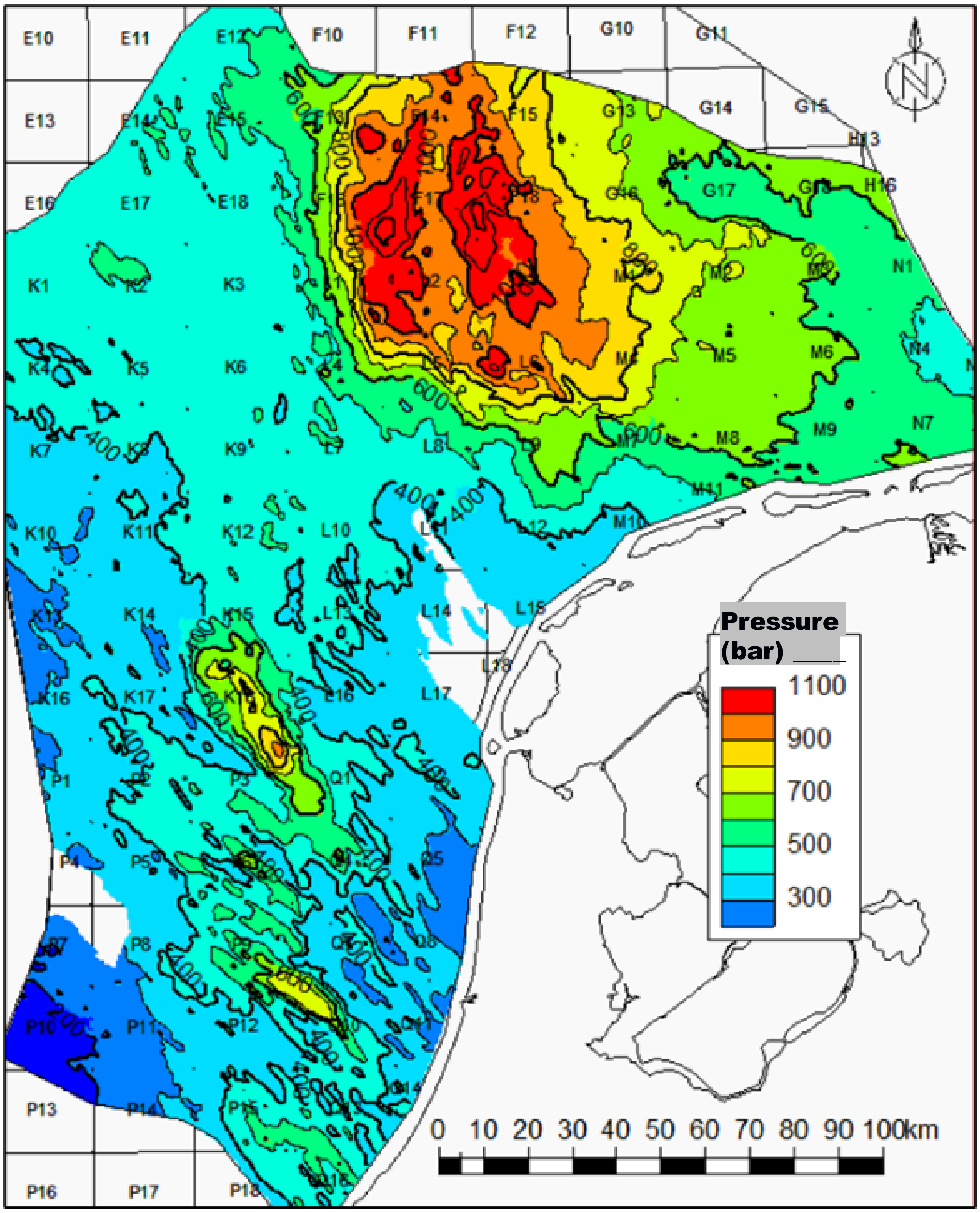

Map 10 - Initial pressures Rotliegend aquifer. The creation process and methodology of the map are elaborated in Section 3.2.3 of this report.

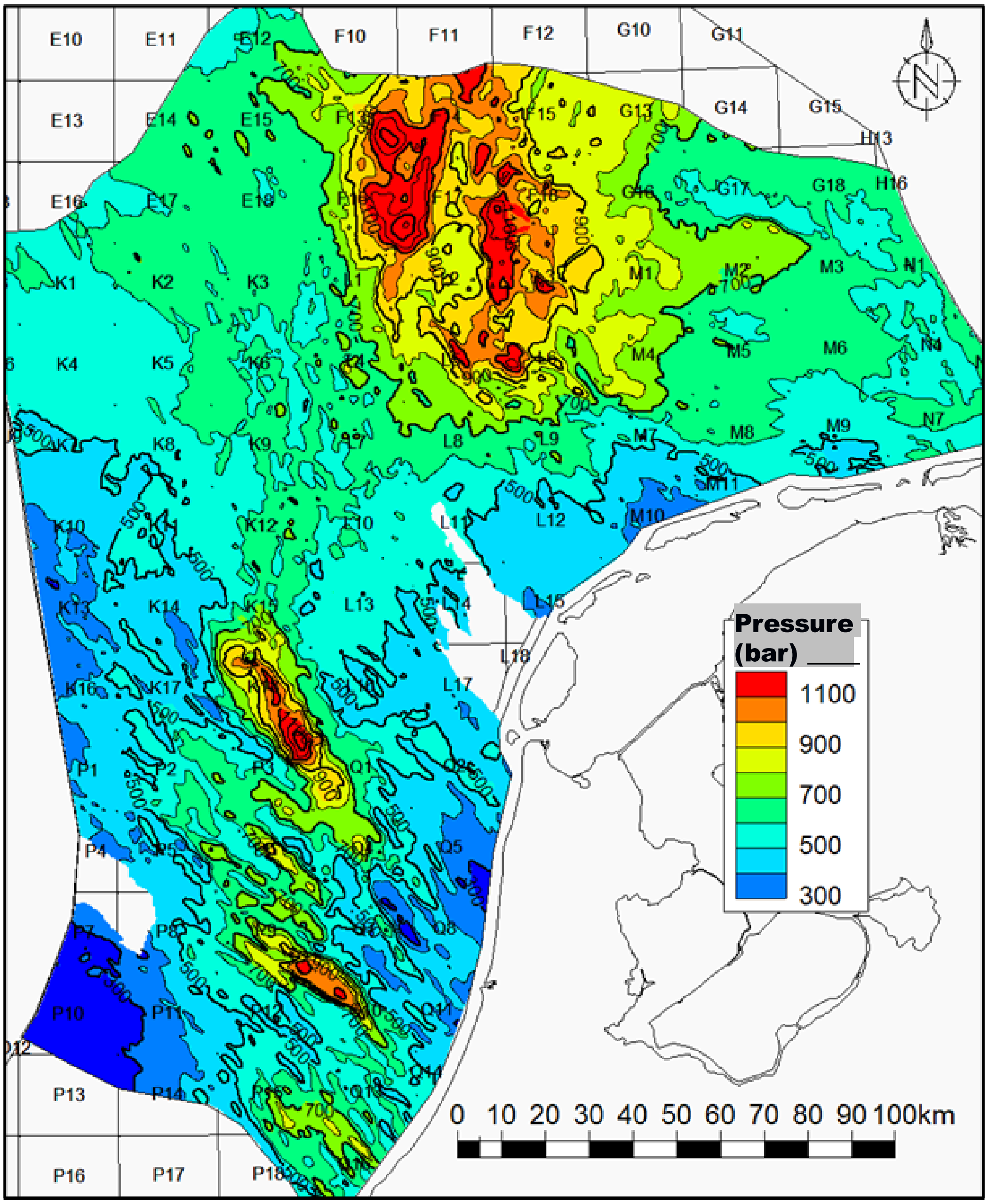

Map 11 - LOT Lower Bound pressures. The creation process and methodology of the map are elaborated in Section 3.2.4 of this report.

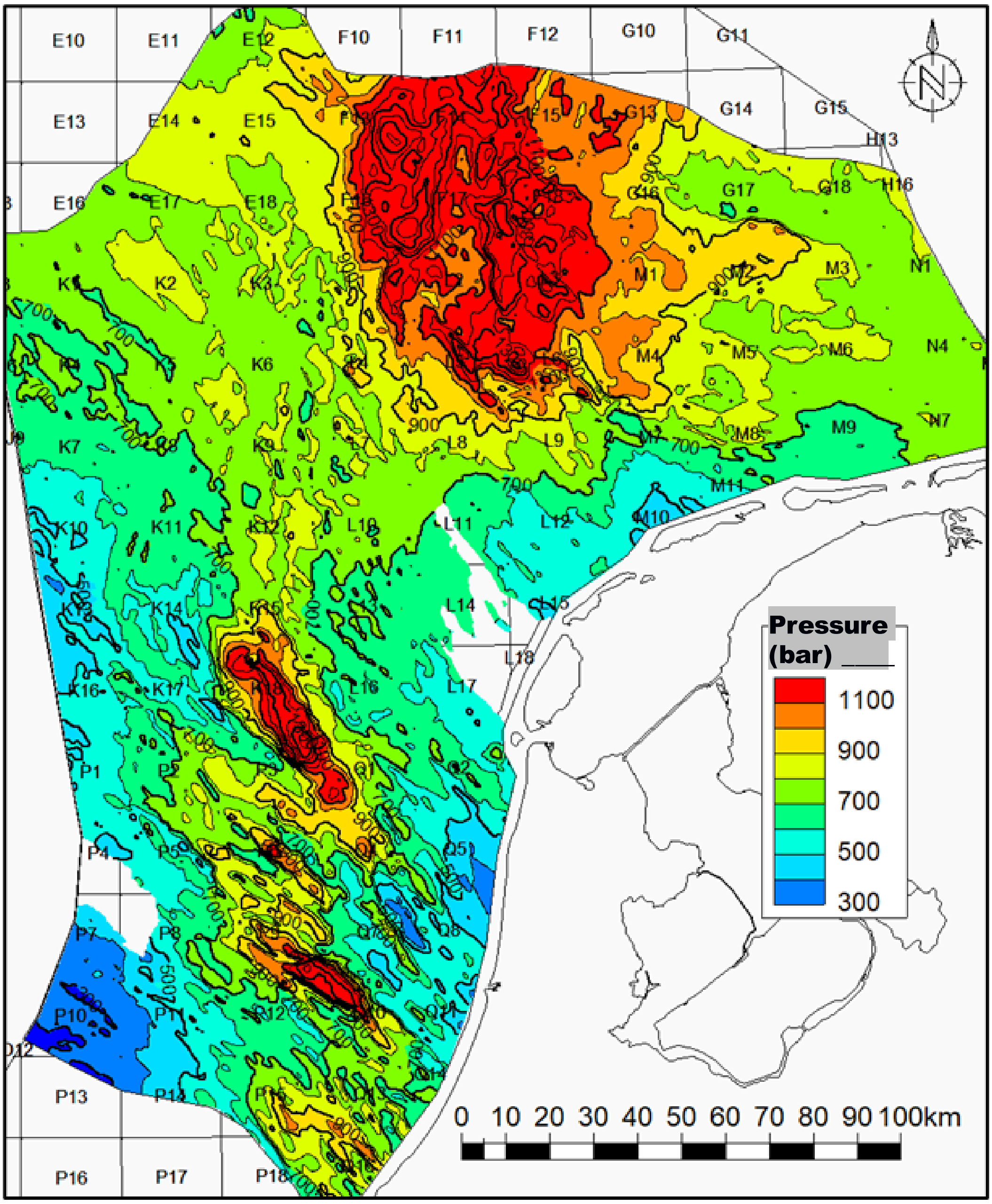

Map 12 - Fracture Gradient pressures. The creation process and methodology of the map are elaborated in Section 3.2.4 of this report.

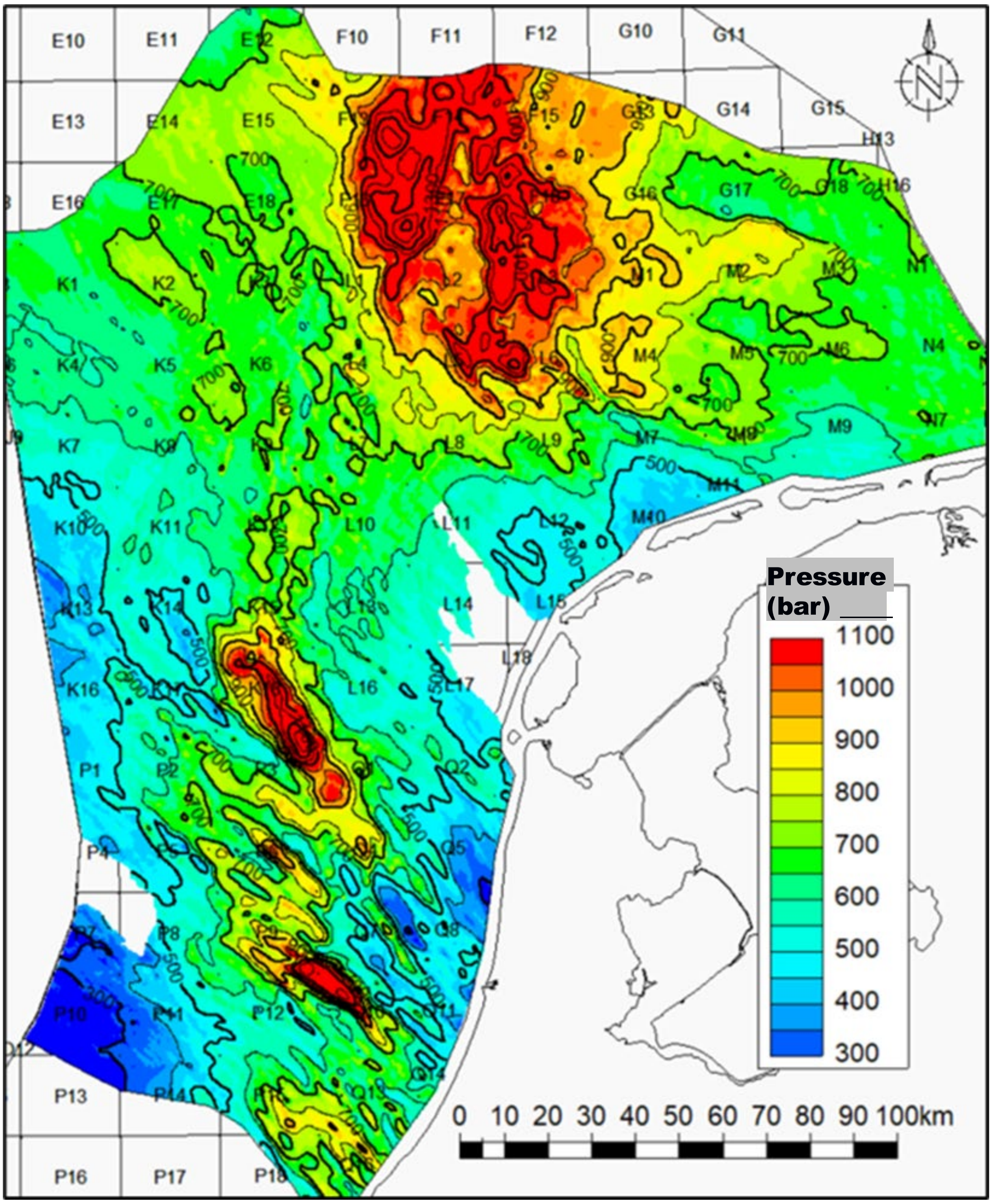

Map 13 - Mid LB-FG gradient pressures (bar). The creation process and methodology of the map are elaborated in Section 3.2.4 of this report.

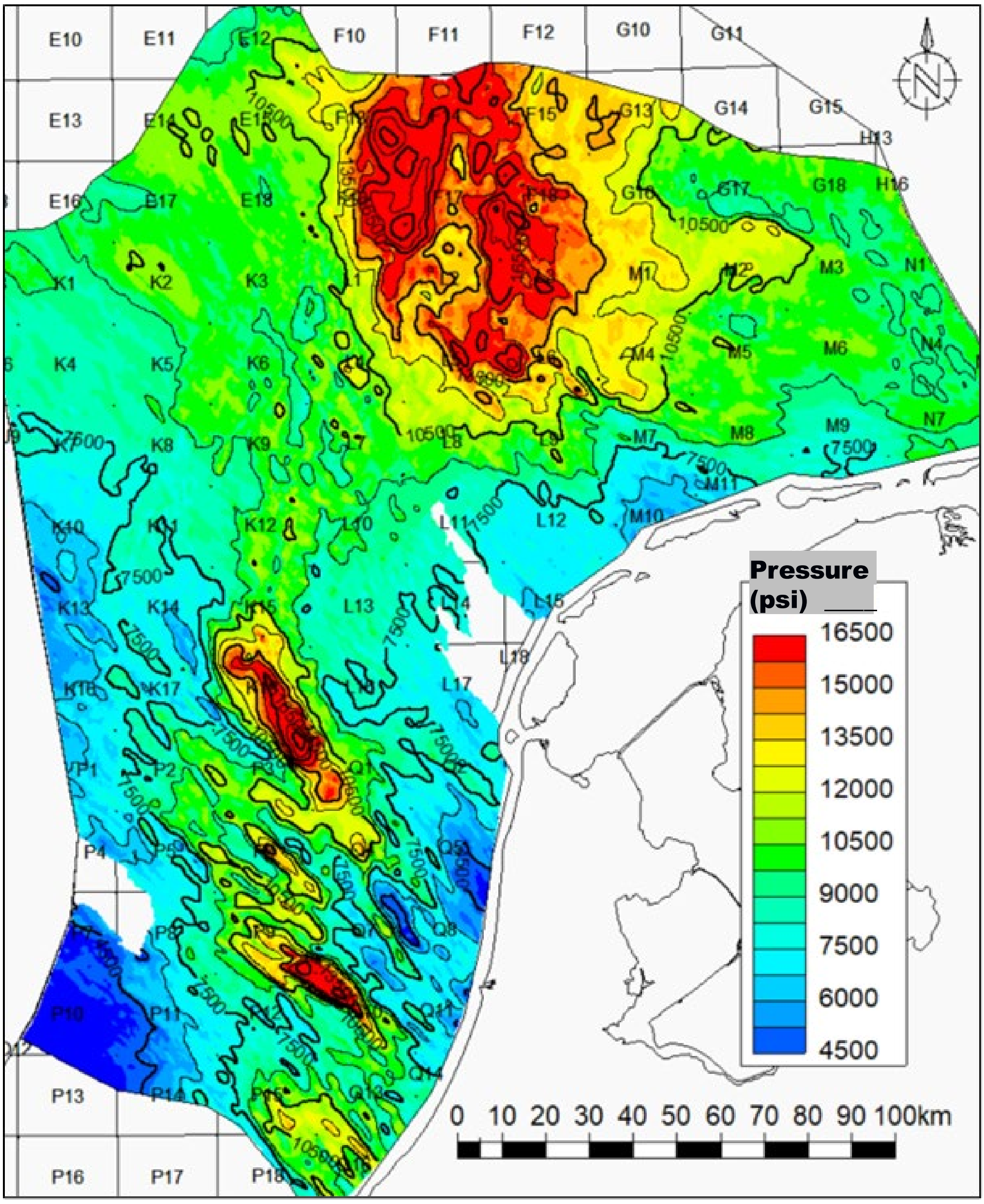

Map 14 - Mid LB-FG gradient pressures (psi). The creation process and methodology of the map are elaborated in Section 3.2.4 of this report.

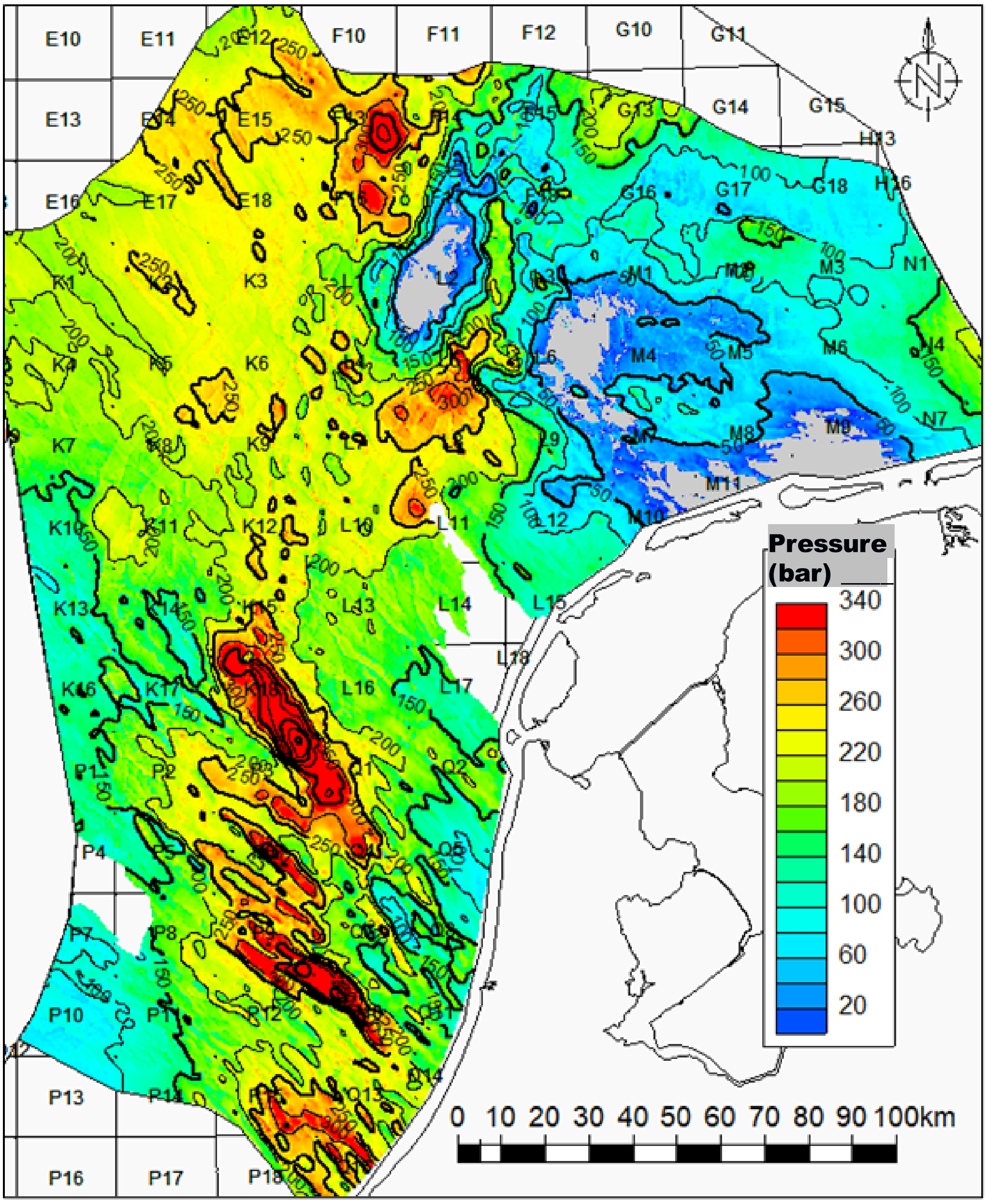

Map 15 - Delta P (ΔP) pressures. The creation process and methodology of the map are elaborated in Section 3.2.5 of this report.

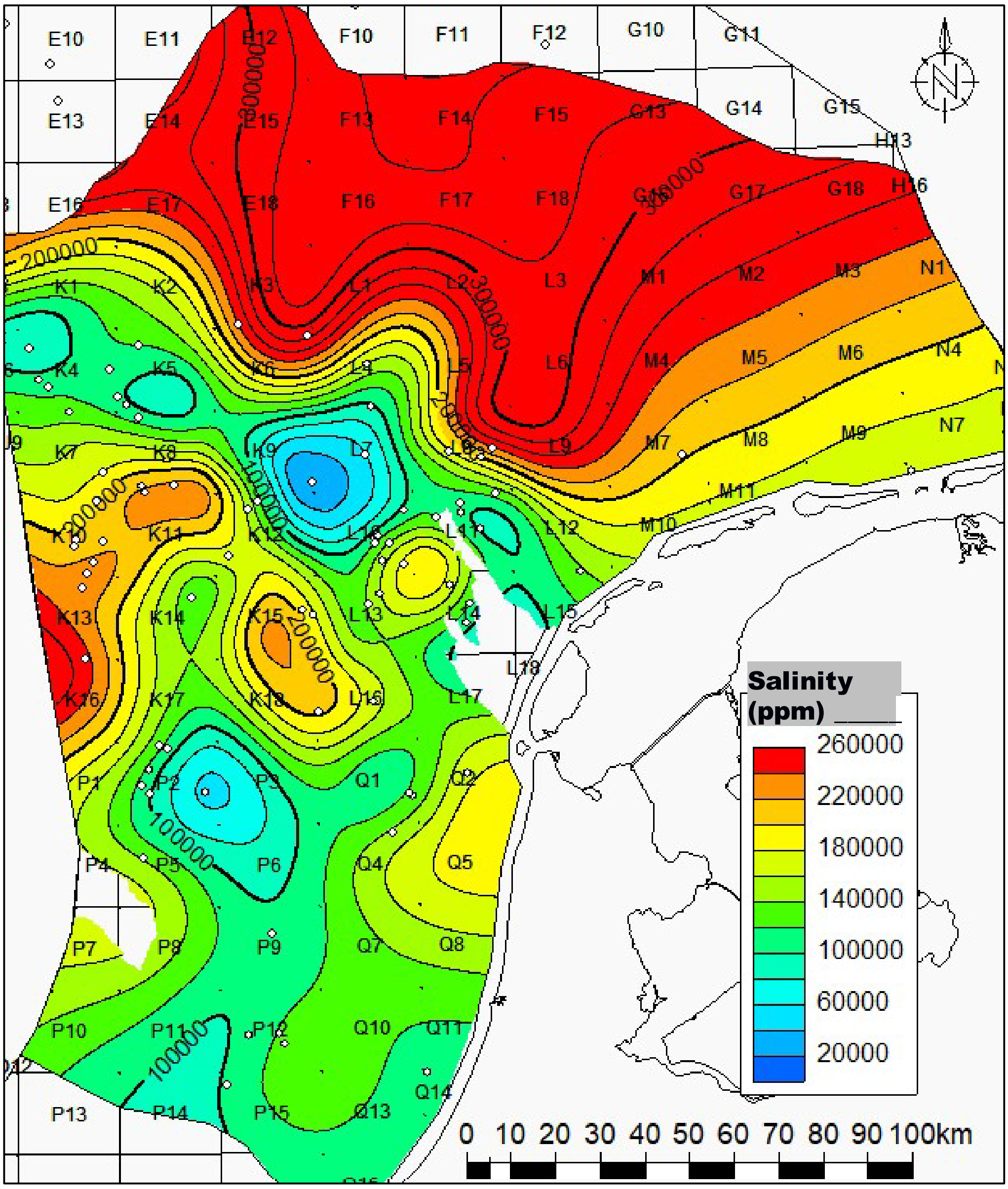

Map 16 – Salinity of the Rotliegend aquifer. The creation process and methodology of the map are elaborated in Section 3.3.1 of this report.

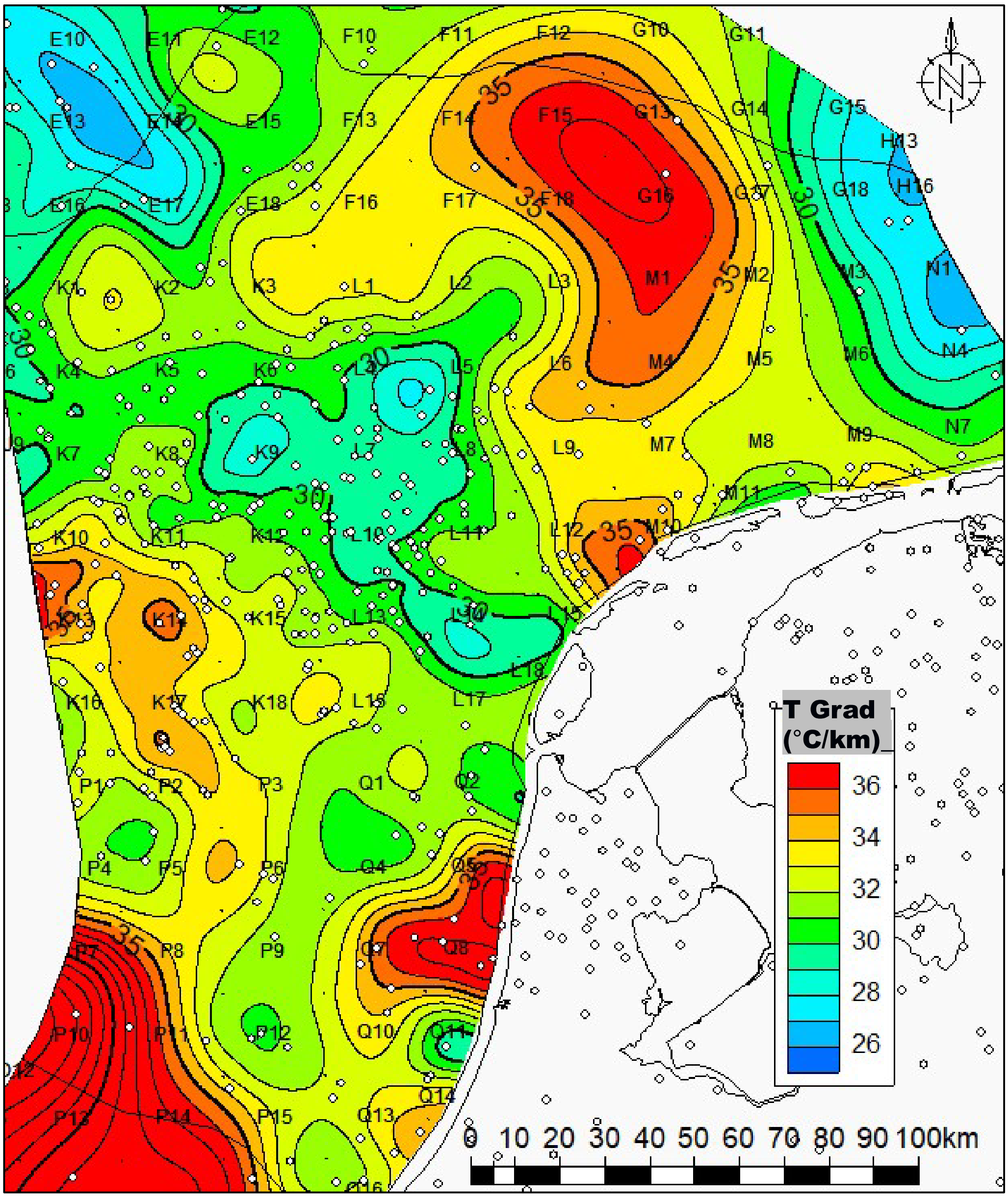

Map 17 - Temperature gradient of the Rotliegend aquifer. The creation process and methodology of the map are elaborated in Section 3.3.1 of this report.

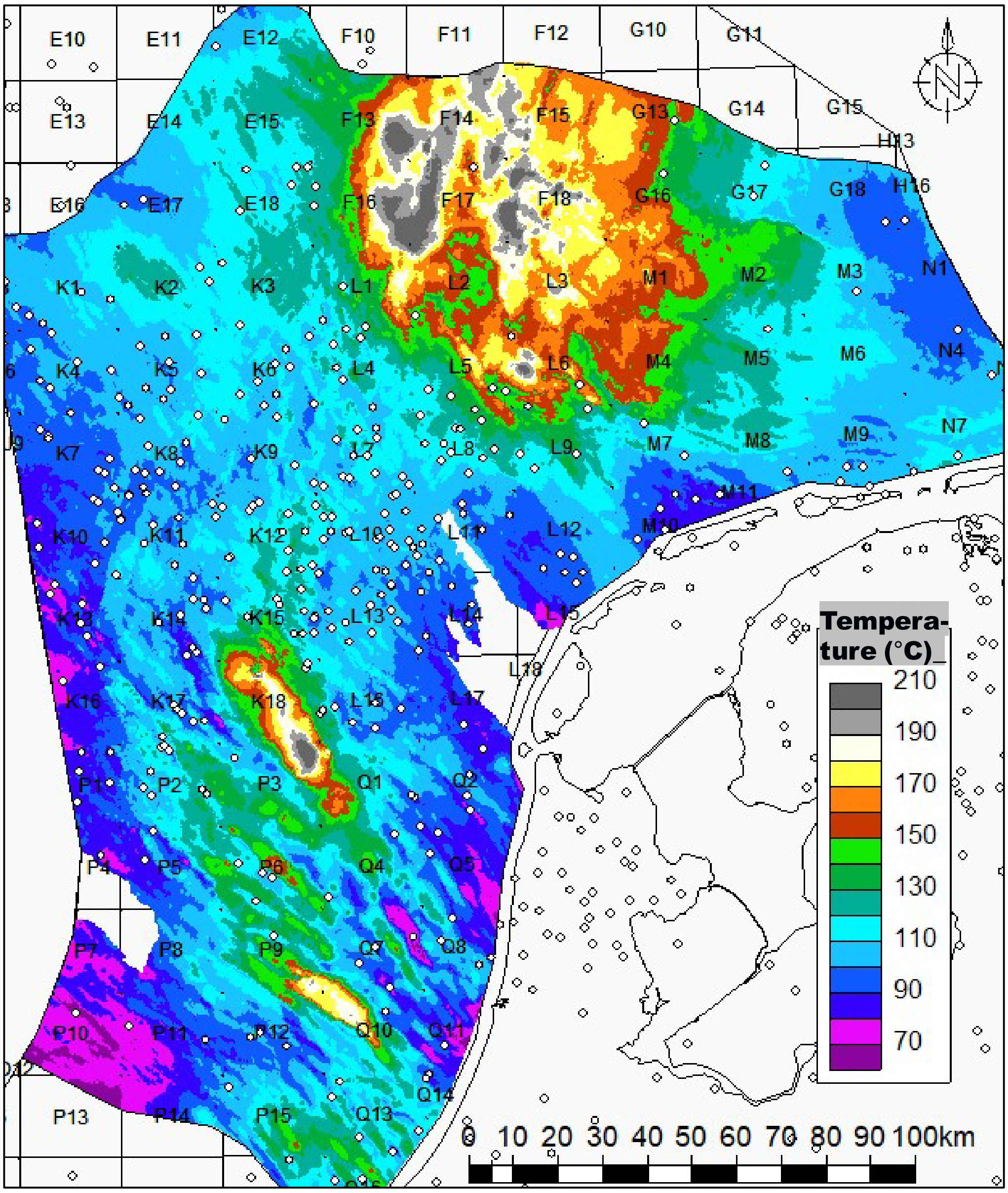

Map 18 - Temperature of the Rotliegend aquifer (°C). The creation process and methodology of the map are elaborated in Section 3.3.1 of this report.

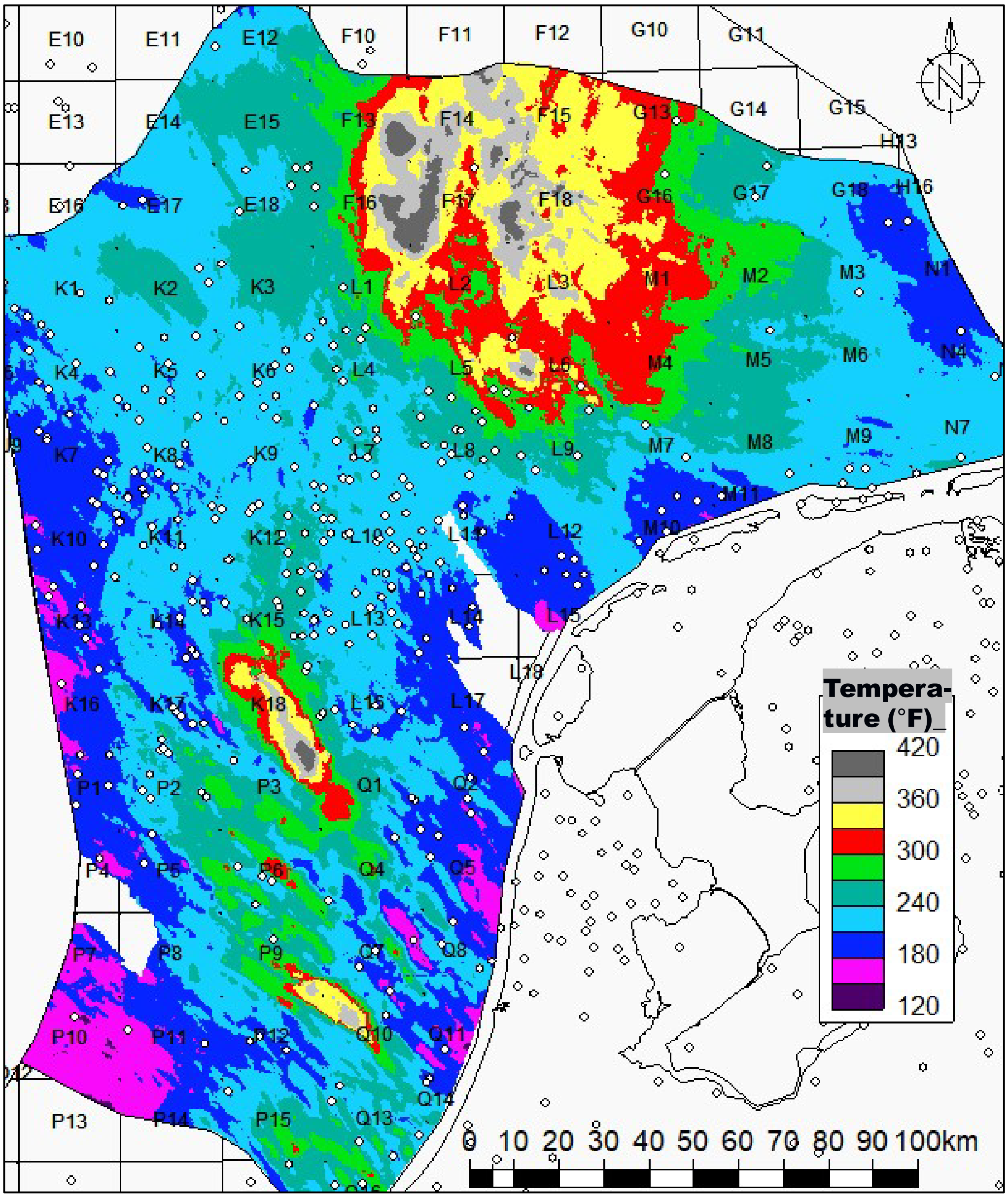

Map 19 - Temperature of the Rotliegend aquifer (°F). The creation process and methodology of the map are elaborated in Section 3.3.1 of this report.

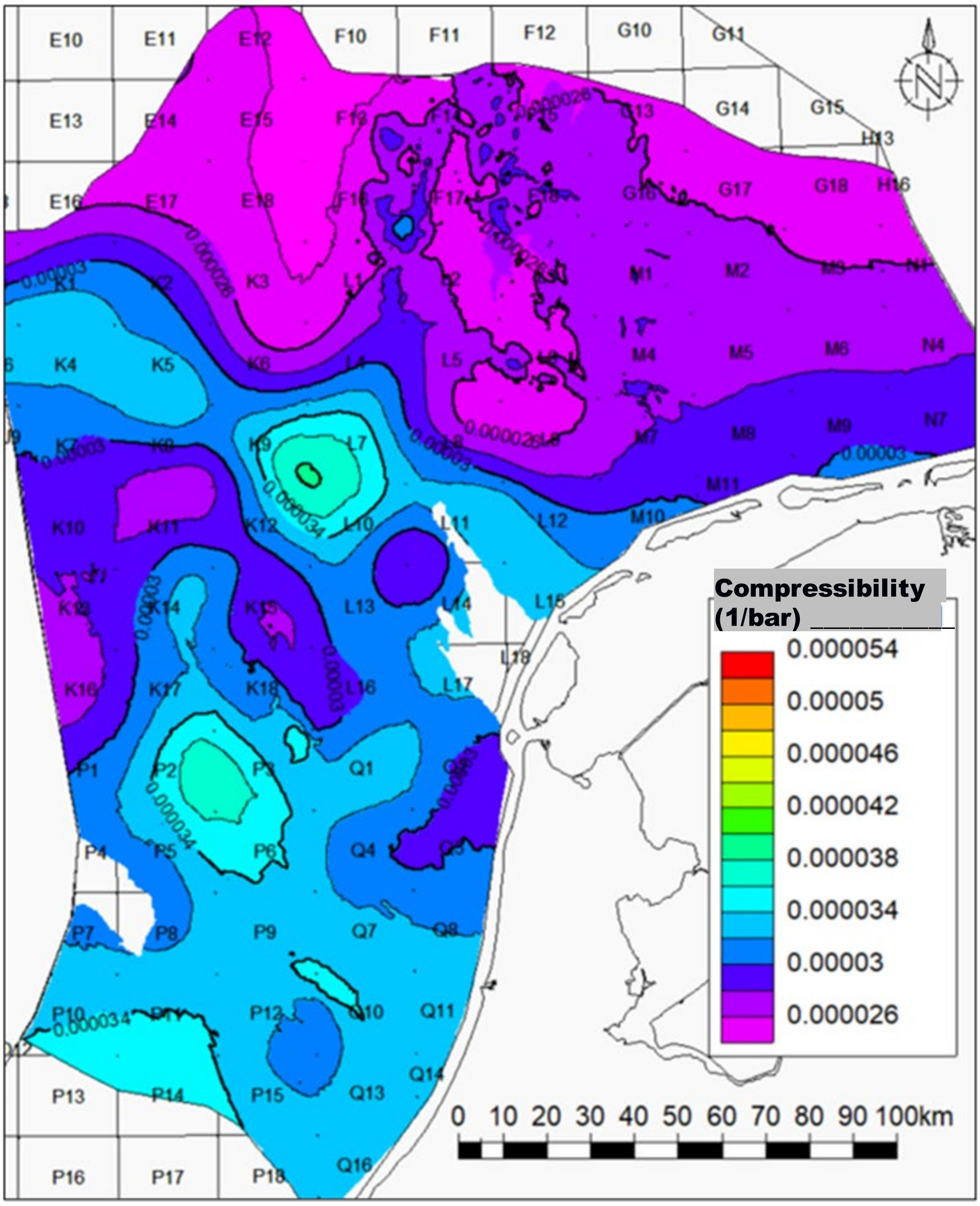

Map 20 – Water compressibility, Rotliegend aquifer. The creation process and methodology of the map are elaborated in Section 3.3.1 of this report.

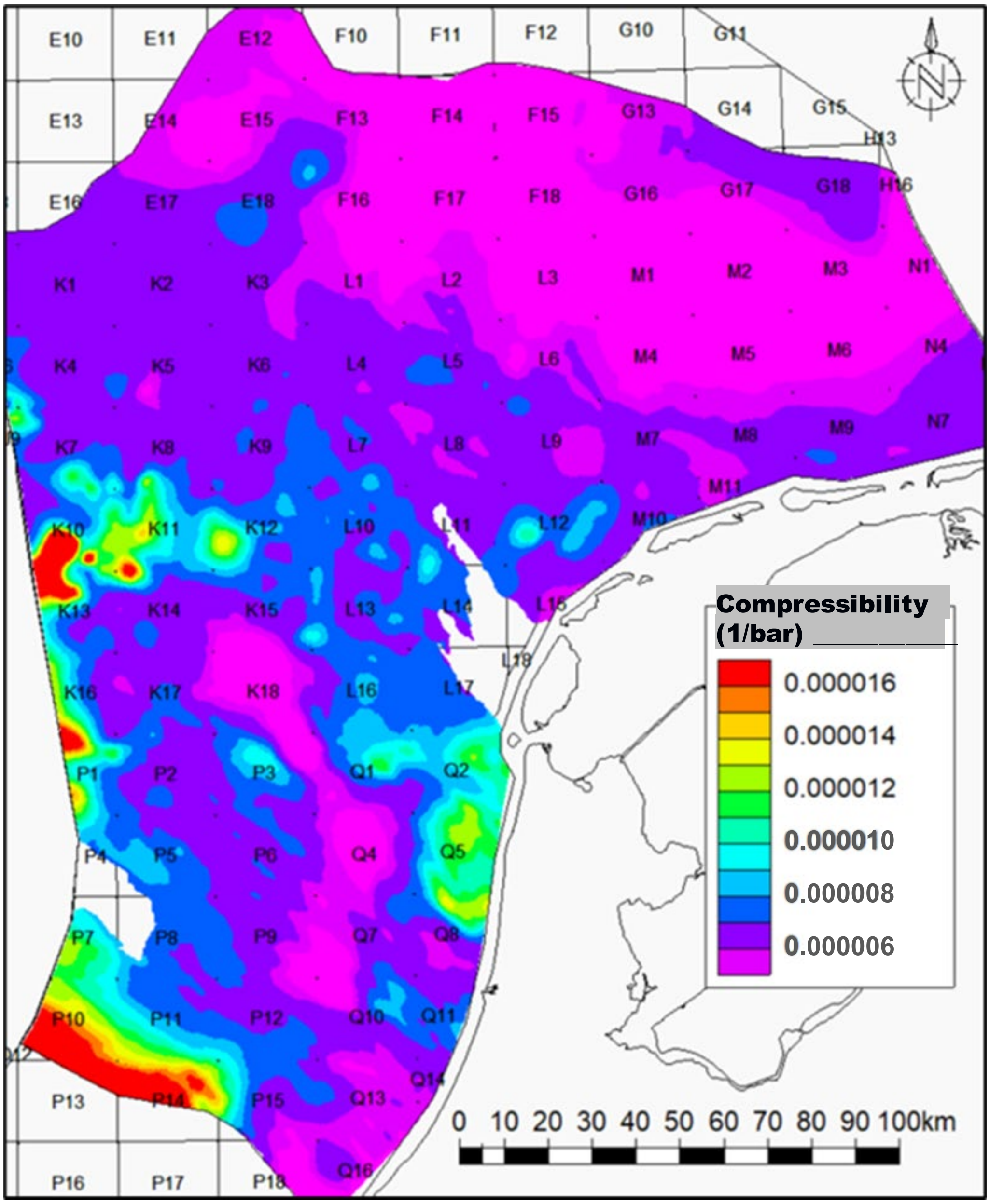

Map 21 - Frame compressibility of the Rotliegend aquifer. The creation process and methodology of the map are elaborated in Section 3.3.2 of this report. For methodology see also Reference 5.

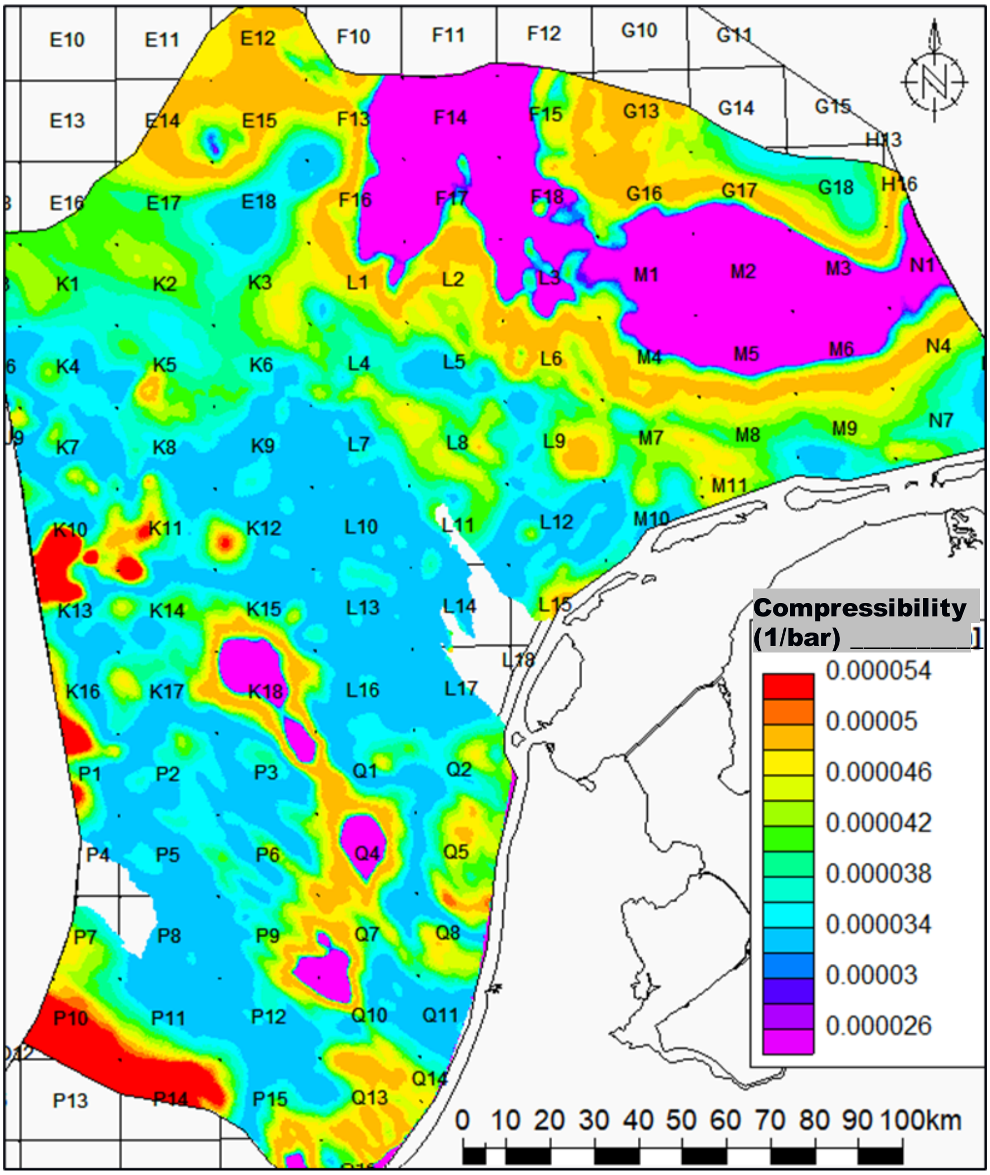

Map 22 - Pore compressibility of the Rotliegend aquifer. The creation process and methodology of the map are elaborated in Section 3.3.2 of this report. For methodology see also Reference 5.

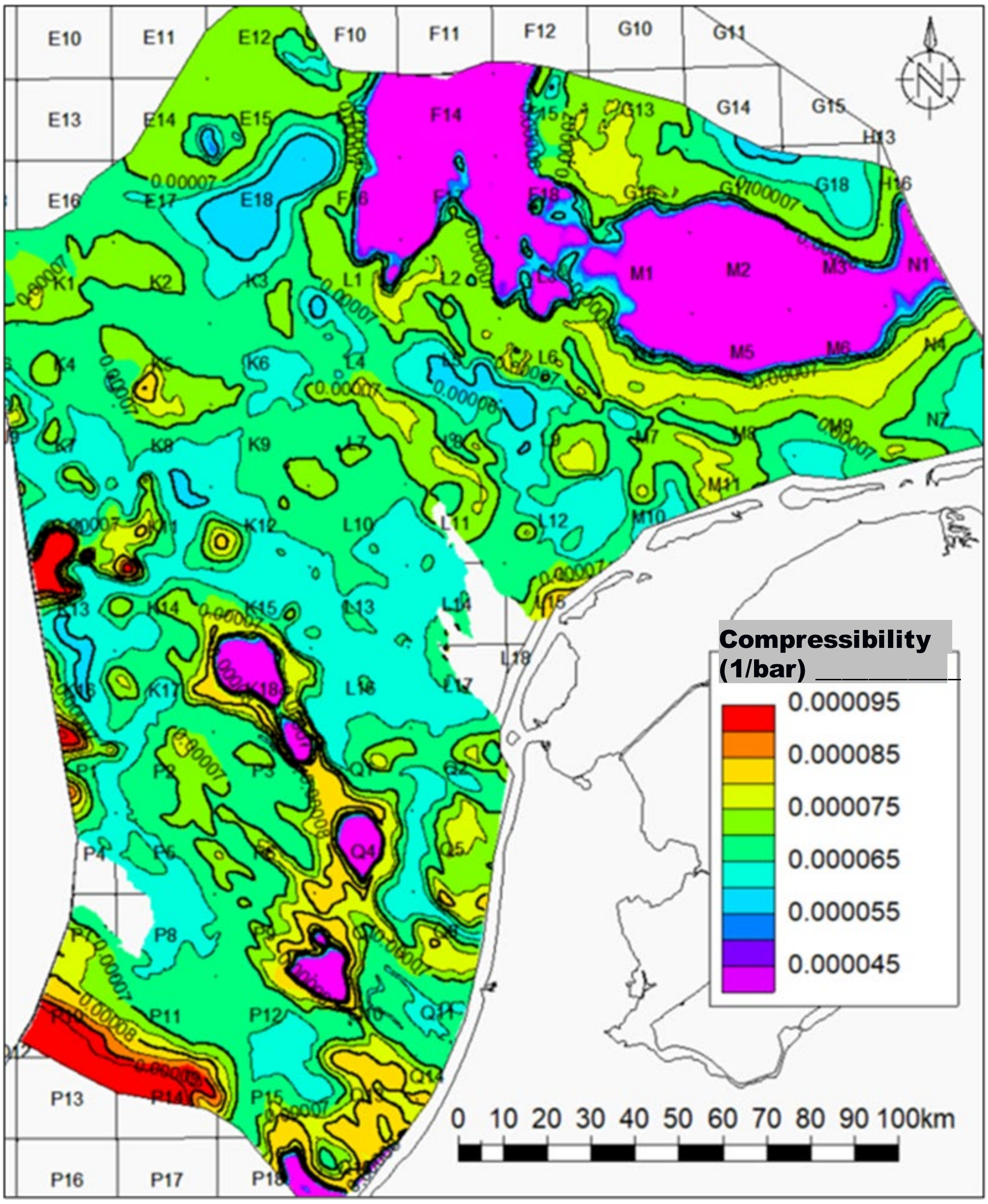

Map 23 - Total compressibility of the Rotliegend aquifer. The creation process and methodology of the map are elaborated in Section 3.3.3 of this report. For methodology see also Reference 5.

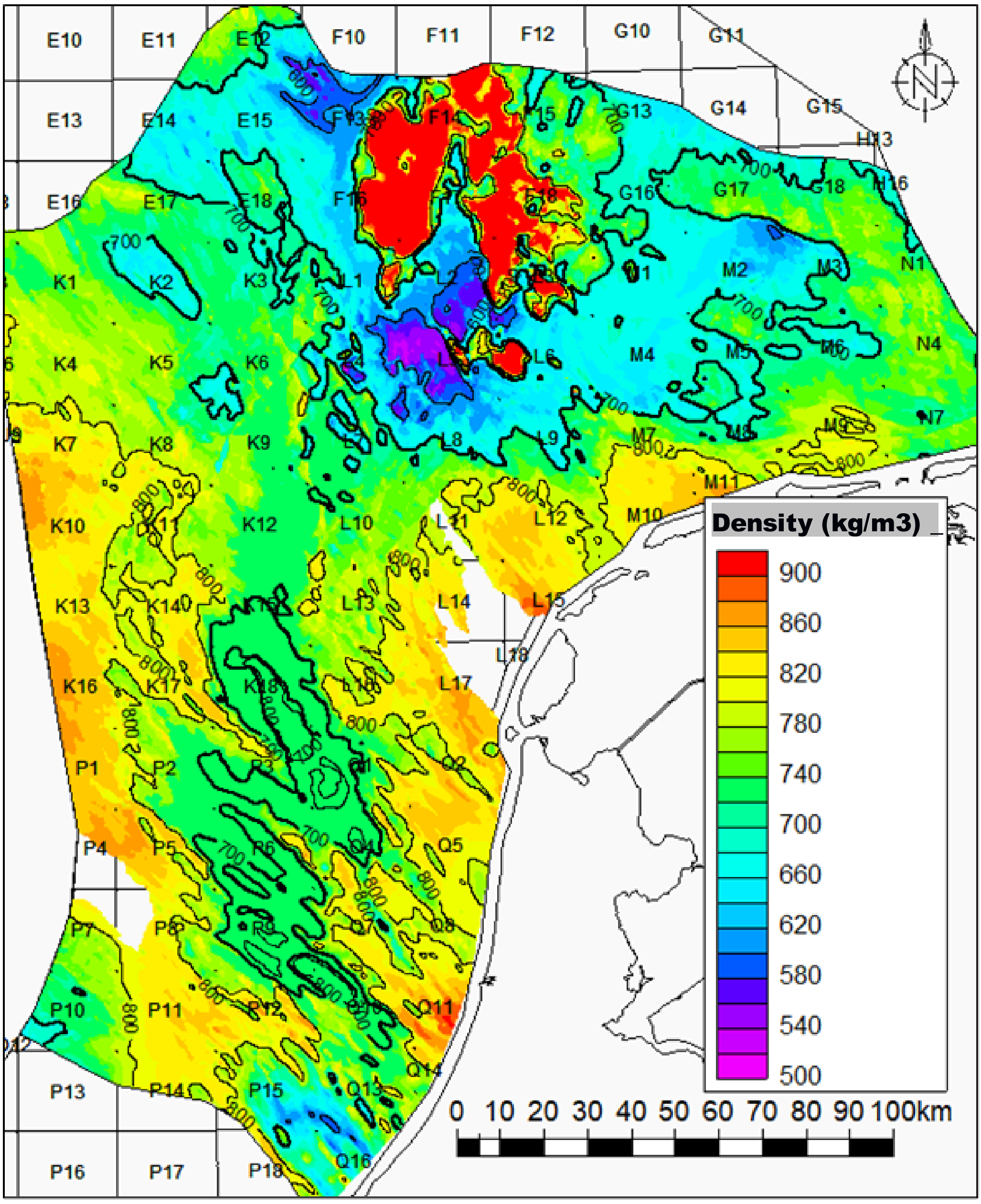

Map 24 - CO_2 plume density of the Rotliegend aquifer. The creation process and methodology of the map are elaborated in Section 3.4 of this report

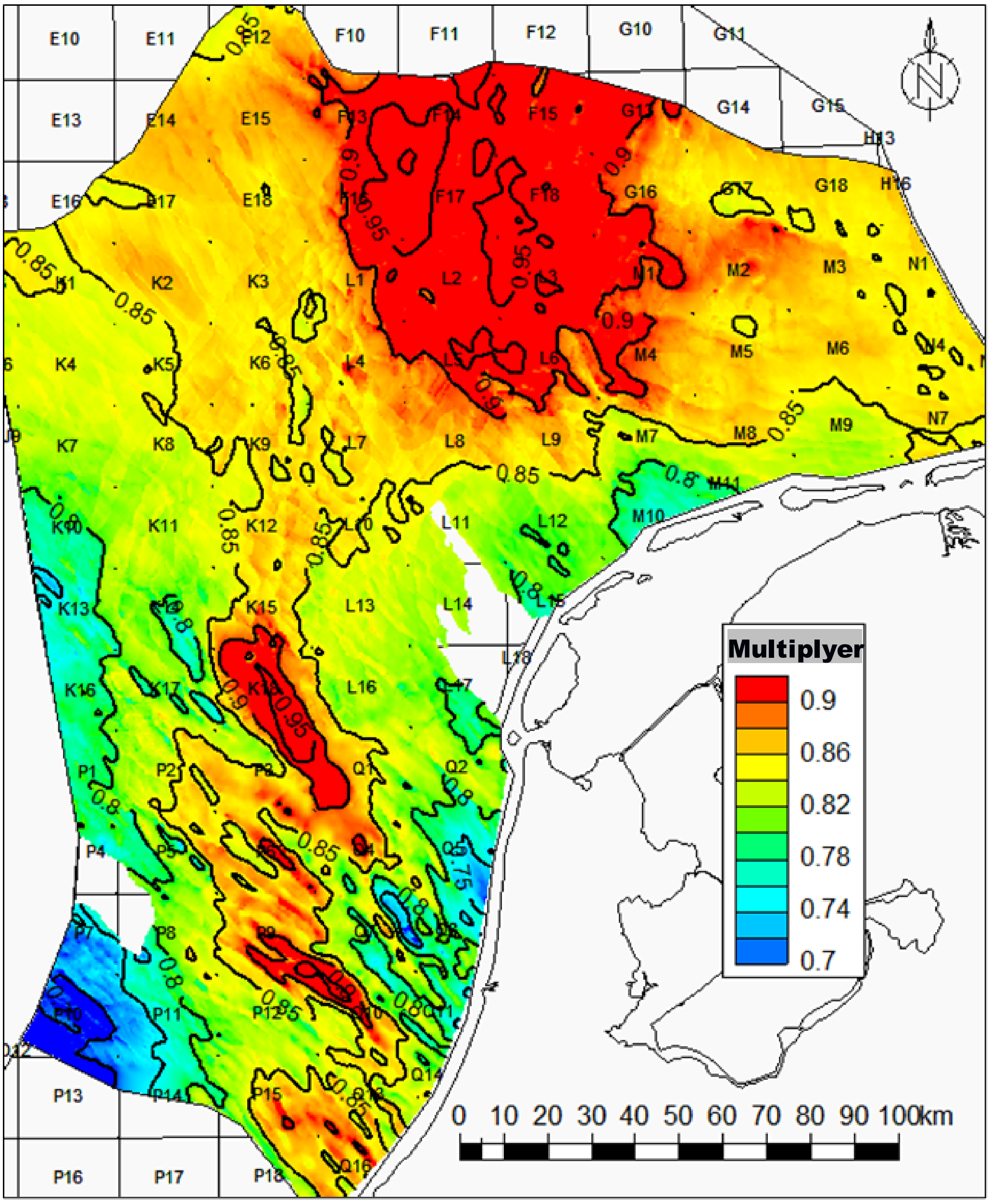

Map 25 - Correction factor. The creation process and methodology of the map are elaborated in Section 0 of this report.

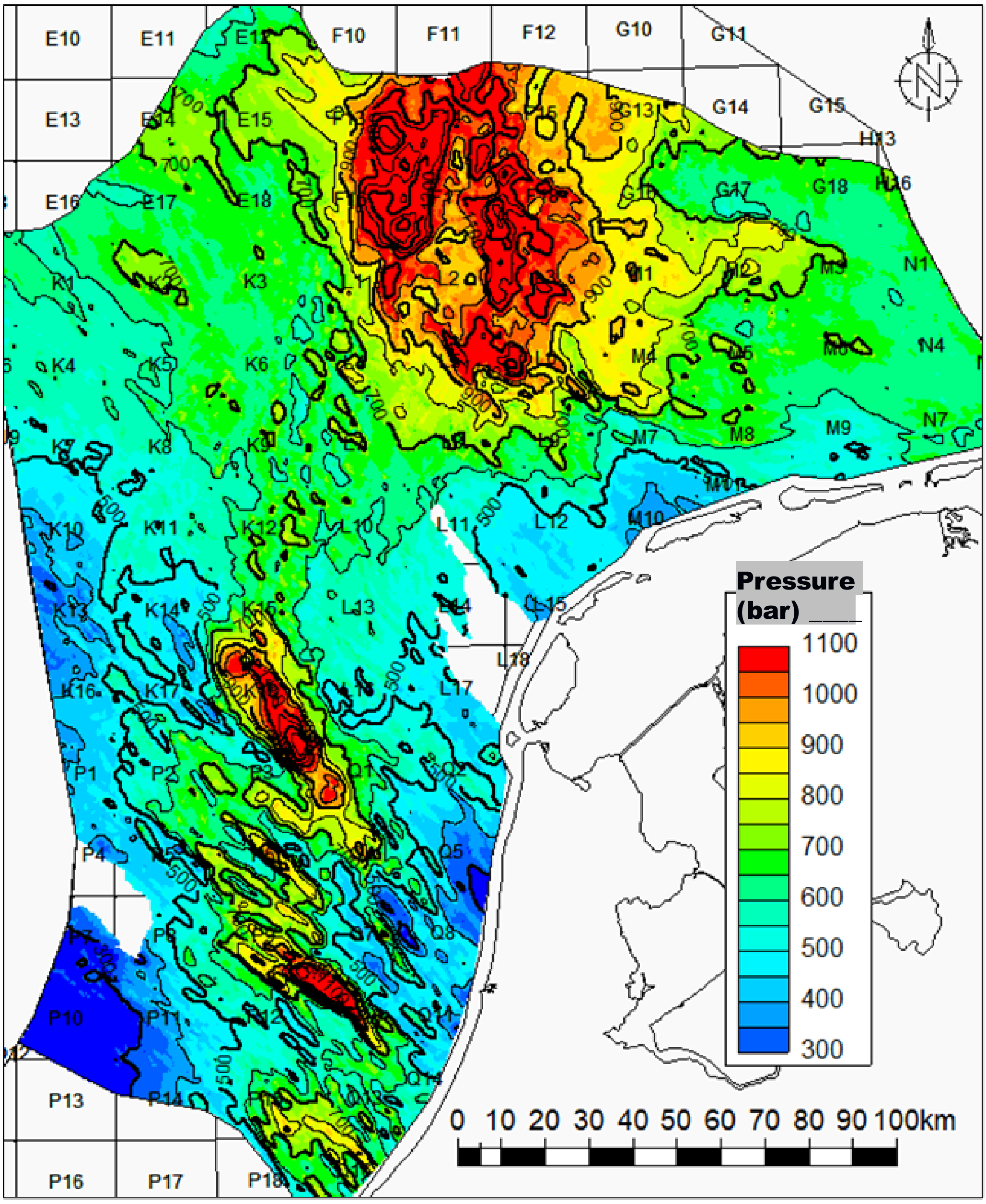

Map 26 - Mid LB-FG gradient pressures corrected (bar). The creation process and methodology of the map are elaborated in Section 0 of this report.

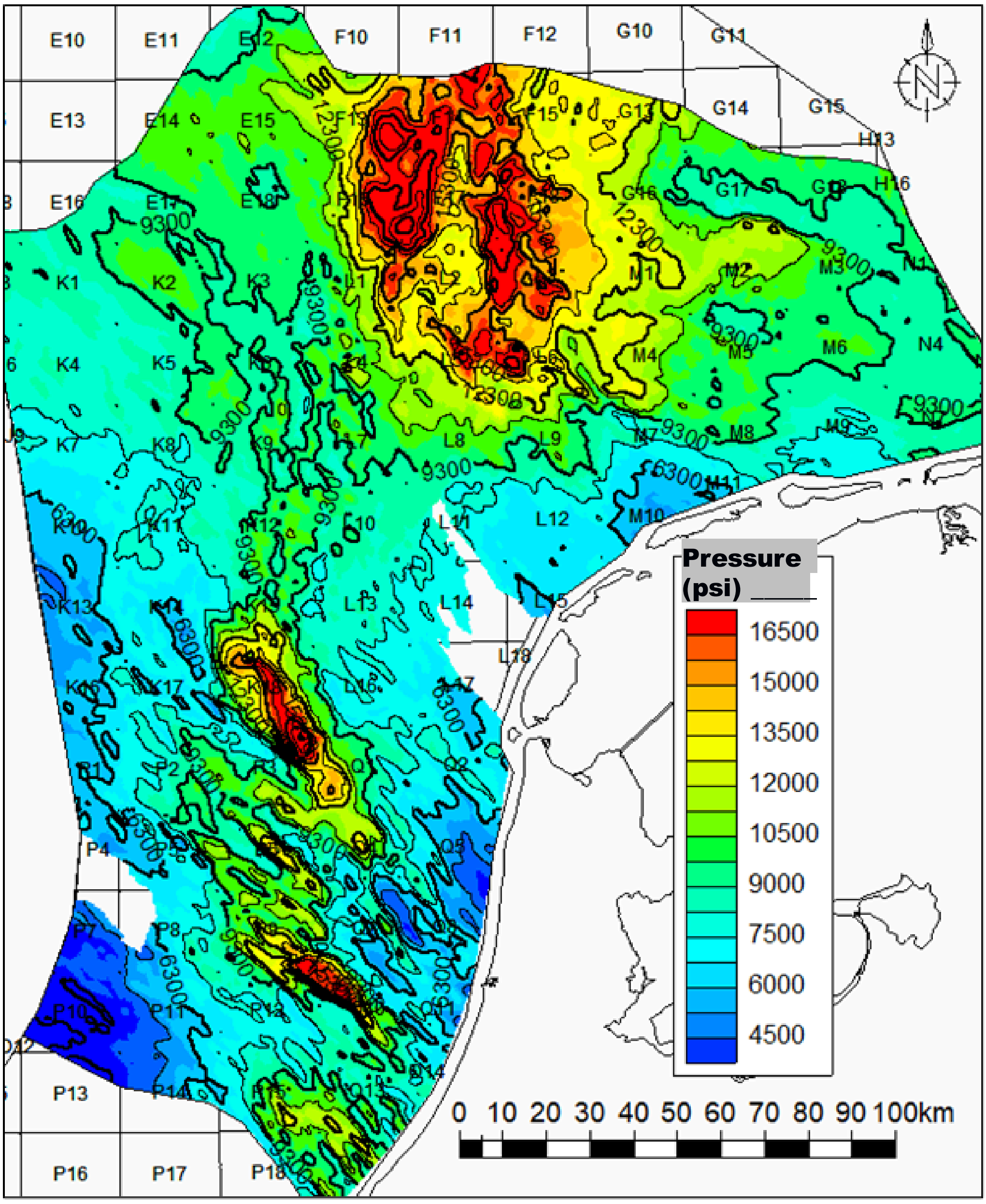

Map 27 - Mid LB-FG gradient pressures corrected (psi). The creation process and methodology of the map are elaborated in Section 3.5.3 of this report.

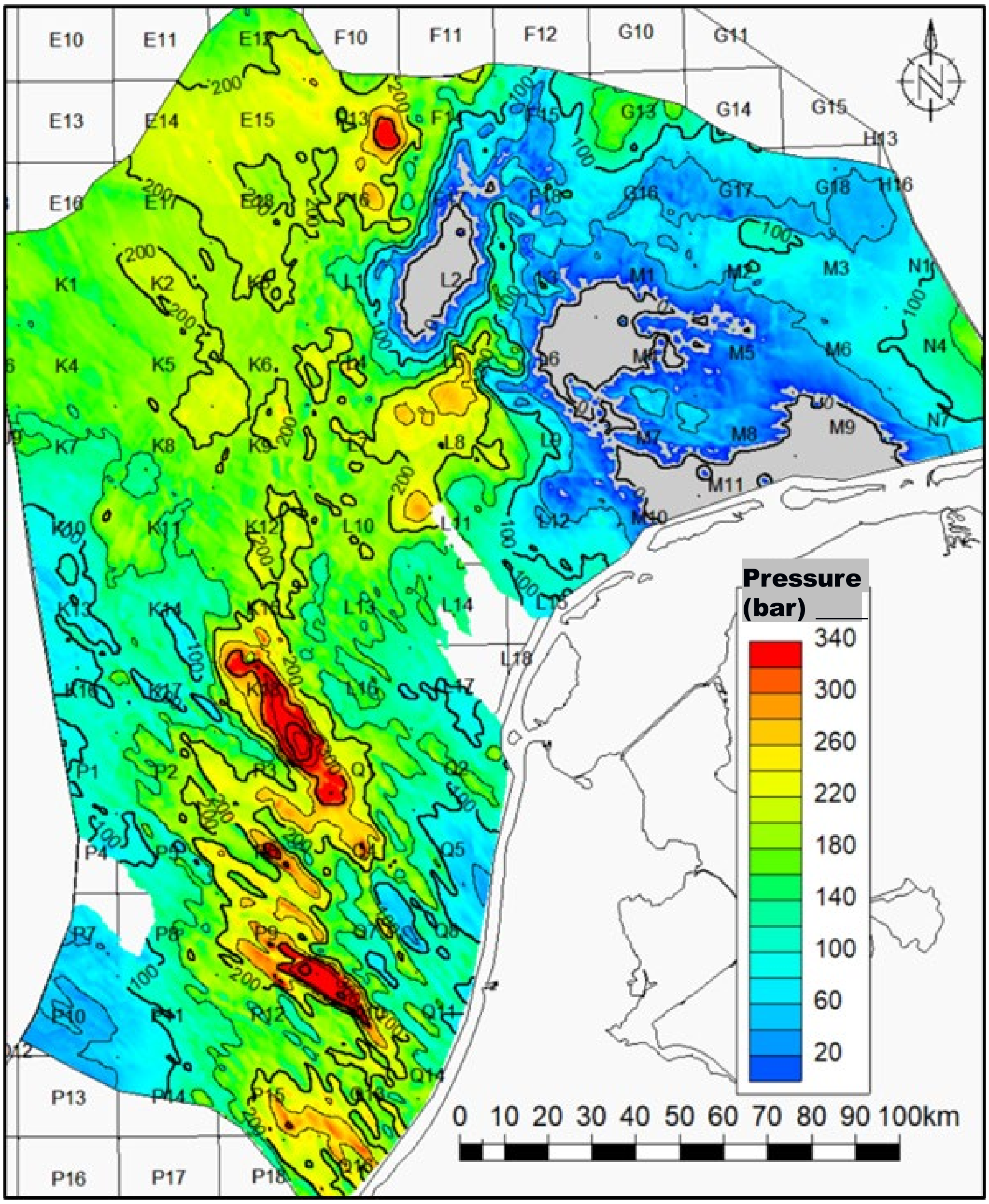

Map 28 - Delta P (ΔP) pressures corrected, Rotliegend aquifer. The creation process and methodology of the map are elaborated in Section 3.5.1 of this report.

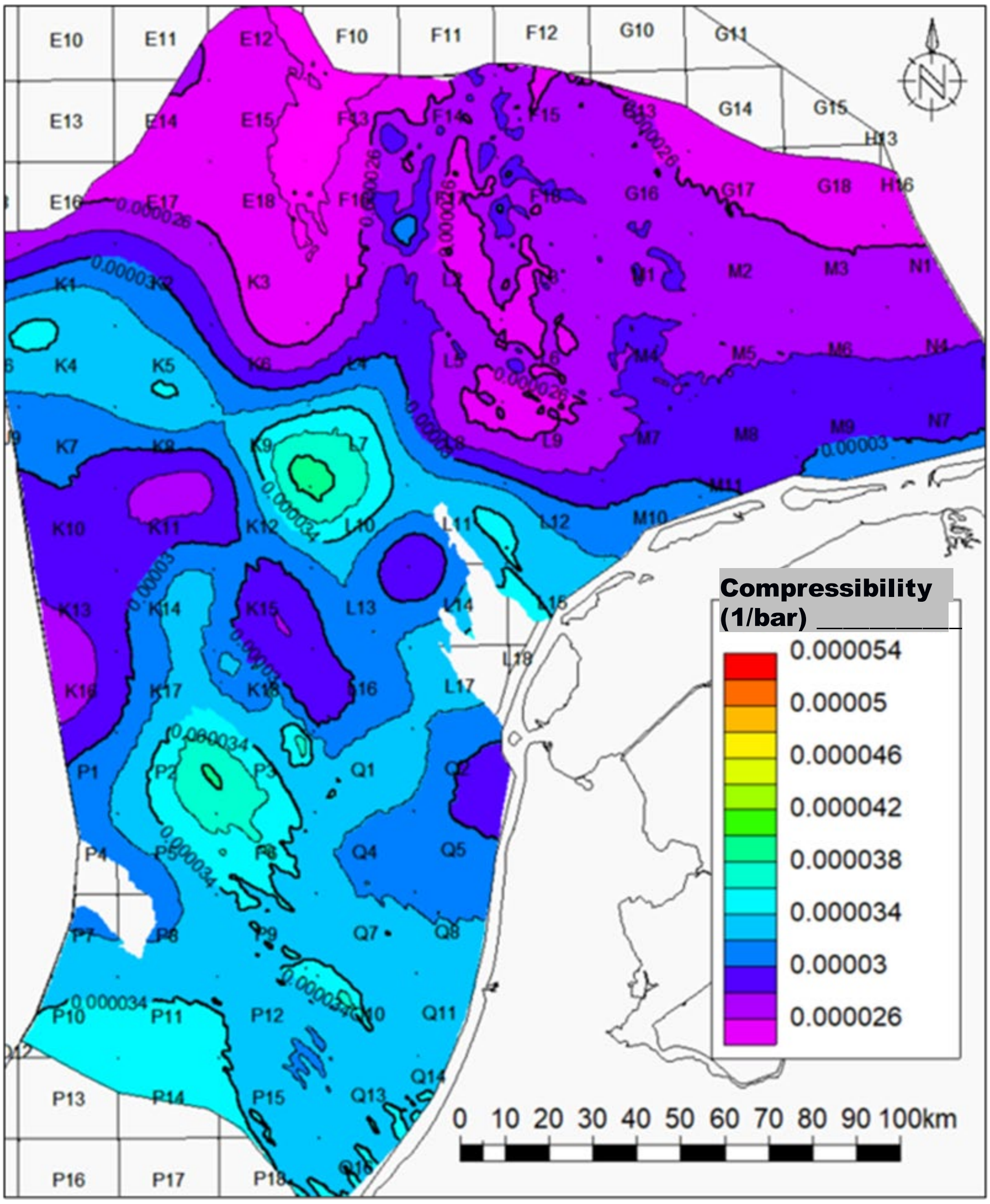

Map 29 - Water compressibility corrected, Rotliegend aquifer. The creation process and methodology of the map are elaborated in Section 3.5.2 of this report.

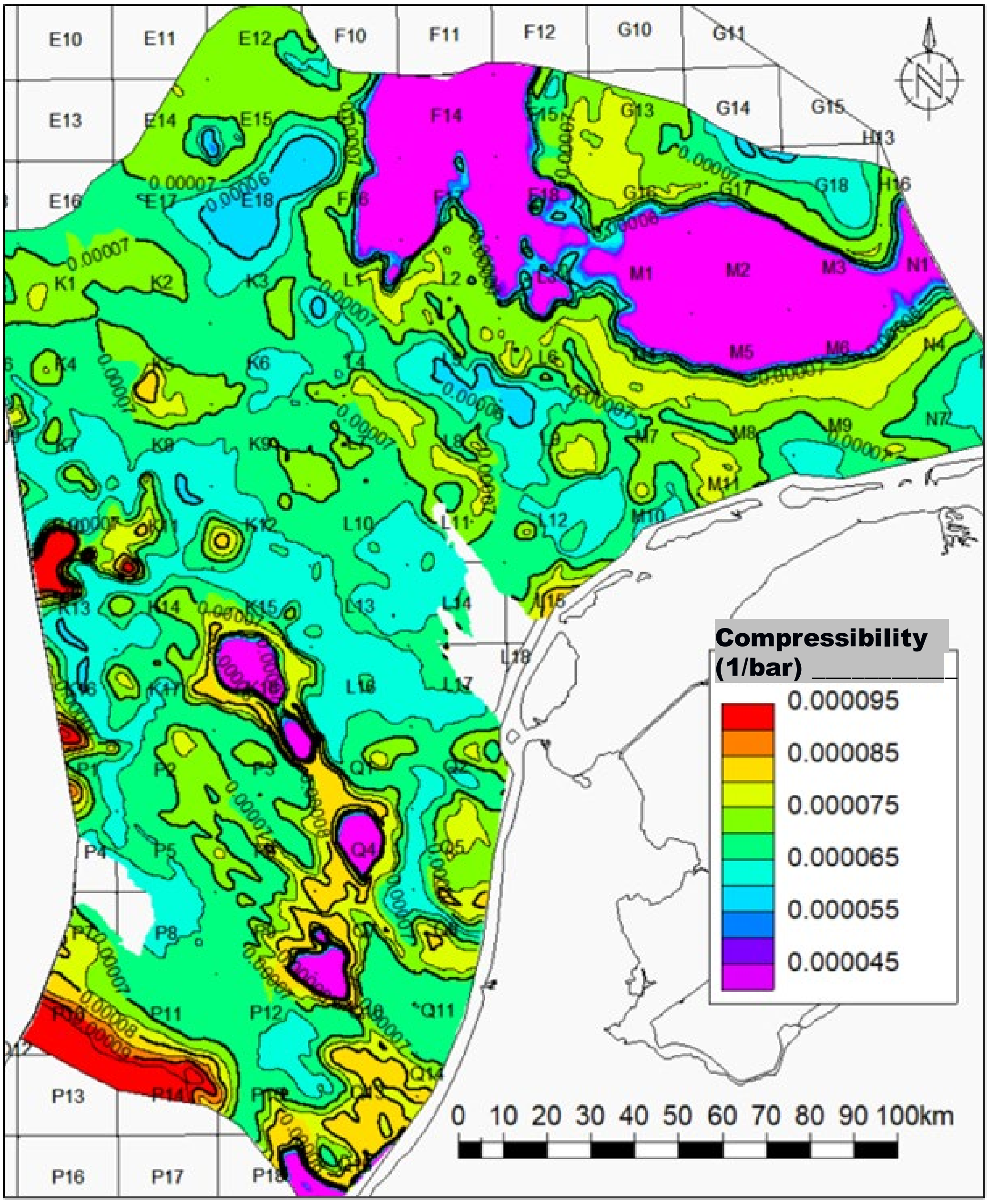

Map 30 - Total compressibility corrected, Rotliegend aquifer. The creation process and methodology of the map are elaborated in Section 3.5.2 of this report.

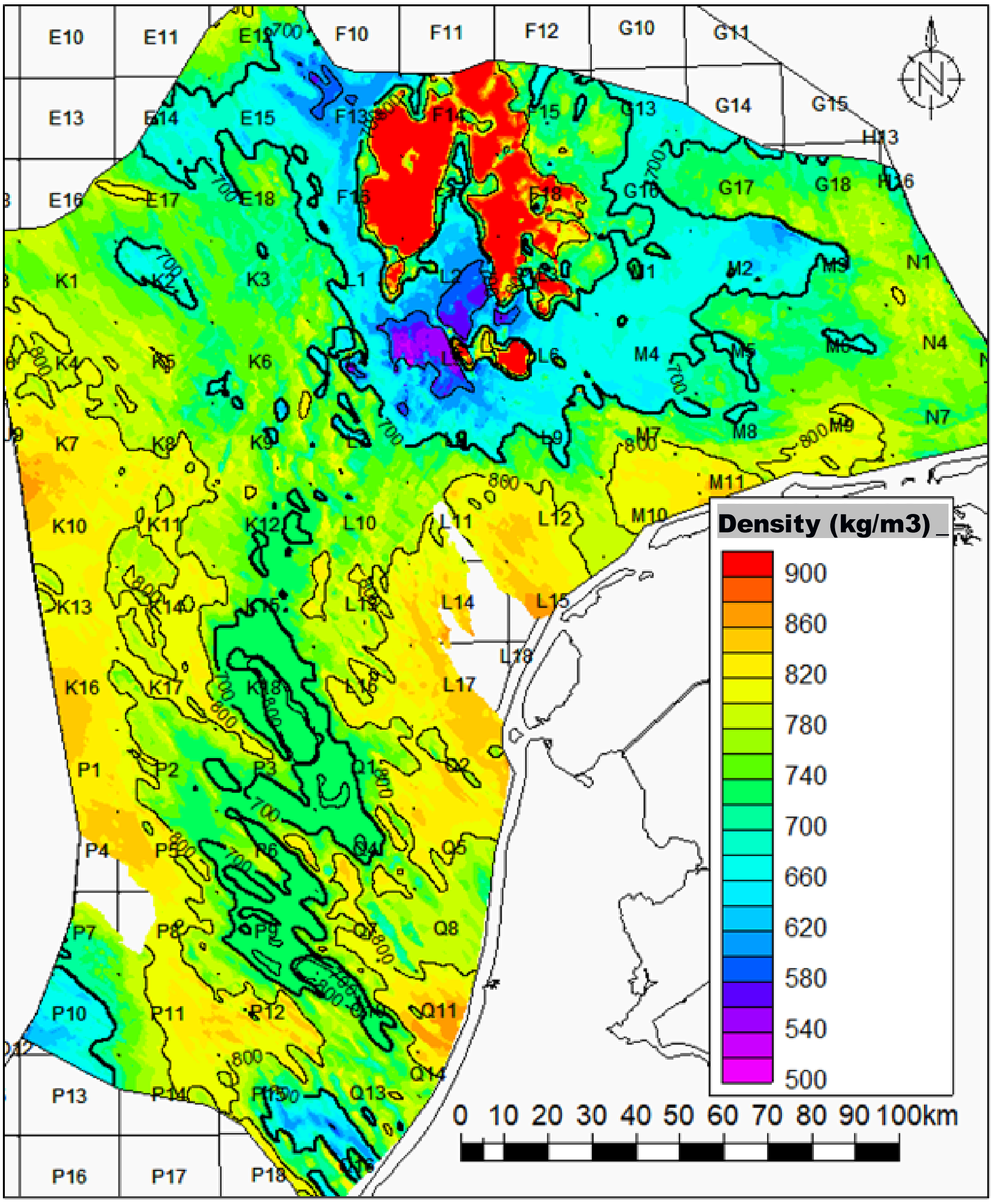

Map 31 - CO_2 plume density corrected, Rotliegend aquifer. The creation process and methodology of the map are elaborated in Section 3.5.3 of this report.

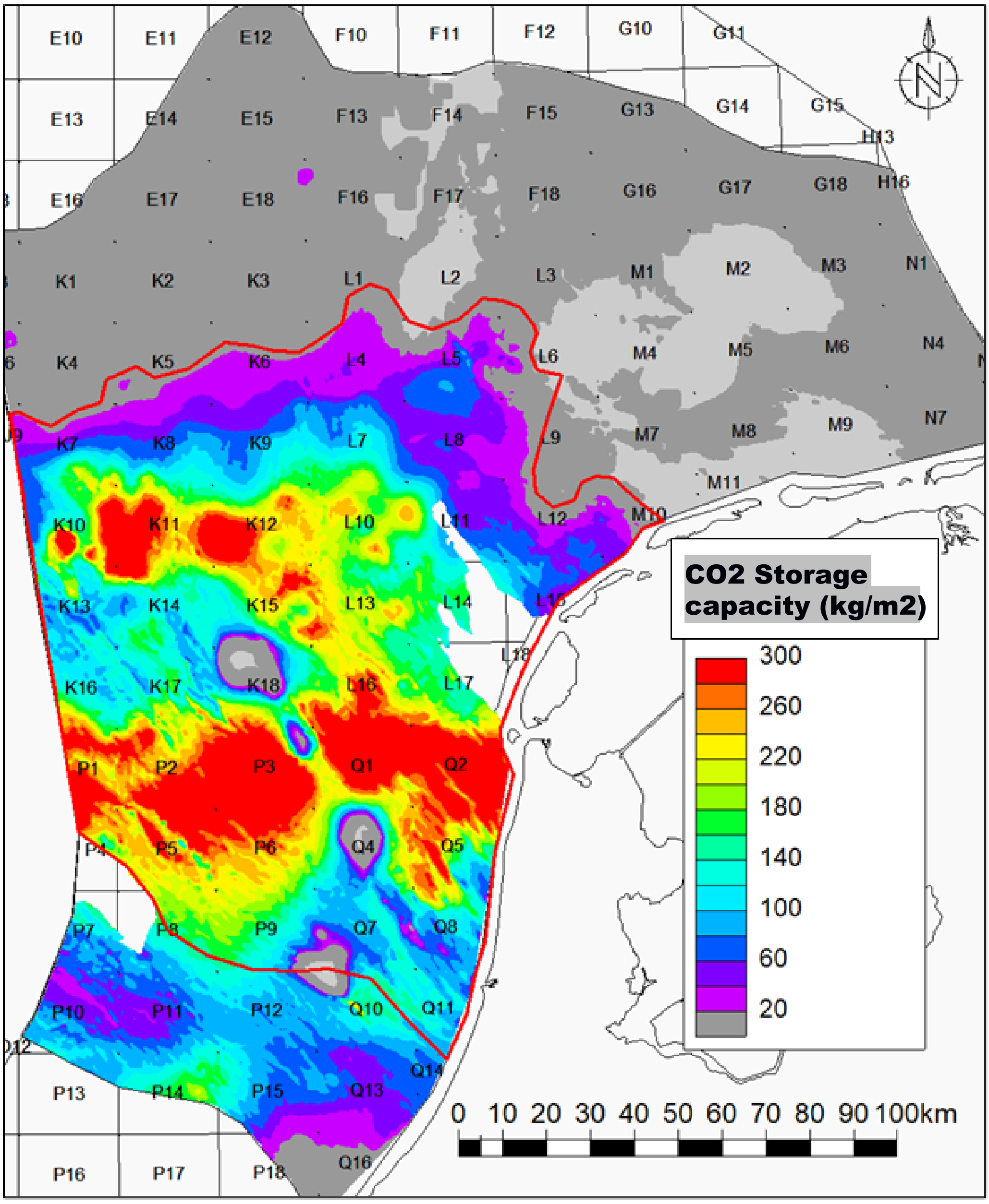

Map 32 - Theoretical CO_2 Storage Capacity, Rotliegend aquifer. The creation process and methodology of the map are elaborated in Section 4.1 of this report.

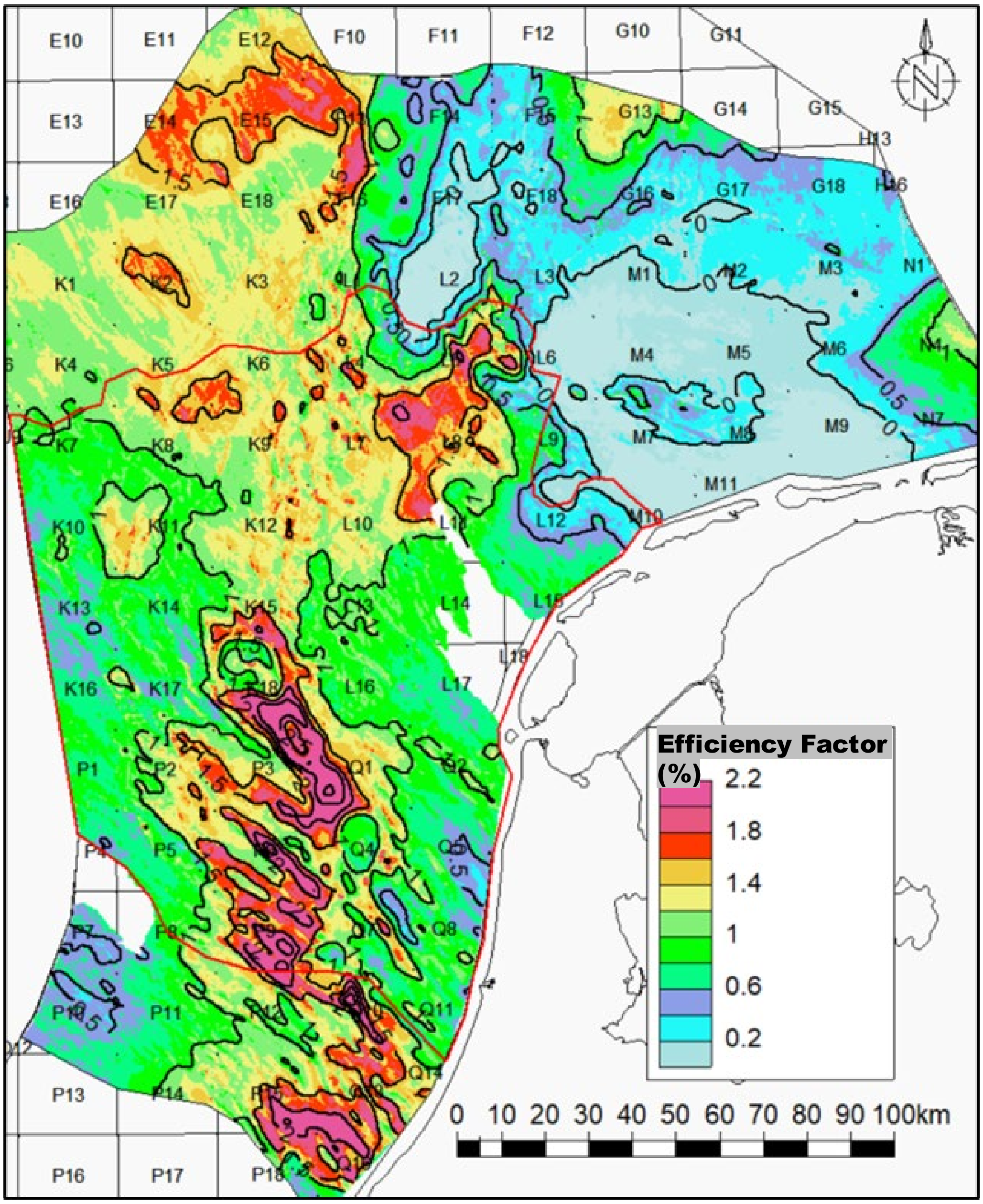

Map 33 - Storage Efficiency Factor, Rotliegend aquifer. The creation process and methodology of the map are elaborated in Section 4.3.2 of this report.

Appendix A - Petrel Equations

The water compressibility map (Cw):

$$C_w = \frac{1}{\left\{10^6\left[0.314+\left(\frac{0.58S}{10^6}\right)+\left(\frac{1.9T}{10^4}\right)-\left(\frac{1.45T^2}{10^6}\right)\right]+\left[(8+(\frac{50S}{10^6})-(\frac{0.125ST}{10^6})\right]p\right\}0.069}$$

S = the salinity of the brine (in ppm, Map 16)
T = the temperature of the brine (in °F, Map 19)
p = the maximum allowed aquifer pressure (in psi, Map 14)

Petrel equation

```
Pow((Pow(10,6) x (0.314+(0.58 x Map_16 /1000000)+(1.9 x Pow(10,-4) x
Map_19)-(1.45 x Pow(10,-6) x Pow(Map_19))))+((8+(50 x Map_16
/1000000)-(0.125 x Map_16 /1000000 x Map_19)) x Map_14),-1)/0.069
```

Map 16 - Salinity, Rotliegend aquifer
Map 19 - Temperature, Rotliegend aquifer (°F)
Map 14 - Mid LB-FG gradient pressures (psi)

The CO₂ plume density map (ρ_{CO_2}):

$$\rho_{CO_2} = 260.416638 + (-7.59534T) + (5.587335p) + (0.038888T^2) + (-0.007272p^2) + (-0.000048T^3) + (0.000001p^3) + (-0.013924\mathrm{Tp}) + (-0.000017T^2\mathrm{p}) + (0.000026\mathrm{T}p^2)$$

T = Aquifer temperature (in deg C, Map 18)
p = Maximum allowed aquifer pressure (in bar, Map 13)

Petrel equation

```
260.416638 + (-7.59534 x Map_19) + (5.587335 x Map_13) + (0.038888 x
Pow(Map_18,2)) + (-0.007272 x Pow(Map_13,2)) + (-0.000048 x
Pow(Map_18,3)) + (0.000001 x Pow(Map_13,3)) + (-0.013924 x
Map_18xMap_13) + (-0.000017 x Pow(Map_18,2) x Map_13) + (0.000026 x
Map_18 x Pow(Map_13,2))
```

Map 18 - Temperature, Rotliegend aquifer (°C)
Map 13 - Mid LB-FG gradient pressures (bar)

Appendix B – Calculation Workflow

B1 - Basic components

$$Theoretical\ CO_2\ Storage\ Capacity = V_p \times \Delta P \times C_t \times \rho_{CO_2}$$

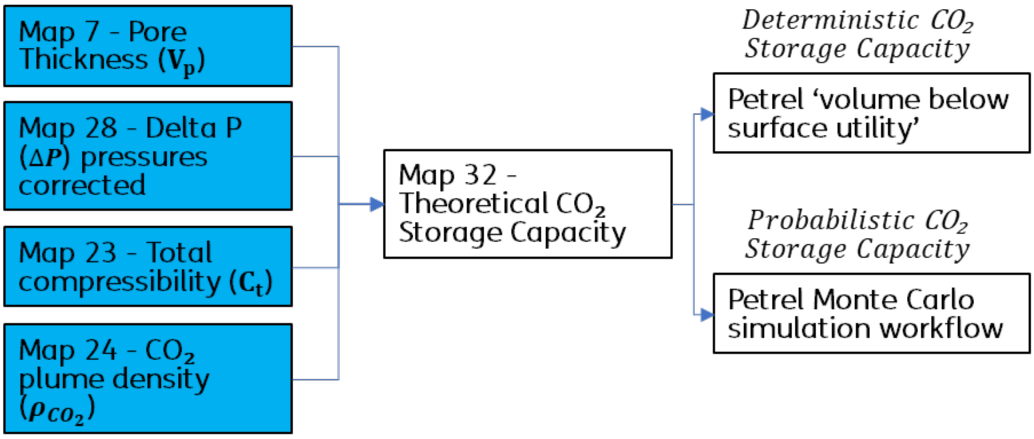

B2 - V_p workflow

$$Theoretical\ CO_2\ Storage\ Capacity = V_p \times \Delta P \times C_t \times \rho_{CO_2}$$

$$V_p\ = Thickness \times Net - to - Gross \times \varphi$$

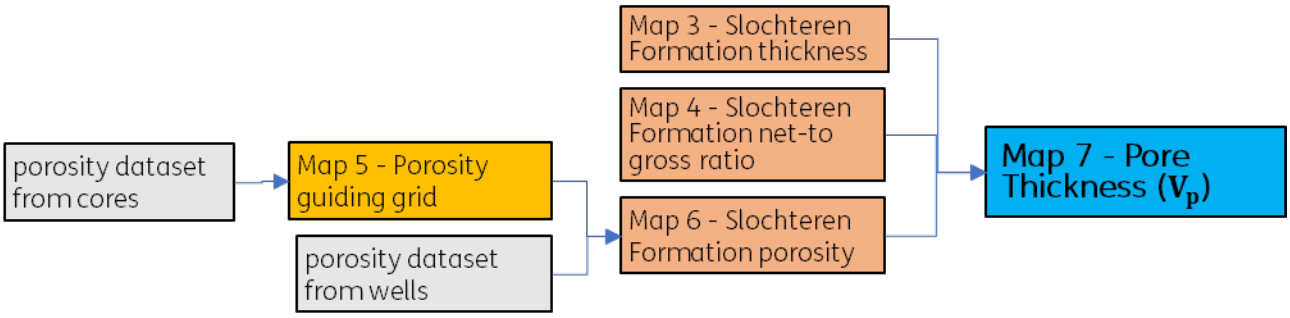

B3 — ΔP workflow

$$Theoretical\ CO_2\ Storage\ Capacity = V_p \times \Delta P \times C_t \times \rho_{CO_2}$$

$$\Delta \mathrm{P} = Initial\ pressure\ at\ crest\ - Max.\ allowed\ pressure\ at\ crest$$

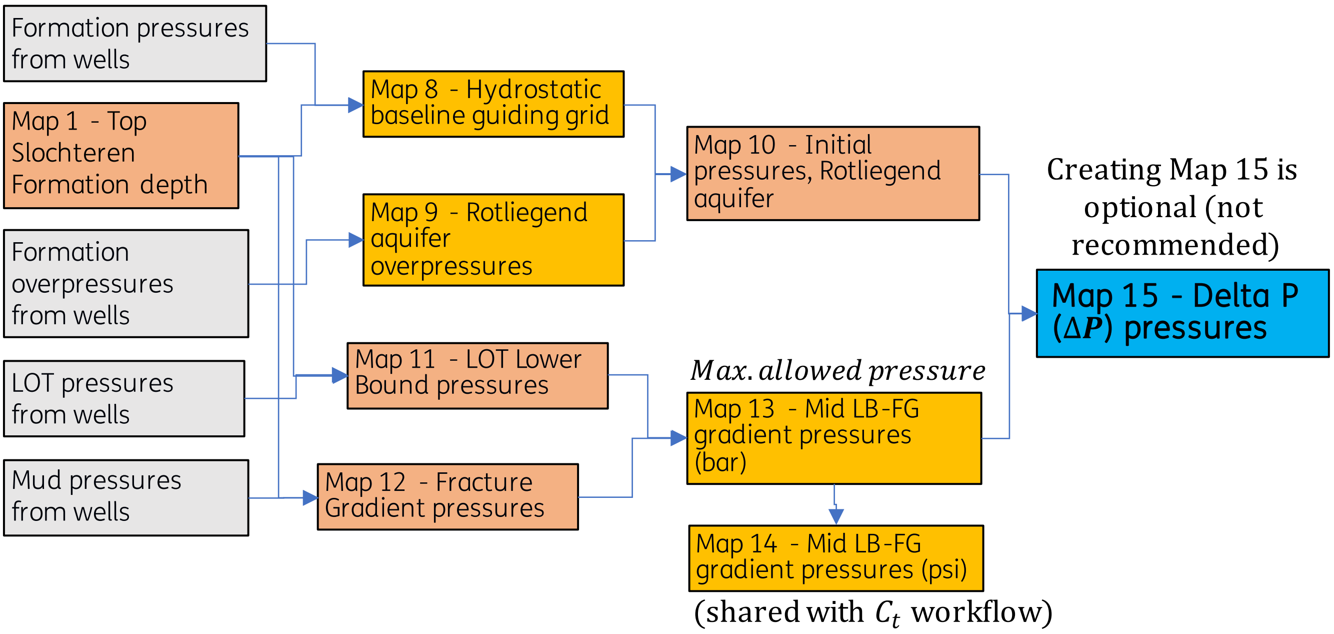

ΔP corrected workflow (Map 13 replaced by Map 26)

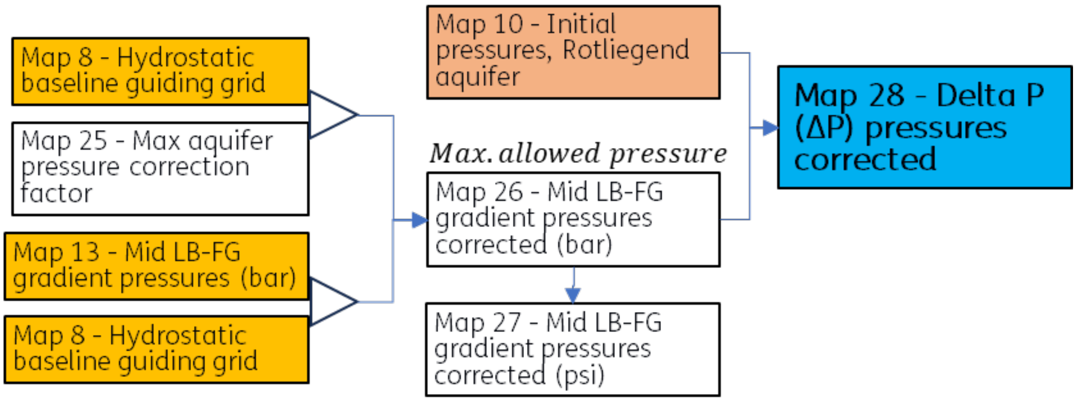

$B4 - C_t$ workflow

$$Theoretical\ CO_2\ Storage\ Capacity = V_p \times \Delta P \times C_t \times \rho_{CO_2}$$

$$C_t = C_w + C_r$$

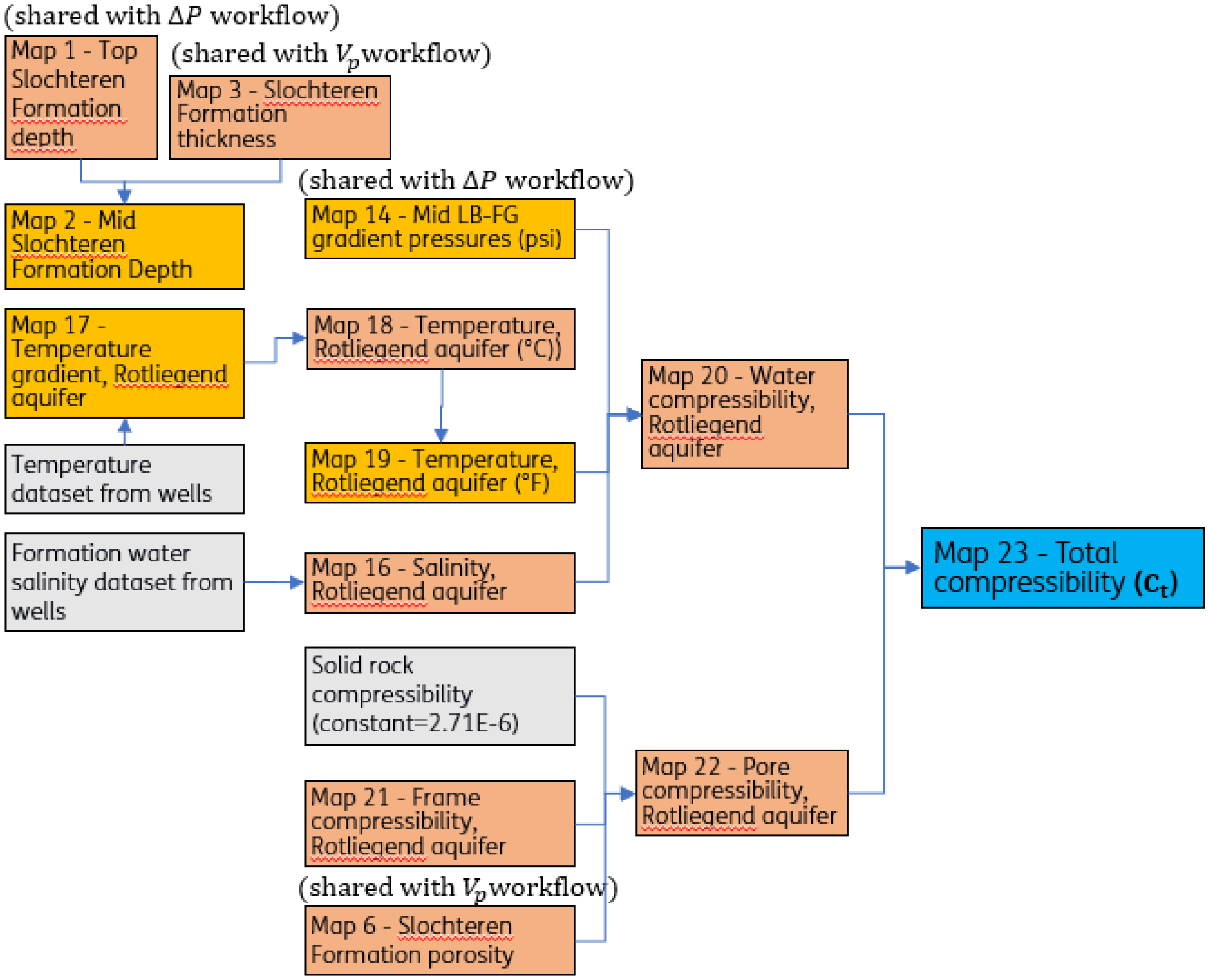

$B5 - \rho_{CO_2}$ workflow

$$Theoretical\ CO_2\ Storage\ Capacity = V_p \times \Delta P \times C_t \times \rho_{CO_2}$$

$$\rho_{CO_2} = plume\ density\ equation,\ see\ paragraph\ 3.4)$$

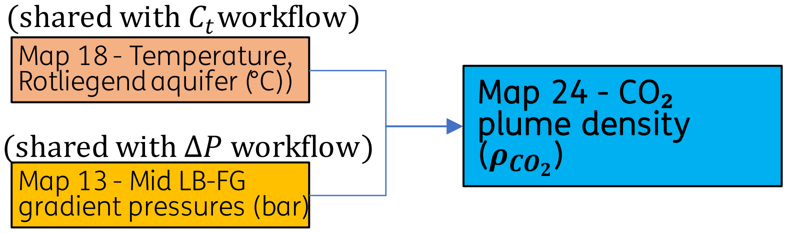

Energy & Materials Transition

Princetonlaan 6
3584 CB Utrecht
www.tno.nl